**UNIVERSIDADE DE LISBOA**
**FACULDADE DE CIÊNCIAS**
**DEPARTAMENTO DE GEOLOGIA**

# BEACH MORPHODYNAMICS AT NAZARÉ COAST USING VIDEO MONITORING

**Ana Maria Almeida Nobre Silva**

Doutoramento em Geologia
Especialidade em Geodinâmica Externa

2014

**UNIVERSIDADE DE LISBOA**
**FACULDADE DE CIÊNCIAS**
**DEPARTAMENTO DE GEOLOGIA**


# BEACH MORPHODYNAMICS AT NAZARÉ COAST USING VIDEO MONITORING

**Ana Maria Almeida Nobre Silva**

Tese orientada pelo Prof. Doutor Rui Pires de Matos Taborda (FCUL) e co-orientada pelo Prof. Doutor João Carlos da Costa Catalão Fernandes (FCUL), especialmente elaborada para a obtenção do grau de doutor em Geologia, Especialidade em Geodinâmica Externa.

2014

This dissertation should be cited as: Silva, A.M.N. (2014). Beach morphodynamics at Nazaré coast using video monitoring. Ph.D. Thesis, University of Lisbon, Portugal, 183 pp.

## ACKNOWLEDGEMENTS

The work on this thesis began in 2008 as part of an ambitious and enthusiastic work program which was only possible due to the valuable help of my supervisor Rui Taborda and to the priceless support given by the Portuguese Navy, particularly the Nazaré *Capitania* and its Captains (Captain José Miguel Farias Pais Neto, Captain António José Henriques de Albuquerque e Silva and Captain Jorge Manuel Lourenço Gorrincha) during this last few years. Also, João Francisco Duarte, from the Hydrographic Institute was an essential element during all this time, his dedication into the logistics allied with the fruitful scientific discussions gave an enormous help into this work. My many thanks to you all.

I would like to thank my co-supervisor João Catalão for his support, suggestions, edits and careful revisions.

The field work, involved a vast number of dedicated and supportive colleagues and friends without whom this work would be much harder, my special thanks to: Sofia Clara, Marco Alves, Hugo Sousa, Raquel Rodrigues, Anabela Dias, Mónica Ribeiro, Ivana Bosnic, Cristina Lira, Rute Ramos, Tanya Silveira, Mafalda Carapuço, Alphonse Nahon, Bárbara Proença, João Cascalho, João Duarte, Rui Taborda and Pedro Costa.

I would like to acknowledge the great working team, sharing offices 6.2.78 and 6.2.79. They, more than colleagues, were always very dear friends during this journey. Thanks to Mónica, Ivana, Cristina, Tanya, Mafalda, Zenaida, Ana Bastos and Paula.

I am also grateful for the amazing pictures of Nazaré, and the Nazaré Wave provided by the professional photographs Jorge Figueira and Renato Cardoso, and, no less amazing, photographs Catarina Guerreiro, João Cascalho, João Duarte and Bárbara Proença. My thanks, also go to Laura Anastácio and to the Nazaré municipality for providing historical pictures of Prainha.

I wish to acknowledge Xavier Bertin for guiding into the SWAN model, his help was essential in my first modeling steps.

Considerable thanks to José Paulo Pinto, from the Hydrographic Institute, for clarification about several oceanographic aspects related to the Nazaré Wave, and to Ana Bastos, Mónica Ribeiro, Ivana Bosnic and Cristina Lira for their careful review of this manuscript.

Financially, this wok was supported by an FCT grant (Fundação para a Ciência e Tecnologia, Ref: SFRH / BD / 41762 / 2007) and in the last several years by the FCT project B2C - Beach to Canyon (PTDC/MAR/114674/2009).

I would like to thank my institutions: University of Lisbon in particular the Department of Geology and IDL (Instituto Dom Luiz) for the logistic support, equipment and workspace.

Apart from work, my eternal thanks to my parents who supported me unconditionally in every aspects of my life; to my brother and sister; to my dear nephews João (always in my heart), Gonçalo, André and Gabriel.

To my giant, incredible and extremely loved universe: deeply grateful to Pedro Costa, Rui and Marta (who I'll meet very soon).

## Thanks

# RESUMO

À semelhança do que ocorre na maior parte das costas arenosas europeias, a costa ocidental portuguesa tem vindo a ser afetada por graves problemas de erosão. Em Portugal estes problemas apresentam uma relevância acrescida, não só pelo papel vital que a zona costeira representa para economia mas também pelo facto do litoral se encontrar exposto a um clima de agitação marítima particularmente energético que mobiliza um grande volume de sedimentos. Neste sentido, o conhecimento do transporte sedimentar longilitoral (TSL), também designado por deriva litoral, é fundamental para sustentar qualquer intervenção no litoral, particularmente intervenções que visem a proteção da linha de costa ou mitigação das tendências erosivas.

A quantificação da deriva litoral efetua-se geralmente através de modelação numérica baseada nos processos atuantes no sistema costeiro, através fórmulas empíricas que relacionam as taxas de transporte sedimentar com o fluxo de energia gerado pelas ondas (c.f. CERC, 1984; Komar and Inman, 1970) e, através de medições de campo. O recurso à modelação numérica para estimar o TSL encontra-se dificultado pela complexidade em representar os processos físicos envolvidos, particularmente em escalas temporais alargadas. Por outro lado, as formulações empíricas que se baseiam no método do fluxo de energia, embora menos problemáticas do ponto de vista da aplicação prática dependem frequentemente de uma calibração específica, materializada por um fator de calibração designado por K. Atualmente, o fator K foi determinado a partir de um número relativamente reduzido de medições, que em geral não são necessariamente representativas das características prevalecentes nas praias expostas do litoral português extremamente energéticas e com um comportamento essencialmente refletivo. Na realidade, a maior parte das medições/aproximações a este fator correspondem a litorais com comportamento dissipativo realizadas em ambientes pouco energéticos.

O presente trabalho tem como principal objetivo contribuir para o conhecimento dos processos associados ao transporte sedimentar longilitoral num ambiente fortemente energético. Este estudo foi concretizado através da análise da evolução morfodinâmica da zona costeira adjacente à Nazaré, através da aplicação de técnicas de aquisição de dados de campo, em particular de vídeo-monitorização, e modelação de processos morfossedimentares.

A praia do Norte, Nazaré, localizada na costa ocidental portuguesa constitui um local estratégico para a instalação de uma sistema de monitorização da linha de costa, baseado em técnicas de vídeo-monitorização, que permita quantificar dinâmica e o balanço sedimentar neste troço costeiro. O promontório da Nazaré, limite sul da praia do Norte,

constitui um local de acumulação sedimentar da deriva litoral dirigida para sul, enquanto o canhão submarino da Nazaré, localizado imediatamente a sul, constitui o maior sumidouro da plataforma continental portuguesa. Esta particular configuração geomorfológica permite que, em determinadas condições (condições oceanográficas que promovam deriva para norte), a praia do Norte esteja desprovida de sedimentos, sendo que a quantificação do seu subsequente enchimento pode servir de suporte para a quantificação da deriva litoral neste troço costeiro.

Neste sentido, foi instalado no promontório da Nazaré, mais concretamente no forte S. Miguel de Arcanjo, a cerca de 50 m de altitude, o sistema de monitorização COSMOS constituído numa primeira fase por uma camara de vídeo direcionada obliquamente para a praia do Norte. A câmara de vídeo, operacional desde dezembro de 2008 adquiriu de forma sistemática (com exceção de algumas falhas de natureza técnica) imagens da praia do Norte.

A aquisição de imagens decorreu a uma frequência de 1 imagem por segundo, durante intervalos de 20 minutos, a cada hora de luz. Para cada conjunto de 10 minutos de imagens foi gerada uma imagem TIMEX de forma a eliminar os efeitos do espraio das ondas. Foram escolhidas 31 imagens TIMEX durante o período entre dezembro de 2008 e maio de 2012, por forma a representar a evolução da praia do Norte numa base mensal.

As imagens representativas de cada mês foram escolhidas tendo por base um nível de água total equivalente, i.e. imagens em que a cota do nível de água se encontrava a 2 m (acima do nível médio do mar - NMM), para que interface água/areia se encontrasse na face de praia e para garantir a comparabilidade entre imagens. Esta interface água/areia, localizada verticalmente a 2 m acima do NMM, foi considerada (e designada) no decorrer do presente trabalho como sendo a linha de costa da praia do Norte.

As estimativas para a cota da linha de costa (i.e. o nível de água) efetuaram-se através de uma fórmula empírica, baseada em medições de campo específicas para a praia do Norte. Esta fórmula estima as cotas do nível da água em função da altura e direção das ondas ao largo e da maré astronómica.

Em cada uma das 31 imagens TIMEX previamente retificadas, detetou-se a posição da linha de costa utilizando o método de classificação automática Máxima Verosimilhança. A partir das linhas de costa, representativas da evolução da praia do Norte durante cerca e 3.5 anos, foram estimados os volumes mensais de areia na praia do Norte. Estes volumes foram estimados através da aplicação do modelo de volume de praia que assume uma configuração de perfil de praia representativa ao longo da área de estudo e estima o volume de areia na praia do Norte até á profundidade de 12 m (relativamente ao NMM).

As variações de volume na praia do Norte, com um intervalo temporal de 1 mês constituíram as observações para o transporte sedimentar nesta praia, enquanto as simulações para o TSL realizaram-se através da fórmula CERC (Rosati et al, 2002). Esta relacionou a magnitude de transporte com a componente longitudinal do fluxo de energia das ondas, na rebentação, que por sua vez foi estimada através de modelação numérica.

Os resultados apontam para uma variabilidade morfológica da praia do Norte extremamente elevada, expressa por variações na posição da linha de costa que chegam aos 160 m, nas imediações do promontório da Nazaré, e que decrescem para norte onde apresentam variações sazonais na ordem dos 70 m. De um modo geral a configuração da linha de costa da praia do Norte varia entre uma forma mais linear, geralmente entre junho e agosto, e uma forma mais arqueada durante os restantes meses.

A praia do Norte apresenta variações volumétricas sazonais que em média atingem os 1.6 milhões de metros cúbicos de areia, e um valor máximo na ordem dos 1.7 milhões de metros cúbicos de areia, ao longo da área de estudo. O aumento de volume de areia na praia do Norte está relacionado com padrões TSL direcionado para sul, enquanto a diminuição de areia na praia poderá estar relacionada com perdas de sedimentos para o canhão submarino da Nazaré, transposição de sedimentos em torno do promontório ou ainda, com TSL para norte da área de estudo.

Foi possível identificar dois sectores com comportamentos distintos, relativamente às variações volumétricas da praia do Norte, um sector mais variável na zona sul junto ao promontório e um sector mais estável na zona norte da área de estudo. O sector sul apresenta um sinal sazonal claro, cujas variações volumétricas são claramente afetadas pela retenção sedimentar no promontório. O sector norte, por outro lado, apresenta um sinal sazonal mais fraco, sendo que a sua variabilidade parece estar mais associada com uma componente interannual.

A integração das aproximações à quantificação do TSL, observações e simulações agrupadas trimestralmente, revelaram uma pequena sobrestimação das simulações (1.15 vezes as observações) que apontam para um fator K na ordem dos 0.34, valor muito aproximado ao referido na literatura. Na sequência dos resultados obtidos, estima-se uma magnitude de deriva anual residual média na ordem de 1 milhão de metros cúbicos, direcionada para sul.

De um modo geral, poderá descrever-se o seguinte modelo de transporte sedimentar para este troço costeiro (que inclui a praia do Norte, Prainha e baía da Nazaré): (1) entrada anual de 1 milhão de metros cúbicos de areia pela sua fronteira norte; (2) transporte predominante de areia para sul induzido pelo regime de agitação predominantemente

(NW); (3) captura da totalidade dos sedimentos pelo canhão submarino da Nazaré imediatamente junto ao promontório ou em frente à baía da Nazaré pelos seus tributários, fechando neste local a célula sedimentar Douro-Nazaré.

Durante o inverno o padrão de circulação de sedimentos, neste troço costeiro, é distinto. A maior dispersão direcional das ondas durante o inverno induz inversões de deriva de natureza pontual que resultam na saída de sedimentos para norte da área monitorizada. Fica ainda por esclarecer, se durante estas condições ocorre a captura de sedimentos para o canhão submarino com diminuição da volumetria total da praia. Para responder a esta questão torna-se essencial o conhecimento do perfil de praia submarino e da sua evolução espácio-temporal bem como alargar a área de monitorização mais para norte.

Em síntese, este trabalho conseguiu definir uma célula de circulação sedimentar na zona costeira da Nazaré e permitiu um conhecimento mais fundamentado acerca do comportamento morfodinâmico em litorais muito energéticos.

**Palavras-Chave:** Morfodinâmica de praias; Transporte sedimentar longilitoral; Vídeo-monitorização; Praia do Norte; Zona costeira; Nazaré.

# ABSTRACT

Most European coasts are subject to erosive processes and the Portuguese coast is not an exception, in fact it has been suffering from severe erosion particularly alarming due to its crucial economic role and its exposure to the highly energetic wave regime which is capable of mobilizing large volumes of sediments. In this sense, a better understanding of the longshore sediment transport (LST), also named longshore drift, is essential to support any coastal interventions, namely those that aim the coastline protection or the mitigation of the erosive tendencies.

The quantification of the longshore drift is typically performed by numerical modeling which is based in the processes acting in the coastal system, by empirical formulae that relate the sediment transport rates with the wave energy flux (c.f. CERC, 1984; Komar and Inman, 1970) and by field data measurements. The use of numerical modeling to estimate LST is hindered by the difficulty on the representation of the physical processes involved, especially in longer time scales. On the other hand, empirical formulae which are based in the energy flux method, although less problematic in terms of its practical application, depend of a specific calibration, through a calibration factor designated by K. Nowadays, the K factor has been established from a limited number of measurements, that are in general non-representative of the prevailing conditions in the high-energetic exposed beaches of the Portuguese coasts, commonly presenting a reflective behaviour. Most of the measurements/approximations of this factor were conducted in coasts with a dissipative behaviour and in low-energy environments.

The main objective of this work is to contribute to the understanding of the processes involved in the longshore sediment transport in a high-energetic environment. This study was carried out through the analysis of the morphodynamic evolution of the coastal zone adjacent to Nazaré, applying field-based data-acquisition techniques, particularly video-monitoring, and morfossedimentary processes modeling.

The Norte beach, Nazaré, located in the western coast of Portugal, is a strategic site for the set-up of a coastline monitoring system, based in video-monitoring techniques, which allows the quantification of the dynamic and the sedimentary budget of this coastal stretch. The Nazaré headland, south limit of the Norte beach, is a sediment accumulation location of the south-directed longshore drift. In contrast, the Nazaré submarine canyon, located immediately to the south, is the major sedimentary sink in the Portuguese continental shelf. This peculiar geomorphological configuration promotes that, under specific conditions (oceanographic settings that induce north-directed longshore transport), the Norte beach

is depleted of sediments, and thus measurement of its subsequent nourishment can serve to the quantification of the longshore drift in this coastal sector.

With that aim, the video-monitoring system COSMOS was installed at the Forte S. Miguel Arcanjo, in the Nazaré headland, at 50m high. The video camera, operational since December 2008, systematically obtained images of the Norte beach (with a few failures due to technical reasons).

The image acquisition occurred with a frequency of 1 image per second, during 20 minutes intervals, at each daylight hour. For each block of 10 minutes images a TIMEX image was generated in order to eliminate the swash effects of waves. Thirty one TIMEX images were selected, covering the period between December 2008 and May 2012, with the aim of representing the Norte beach evolution in a monthly basis.

The images representing each month where selected based in an equivalent total water level, (i.e. images where the water level height was 2 m above mean sea level - MSL), to guarantee that the water/sand interface was located in the beach face and, therefore assure comparability between images. This interface water/sediment, located vertically at 2 m above MSL, was considered (and entitled) in the present work as the coastline of the Norte beach.

The estimations for the coastline elevation (i.e. the water level) were obtained through an (site specific) empirical formula which was based in field measurements for the Norte beach. This formula estimates the elevation of the water level as a function of height and direction of the offshore waves and of the astronomical tide.

In each the previously rectified 31 TIMEX images, the coastline position was detected using the automatic classification by Maximum Likelihood. From these coastlines, representing the evolution of the Norte beach during 3 and ½ years, monthly sand volumes were estimated for the Norte beach. These volumes were estimated through the application of a beach volume model that assumes the beach profile configuration representative of the whole study area and calculates the sand volume of the Norte beach up to the depth of 12 m (Mean Sea Level).

The volume variations in Norte beach, within a 1 month window, relates to the observations of sediment transport in this beach, while the LST simulations were achieved though the CERC formula (Rosati et al., 2002). This formula related the magnitude of transport with a longitudinal component of the wave energy flux, at the breaking, which on the other hand was estimated though numerical modeling.

Results indicate an extremely high morphological variability in the Norte beach, this is translated by the variations of the coastline that reach 160 m, in areas adjacent to the Nazaré headland, and decrease northward were they present seasonal variations in the order of 70 m. From a broader perspective, the Norte beach coastline configuration follows a more linear variation, usually between June and August, and a more arcuate configuration during the remaining months.

Norte beach presents seasonal volumetric variations that on average reach the 1.6 cubic meters of sand, and a maximum value of 1.7 cubic meters of sand along the study area. The Norte beach sand volume increase is related with south-directed LST patterns, while the decrease in beach sand might be related with loss of sediment to the Nazaré submarine canyon, to the sediment bypass of the promontory or, with north-directed LST out of the study area.

It was possible to identify two sectors with distinctive behaviours in what concerns Norte beach volumetric variations; one sector, more variable, at the south and adjacent to the promontory and a more stable sector, in the north section of the study area. The south sector presents clear seasonal signatures, with volumetric variations clearly affected by sediment retention in the promontory. While, the north sector presents a weaker seasonal signature, and its variability seems to be more associated with an interannual component.

The integration of the LST approximations, observations and simulations trimonthly grouped, revealed a minor overestimation of the simulations (1.15 times the observations) that lead to a K factor in the order of 0.34, a value that is very close to the ones found in the literature. Based in the results obtained, it can be estimated a net annual drift magnitude in the order of 1 million cubic meters, south-directed.

Overall, the following model can be used to describe the sediment transport within this coastal sector (that includes Norte beach, Prainha and Nazaré bay): (1) annual input of 1 million cubic meters of sand through its northern boundary; (2) dominant sand transport directed to the south in response to the predominant wave regime (NW); (3) total capture of sediments by the Nazaré submarine canyon (in the vicinity of the headland) or by its tributaries (in front of Nazaré bay), closing in this location the sediment cell Douro-Nazaré.

During winter, in this coastal sector, the sediment circulation pattern is different. The winter major directional wave dispersion, induces drift inversions that result in the loss of sediment to north of the monitored area. It is still uncertain, if during these conditions occurs the sediment capture into the canyon, by the submarine profile, inducing a decrease of the total volume of the beach. To answer to this question it is crucial to know the

submarine beach profile and its evolution in space and time, as well as enlarge the monitoring area to the north.

As a summary, this work succeed to define a sediment circulation cell in the Nazaré coastal zone and allowed a more grounded knowledge about the morphodynamic behaviour at highly-energetic coastal stretches.

**Key-Words:** Beach morphodynamics; Longshore sediment transport; Video monitoring; Norte beach; Coastal zone; Nazaré.

# CONTENTS

# CHAPTER 1

# General Introduction

# CHAPTER 1 – GENERAL INTRODUCTION

**This chapter presents a description of the motivation that led to the present work, research approach and thesis outline.**

## 1.1. MOTIVATION

Longshore sediment transport (LST) or longshore drift is an extremely influential factor of the coastal geomorphology. Understanding longshore drift patterns, magnitudes and gradients is essential to characterize shoreline evolution and the sedimentary budget thus contributing for many coastal engineering and science studies.

Scientific community believes that to understand longshore sediment dynamics and its gradients is fundamental to minimize the erosive trends that affect most of the world's sandy coastlines.

LST rates can be measured in the field or can be estimated by processes based modeling, by empirical formulae, which normally relate volume of transport rates with wave energy flux (c.f. CERC, 1984; Komar and Inman, 1970).

Despite the vast plethora on measurement techniques, the complexity of processes controlling the LST and the instantaneous nature of some of these techniques difficult accurate estimates. Still, field measurements offer the most accurate estimates for LST and provide essential data to define the K factor, used in calibration of the wave energy flux approach.

Direct field measurements include sediment accumulations rates in harbours, inlets or groins (e.g. Barceló, 1970; Komar, 1990), short-term impoundment (Bodge and Dean, 1987), nourishment loss (Teixeira, 2009), sand tracers (e.g. Komar and Inman, 1970; Duane and James, 1980; Kraus et al., 1981, 1982; Fields and Weishar, 1987; Ciavola et al., 1997; Taborda et al., 1999; Vila-Concejo et al. 2004; Silva et al., 2007), streamer traps (Dean et al., 1987; Kraus and Dean, 1987; Rosati et al., 1991; Wang et al., 1998, 2002a), optical devices (Downing et al., 1981; Beach and Sternberg, 1988; Aagaard et al., 2002) and acoustic sensors (Vincent and Green, 1990; Vincent et al., 1991).

Empirical formulae were mainly developed for low energetic/dissipative beaches, thus generally cannot be directly extrapolated to higher energetic and/or reflective environments. In fact, still few measurements exist for the K approximations along these energetic coastal stretches (Rosati et al., 2002). Therefore, the proportional K factor is often used as an empirical calibration factor between estimates and observations.

LST quantifications based on sediment accumulation in artificial structures or by the inverse process, i.e. quantification of erosion rates downdrift of the blocking structure, are firstly referenced in the work of Watts (1953) followed by numerous authors during the XX$^{th}$ century (see Komar, 1998 for a critical review of this theme). Main limitations to this method are local effects on waves and currents induced by structures, sand bypassing in front of the structure and the time involved to retain enough sediments that could induce shoreline changes unequivocally higher than the uncertainties of the measurement techniques.

Naturally, sediment retention and associated LST quantifications can also be performed in natural structures such headlands, sand spits, inlets and estuaries. In the former, sand retention processes and coastline evolution are similar to the ones observed in artificial structures. However, in headland settings is not generally possible to define neither the conditions where the retention process began, nor the transposing processes (time and magnitude).

Yet, in some cases the coastline evolution related with the retention processes can be identified. This generally occurs where the downdrift boundary of a littoral cell only allows one way sediment transposition (e.g. related to existence of a submarine canyon). In these cases, longshore drift inversions lead to a sedimentary depletion of the updrift beach adjacent to the headland; if longshore drift inversion is persistent enough to retreat the coastline to a minimum the subsequent infill of the beach can be used to access longshore drift. This method is only suitable when the magnitude of coastline variations, in relation to longshore processes, clearly dominates the cross-shore component.

The Norte beach, and the Nazaré coast, located at the southern limit of the Douro-Nazaré littoral cell emerge as a strategic place to focus investigation on the sedimentary dynamics and the sedimentary budget of this coastal stretch. The Nazaré headland acts as a sedimentary retainer of the southward-directed drift, the presence of the Nazaré submarine canyon prevents sediment entry through the southern boundary (defining a kind of gated boundary) which promotes, in particular conditions, the depletion of the beach. These important advantages support valuable quantifications about the littoral drift at this coastal stretch and, ultimately, improve the calibration of the LST formulations for this coast.

Additionally, the Norte beach is a perfect place for beach video monitoring. In fact, the fort and lighthouse in Nazaré headland confer perfect conditions for the installation of a continuous video monitoring system which enables monitoring the coastline variations over several years (Figure 1.1).

The COSMOS video monitoring system (Taborda e Silva, 2012 - *Chapter 3 - COSMOS Video Monitoring System* ), installed at a high place (about 50 m above mean sea level – MSL) allows the oblique perspective of the Norte beach. Acquisition of long-term high-resolution images of the Norte beach, particularly focusing on the coastline position and evolution, can support the quantification of morphological changes and subsequently contribute for the sedimentary budget assessment at this coast.

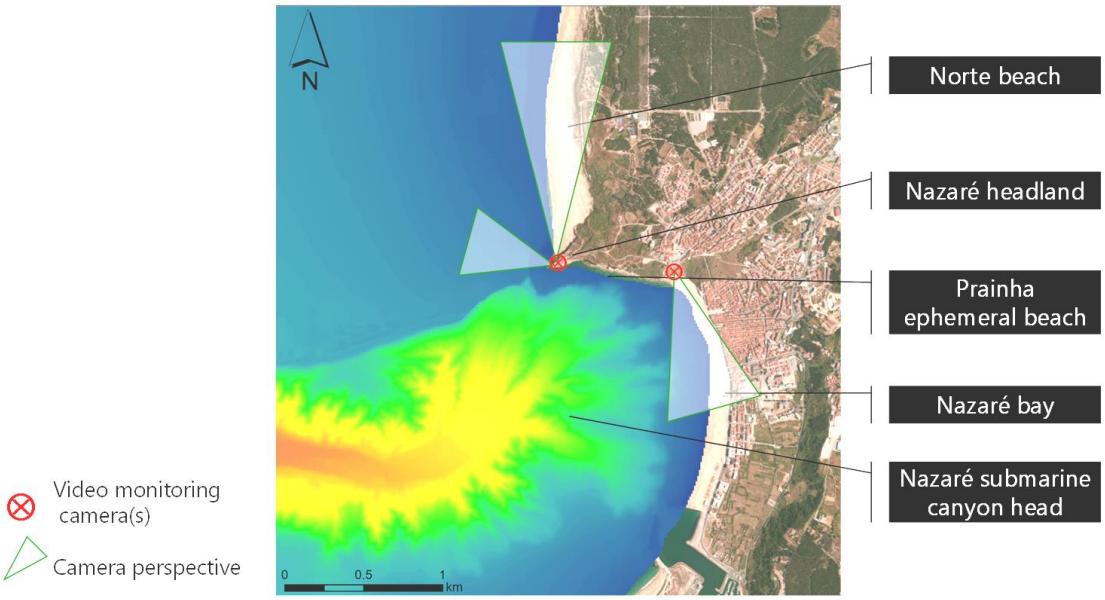


**Figure 1.1 – The Nazaré coast and the COSMOS video monitoring cameras perspectives.**

Moreover, the video monitoring techniques have been widely used in coastline evolution studies with demonstrated proves of its applicability and accuracy (see for example Silva et al., 2009 - *Chapter 2 – Video Monitoring* and Silva and Taborda, 2014 - *Chapter 7 – Norte beach morphodynamics – long-term perspective through video monitoring* for a wide list of bibliographic references).

Overall sedimentary dynamics at the northwest coast of Portugal is highly influenced by the North Atlantic wave regime, which is particularly energetic. Coastal erosion has been an issue affecting the generality of the Portuguese coast particularly due to the high potential LST and decreased sediment availability.

Between the Douro river mouth and Nazaré, a wide coastal cell can be recognized by having common wave exposure and common continental shelf morphology that induce similar longshore sediment transport behaviour (Figure 1.2). The amount of material

involved in this process has been estimated in about one million cubic meters per year, net southward-directed, as discussed in Silva, et al., 2012 - *Chapter 5 – Longshore Sand Transport Variability at the Northwest Coast of Portugal*.

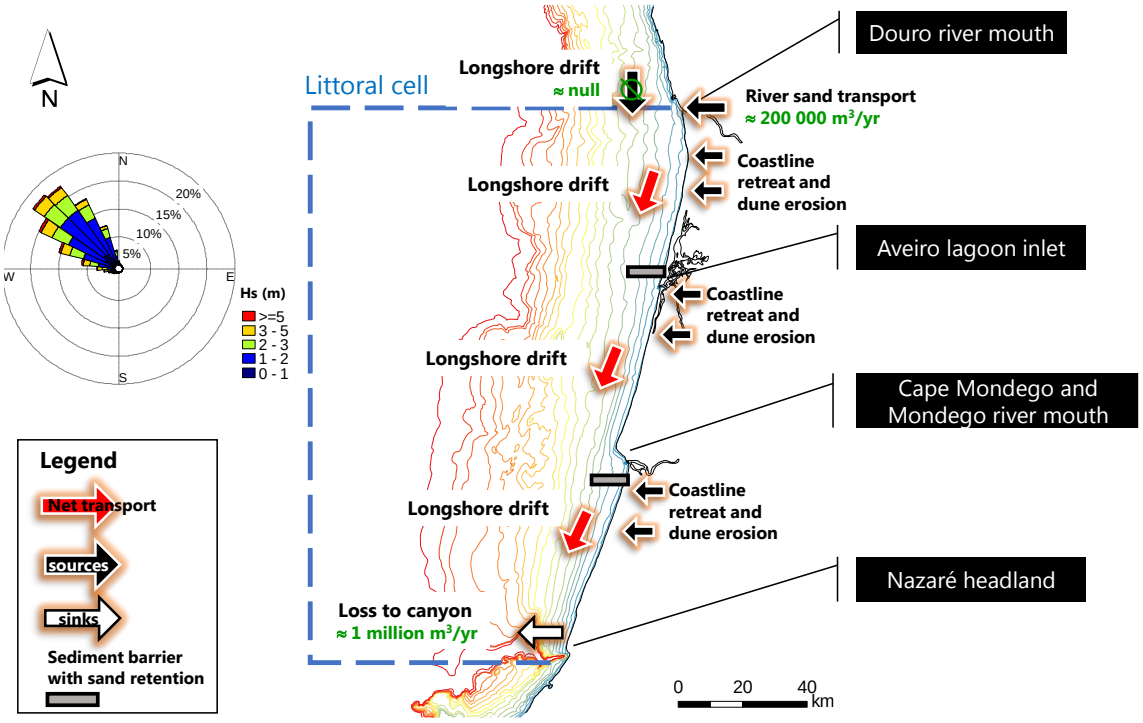


**Figure 1.2 – Sedimentary budget on the Douro-Nazaré littoral cell (the rose diagram represents the offshore wave conditions between 1953 and 2008; Dodet et al., 2010).**

This coastal cell comprehends about 160 km of sandy coastline interrupted by Aveiro lagoon, Mondego cape and Mondego river mouth. Although some of these interruptions are natural barriers bypassed by sediments, the Aveiro inlet jetties and the groin field southward of Aveiro have strongly disturbed the sediment supply with severe erosion consequences downdrift (Andrade et al., 2002, Taborda et al., 2005 and Taveira-Pinto et al., 2009).

At the northern boundary sedimentary input is very scarce. Presently, sediment contribution from the updrift adjacent cell is null, while the sediment contribution from the Douro river is estimated in 200 000 $m^3$/yr (Vicente and Clímaco, 2012). Along this coast, sediment contribution from the drainage basins, once capable of feeding the downdrift littoral, are nowadays negligible (concerning sand contents) and coastal retreat and/or

dune erosion have been more and more reported. These erosive episodes occur as a natural system response to assure the potential LST which maintain its capability.

Is presently settled that the net (southward-directed) longshore drift when reaches the Nazaré submarine canyon is captured and escapes from coastal system, closing this littoral cell in its southern boundary.

The most important concern about this coastal stretch is that balance of the sedimentary budget is being assured through erosive tendencies. The magnitude of sediments provided by river transport and LST is not in equilibrium with the magnitude of sediments loss to the canyon (Table 1.1). Nowadays, principal sediment sources at this cell are related with sediments provided by coastline retreat and dune erosion once sediment input (sand content) due to fluvial transport is very small or even null.

**Table 1.1 – Sedimentary budget components on the Douro-Nazaré littoral cell.**

| | |
|---|---|
| ***Sources*** | • River transport<br>• Coastline retreat |
| ***Sinks*** | • Down-canyon transport |
| ***Balance*** | • Coastal cell with erosion tendency |

In summary, motivation of this thesis relates to the need of quantifying the longshore sediment transport in high energetic environments. To achieve this goal it was necessary to recognize the links between oceanographic forcing and shoreline evolution patterns at the Norte beach and, simultaneously, understand the sedimentary budget at the Nazaré coast.

## 1.2. OBJECTIVES

Main objective of the present thesis is to quantify longshore sediment transport in high energetic environments, evaluating the morphodynamics of the Nazaré coast, particularly focusing on the morphodynamics of Norte beach through video monitoring techniques.

Several complementary objectives can be drawn:

- Validate the use of video monitoring techniques in the study of beach morphodynamics, mostly in what concerns coastline detection.

- Implement a video monitoring system in Norte beach. This task includes, not only hardware installation, but also software components and all logistics and maintenance associated to a long-term video monitoring system.
- Wave propagation and morphological modeling of the coastal zone with SWAN and XBeach models.
- Characterize the long-term LST and it's seasonal to decadal variability at this coastal stretch. The long-term LST quantifications will be achieved through the use of empirical LST formulae coupled with long-term simulated wave information.
- Quantify and describe the shoreline variability of the Norte beach during a large period (pluriannual scale) through video imagery.
- Understand long-term (yearly to decadal) beach morphological changes at the Norte beach based on the shoreline variability monitoring.
- Comprehend morphodynamics and sedimentary budget at the Norte beach and at the Nazaré coast (including Prainha and Nazaré bay beach).
- Improve the knowledge about the sedimentary budget of the Douro-Nazaré coastal cell and calibrate LST formulae though the estimation of the K parameter.

## 1.3. THESIS OUTLINE

This study covers a wide range of topics from video monitoring implementation, oceanographic forcing modeling, longshore sediment transport evaluations, to shoreline variability and volume quantifications which were structured in eight chapters:

Chapter one, *General Introduction,* correspond to a description of the thesis objectives, motivations and outline.

Chapter two, *Video Monitoring,* presents the methods of the present research. Although the study site is not the focus of this study, the work presented in this chapter demonstrates and validates the use of video monitoring in the detection of shoreline position.

Chapter three, *COSMOS Video Monitoring System*, has a comprehensive description of the video monitoring system installed in the Norte beach, including photogrammetric and mathematical principles behind the video monitoring and the processes involved between image acquisition and feature extraction.

Chapter four, *Hydrodynamic and Morphodynamic Modeling*, describes the efforts made to model the oceanographic forcing and morphological responses of this high energetic and complex coastal system.

Chapter five, *Longshore Sand Transport Variability at the Northwest Coast of Portugal,* includes the evaluation of the variability of the longshore drift at seasonal to decadal scales. Herein, the longshore drift magnitudes and gradients updrift of the monitored area, the Norte beach, is established.

Chapter six, *Shoreline variability at the Norte beach,* presents the first video derived results. This chapter includes the monitoring of shoreline position for about three and half years, which allowed the study of the Norte beach seasonal variability.

Chapter seven, *Norte Beach Morphodynamics – Long-term Perspective through Video Monitoring,* includes a state of the art on long-term beach monitoring using video techniques, quantification of beach volumes and wave forcing characterization of Norte beach over a period of three and half years

Finally, chapter eight, *Synthesis of the Morphodynamics of the Nazaré coast and conclusions*, synthesize the morphodynamic conceptual model of this coastal stretch and adds some information and discussion on a few themes/results that were not included in aforementioned chapters. This concluding chapter provides important insights on overall beach morphodynamics and sedimentary budget of this coastal cell.

# CHAPTER 2

# Video Monitoring

# CHAPTER 2 – VIDEO MONITORING

**This chapter is based on a manuscript published in the Journal of Coastal Research:**

Ana Nobre Silva; Rui Taborda; João Catalão and Paula Freire, 2009. "*DTM Extraction using video-monitoring techniques: application to a fetch limited beach*". Journal of Coastal Research, Special Issue 56, pages 203-207.

## 2.1. ABSTRACT

In this work, a video-monitoring system applicable to the study of beach morphodynamics was developed and applied to the DTM extraction of the intertidal zone of a fetch limited beach (Alfeite, Portugal). This low-cost system, intended to complement standard survey tools, has the additional benefit of enabling the continuous monitoring of beach meso-scale process (spatial/temporal scales in the order of kilometres and years, respectively).

The development of this system, based on terrestrial photogrammetric techniques, involved three main steps: i) camera calibration, where the internal camera parameters were determined in the laboratory using open-source software; ii) the development of image correction subroutines, which aimed to correct the relatively large image distortions induced by camera optics; this procedure revealed to be essential as the system was built upon standard non-metric surveillance cameras; iii) the development of image rectification subroutines to transform oblique images into vertically equivalent images; this transformation was based on external camera orientation parameters obtained in the field through the surveying of ground control points.

Alfeite beach DTM extraction was performed through the shoreline digitalization, in geo-referenced rectified images acquired every 10 min, during the flood. The overlapped set of shoreline curves, properly referred to a vertical datum by means of tide measurements, characterized the intertidal beach morphology.

The obtained results were compared with the ones acquired with classic survey techniques revealing very encouraging results; the overall vertical rms was 0.08 m with a maximum value of 0.15 m at 390 m of the camera.

## 2.2. INTRODUCTION

Coastal morphodynamics represents an important issue as littoral systems are extremely dynamic and encompass a high socio-economic value. Nowadays, a conscious understanding and characterization of coastal dynamics is essential not only for scientific

knowledge but also for a correct and sustainable management of littoral. The complexity of the littoral processes ranges from very small spatial/temporal scales as wave breaking, currents, sand bar and beach cusps movements to large spatial/temporal scales like coastline evolution, erosion and accretion response to sea level changes amongst others processes.

Littoral video-monitoring techniques are based on the fact that nearly any nearshore phenomena that can be discerned visually can be quantified by image processing techniques (Holland et al., 1997; Aarninkhof, 2003; Holman and Stanley, 2007), namely breaking zone location (Holman et al., 1993) and shoreline position (Plant and Holman, 1997; Dronkers, 2001; Alexander and Holman, 2004; Armaroli et al., 2004; Conley et al., 2007; Siegle et al, 2007).

In the 80's the video monitoring techniques suffered important developments by the Coastal Imaging Laboratory (CIL) at Oregon State University by means of video and image processing tools directed to the monitoring and measuring of the morphodynamic changes and the physical processes acting on the littoral, which resulted on a worldwide network of video-cameras, the ARGUS monitoring system.

Beach video monitoring has the advantage to be a cheap, continuous and automatic technique for data acquisition of the visible littoral phenomena along large periods. Although images can be obscured by fog and rain during storms, it provide important information before and after storm (Smith and Bryan, 2007) in spatial and temporal scales suitable of the beach physical processes (Holman and Stanley, 2007), providing the higher resolution remote detection technique, for morphodynamic monitoring, over large periods (Aarninkhof, 2003).

The major disadvantages of video monitoring systems are the impossibility of data acquisition during the night and the variable linear scale factor along the image, inherent to the oblique acquisition geometry which reduces the accuracy further from the camera (Smith and Bryan, 2007). The reliability, accuracy and versatility of the coastal video systems have been tested and reviewed in scientific literature (Davidson et al., 2007). Coastal video systems have been recognized as a very effective coastal management tool, uniquely providing data with excellent spatial and temporal resolution and coverage (Van Koningsveld et al., 2007).

The shoreline detection through the identification of the water/sand interface in the video images allow the quantification of the shoreline evolution in large temporal scales (years) through small scales (seconds), including the shoreline detection along a tidal cycle that, together with the sea level measured or estimated, allow the automatic intertidal

bathymetry mapping (Aarninkhof et al., 2003; Madsen and Plant, 2001; Plant and Holman, 1997).

The video monitoring systems are generally supported by terrestrial photogrammetric principles as the collinearity condition equations which state that the camera center, the object point and its photo image lie along a straight line in three-dimensional space (Wolf and Dewitt, 2000). The knowledge of this geometric relation is essential to extract quantitative information of the objects strictly from its images by the transformation of the image coordinates (x, y) into real world coordinates (X, Y, Z).

In order to obtain accurate results, from a video monitoring system, three main steps must be performed: 1) camera calibration, in which internal camera parameters responsible for the image distortions are measured in the laboratory in order to characterize the camera distortion model; 2) image correction, which intend to create a distortion free image using the previously determined internal camera parameters; and 3) image rectification to transform originally oblique images into vertically equivalent images in which precise measurements can be made.

In Portugal beach video-monitoring systems are still at initial stages of development mainly because of the relative high cost of commercial systems that has made the littoral video-monitoring inaccessible to management organizations and also to the scientific community. For that reason the development of a low cost video-monitoring system, which is the main goal of this work, is fully justified. This was achieved through the development of a video-monitoring system, built upon rigorously calibrated non-metric IP surveillance cameras, able to accurately quantify coastal processes.

## 2.3. STUDY SITE

Alfeite beach, located at Alfeite sand spit in the inner bay of Tagus estuary, Portugal (Figure 2.1). Alfeite beach is a fetch limited beach extended for about 2600 m, from Quinta do Alfeite to Ponta dos Corvos, characterized by a narrow and steep foreshore (slope of 0.10) and a broad sub-horizontal low-tide terrace (Freire, 2003). Under a semi-diurnal mesotidal regime Alfeite beach is characterized by tidal range, in Lisbon, from 1.5 m to 3.2 m, respectively in spring and neap tides (Portela and Neves, 1994).

Alfeite beach has an E-W orientation and is characterized by a low energy, locally generated, wave regime with mean wave height of 0.11 m and median gain size diameter of 0.21$\phi$ (Freire et al., 2007). The choice of Alfeite beach, as experimental test site, was

justified by its low energy wave regime which simplifies the shoreline detection procedure due to negligible wave swash motion.

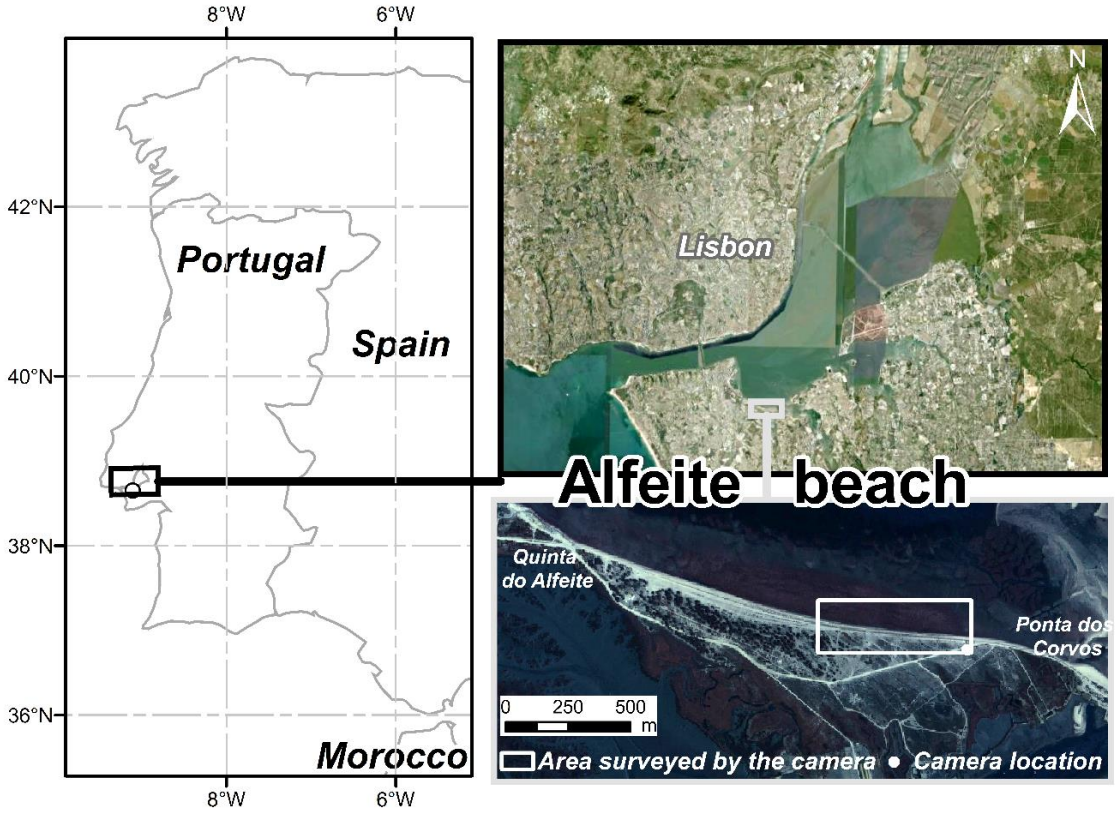


**Figure 2.1 - Alfeite beach and video camera location.**

## 2.4. METHODS

### 2.4.1. CAMERA CALIBRATION

The camera calibration consists in the computation of camera internal parameters (i.e. effective focal length, the principal point position, pixel skew and the coefficients of distortion). In the present work the internal camera parameters were measured in laboratory using the open-source computer application Camera Calibration Toolbox for MATLAB developed by Vision Caltech (2009) in which images of a calibration object were recorded from several camera orientations.

### 2.4.2. DATA ACQUISITION

Alfeite beach images were acquired from a video camera positioned in a high place (near 8m above mean sea level) and directed obliquely to the shoreline (Figure 2.2) during the tidal flood between 12:00 and 16:15 of 1 June of 2007. The video-monitoring camera, with a 1.2 mega pixel resolution, was connected to a laptop using an Ethernet cable and recorded oblique images of Alfeite beach every 1 minute. Simultaneously, water level was measured using a pressure transducer placed at the beach face.

**Figure 2.2 - Video camera setup on an electric pole.**

### 2.4.3. IMAGE CORRECTION

Image distortions induced by camera optics were corrected using developed MATLAB subroutines based on Heikkila and Silvén (1997) distortion model, which accounts both for tangential and radial distortion components. Using the internal camera parameters, computed in laboratory calibration, undistorted images (Figure 2.3B) were created by inverse mapping from original Alfeite images (Figure 2.3A).


**Figure 2.3 - Oblique Alfeite beach image. (A - Original image and B – Corrected image).**

### 2.4.4. RECTIFICATION

Image rectification is the process that transforms an oblique image into a vertical equivalent one, free from deformations induced by the camera obliquity (Wolf and Dewitt, 2000). The external camera parameters were computed based on the correspondence between several field ground control points (GCP) coordinates, positioned with Trimble 4000 SST GPS, and the respective image coordinates. The Alfeite corrected images were rectified using external camera parameters (three coordinate camera position, X, Y and Z and three orientation angles $\alpha$, $\omega$ and $\kappa$) and the water level, at acquisition time, as reference level. Inverse mapping MATLAB subroutines were developed to create vertically equivalent images (rectified images) (Figure 2.4) from distortion free images (corrected images).

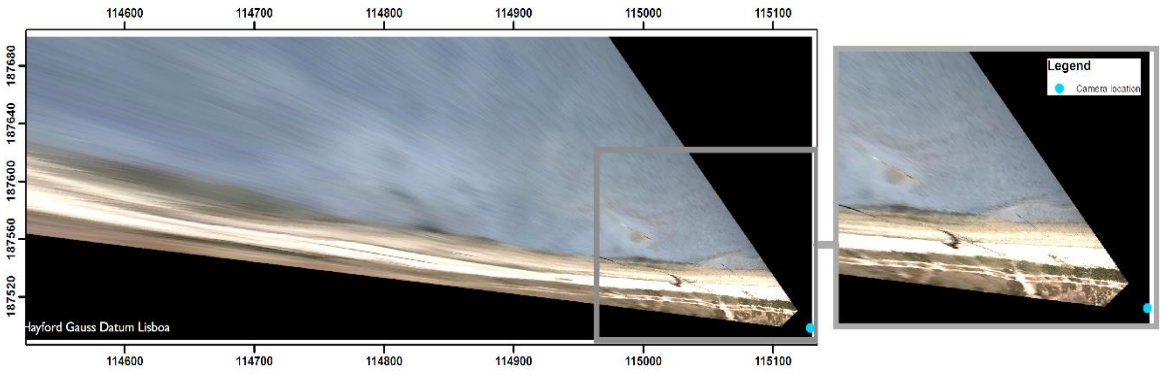


**Figure 2.4 - Rectified image of Alfeite beach.**

### 2.4.5. DIGITAL TERRAIN MODEL EXTRACTION

The intertidal digital terrain model was extracted from the shoreline detection every 10 minutes, during the flood, over the Alfeite rectified and geo-referenced consecutive images. To every shoreline, the water level height corresponding to the time of image acquisition was attributed, producing an intertidal contour map and a digital terrain model as a triangulated irregular network (TIN) (Figure 2.5). Total station topographic profiles were performed to compare video-monitoring results with classic survey results.

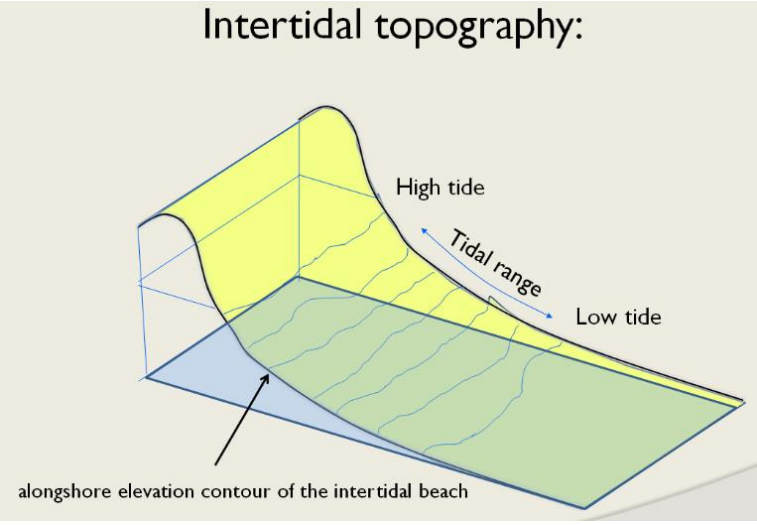


**Figure 2.5 - Conceptual model of DTM extraction using the changes on the water level (adapted from Aarninkhof, 2003).**

## 2.5. RESULTS AND DISCUSSION

The laboratory calibration was able to characterize camera internal parameters with a calibration error of 0.25 of the pixel dimension. From every 10 minute rectified image a contour line was digitized resulting on a contour map and a respective digital terrain model of the intertidal zone at Alfeite beach (Figure 2.6).

Results show an important loss of pixel resolution with camera distance, especially in longshore direction (Δy), e.g. at 500 m distance the longshore pixel resolution is about 20 m. The cross-shore direction (Δx) is less degraded with distance and shows a pixel resolution less than 1 m along the x axis (Figure 2.7). In shoreline detection studies the cross-shore pixel resolution component is the main influent factor as the shoreline is mainly identified along this direction (reducing the uncertainties).

The comparison between video-monitoring results and classic survey techniques revealed very good results with a low rms vertical error, of about 0.08 m. The maximum vertical error, 0.15 m, was observed at 390 m distance from the camera, decreasing toward the camera location (Figure 2.8). At camera distances lower than 250 m the rms error was mainly below 10 cm, with a single exception (0.11 m) at 170 m from the camera. Similar results were obtained by Aarninkhof et al. (2003), with major deviations further from the camera, lower than 15 cm, along 85 % of the 2 km beach studied. Plant and Holman (1997) reported a 0.24 m rms vertical error, later corrected to 0.06 cm by empirical corrections for the water level.

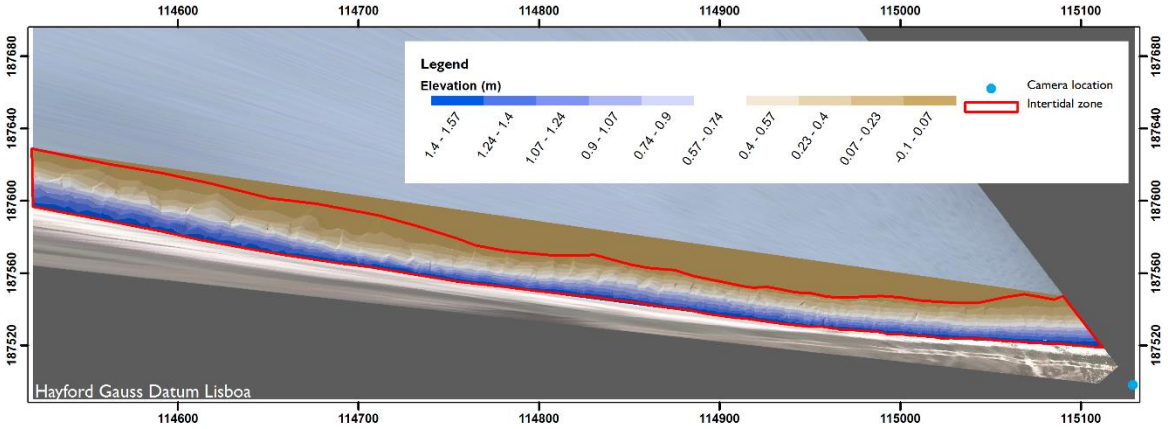


**Figure 2.6 - Alfeite beach intertidal digital terrain model (vertical datum – mean sea level).**

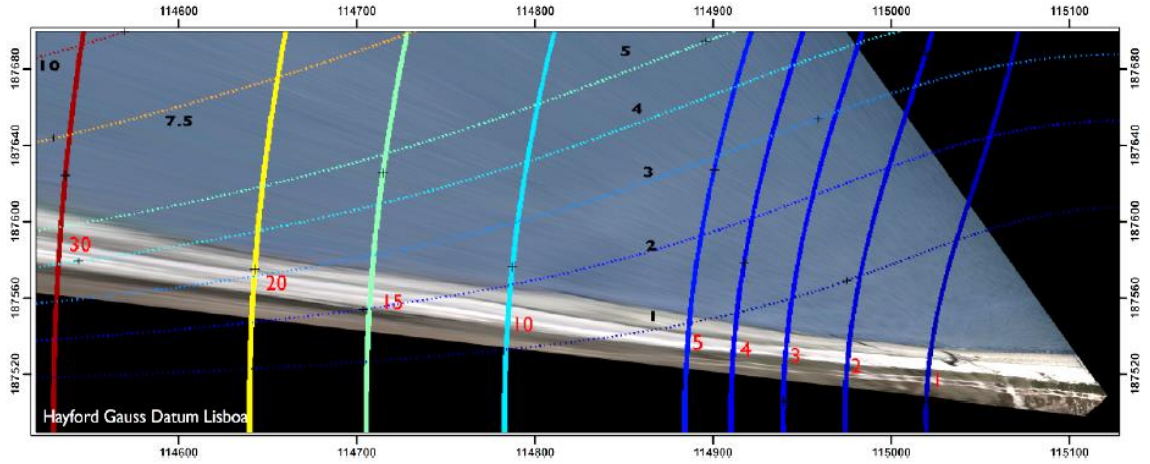


**Figure 2.7 - Spatial pixel resolution along assumed Alfeite beach coordinate system. Bold lines represent pixel resolution along longitudinal component (Δy) and dashed lines the pixel resolution along cross-shore component (Δx).**

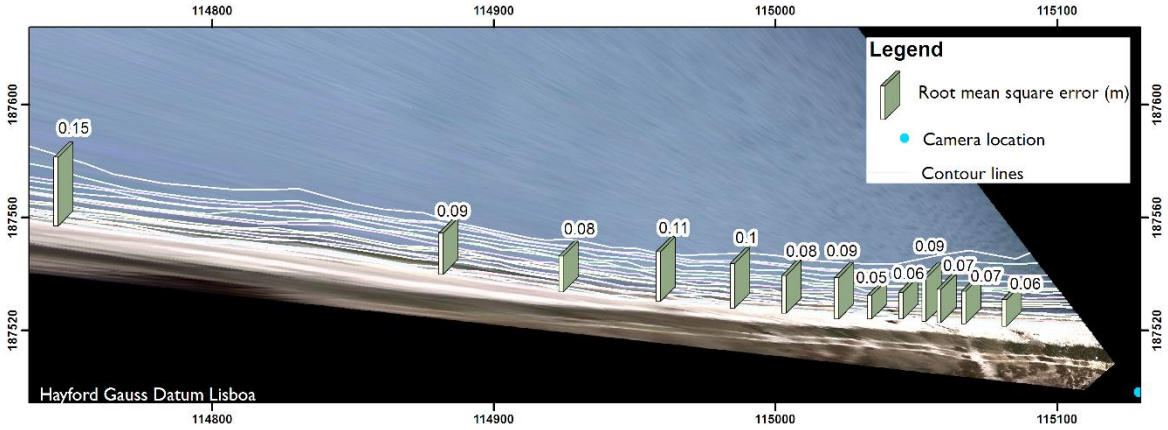


**Figure 2.8 - Root mean vertical error along the control topographic profiles.**

## 2.6. CONCLUSIONS

The present work describes the development of a portable video-monitoring system, based on low cost IP non-metric cameras.

Promising results were obtained as this system was able to extract a digital terrain model of an intertidal zone with similar accuracy to standard surveying methods. The use of these systems can significantly extend the spatial/temporal resolution of beach monitoring programs, contributing therefore to a littoral management supported on a knowledge based approach.

## 2.7. ACKNOWLEDGEMENT

This paper is a contribution from project BERNA - Beach Evolution in Areas of Restricted fetch: experimental and numerical analysis (POCTI/CTA/45431/2002), supported by FCT (Foundation for Science and Technology) and Ana Silva benefited of a PhD grant from the same institution (SFRH / BD / 41762 / 2007).

# CHAPTER 3

# COSMOS Video Monitoring System

# CHAPTER 3 - COSMOS VIDEO MONITORING SYSTEM

**This chapter is based on a manuscript published in Computers and Geosciences:**

Rui Taborda and Ana Nobre Silva, 2012. "*COSMOS: a lightweight coastal video monitoring system*". Computers & Geosciences, Volume 49, pages 248-255. DOI: 10.1016/j.cageo.2012.07.013 EID: 2-s2.0-84866791641

## 3.1. ABSTRACT

The use of video systems for coastal monitoring purposes experienced a huge development over the last years. The main aim of this work is to present a new lightweight video monitoring system (COSMOS) that has been developed to target several key characteristics including portability, low-cost, robustness and easy installation. These characteristics were accomplished through the use of standard IP surveillance cameras and in-house developed software to correct the relative large distortion induced by the use of cameras with non-metric lens.

This monitoring system has already been successfully tested in several coastal and estuarine sites with different objectives, illustrating its versatility and wide range of applicability. Research efforts are being made so that these systems can provide reliable real-time beach state indicators turning them into a key element in what concerns coastal hazard warning systems.

## 3.2. INTRODUCTION

One key element for integrated coastal zone management is a correct understanding of the coastal zone evolution. However, the permanent evaluation of morphological changes of a coast is a non-trivial task, due to the complex and intrinsically non-steady nature of the processes.

Terrestrial photogrammetric techniques have been applied to the study of coastal processes since the middle of the twentieth century. In the eighties, video systems emerged as a promising monitoring technique and, since then, started to be used as a standard tool for the study of coastal changes as they can provide synoptic datasets with high spatial and temporal resolution.

The application of video systems to the study of the coastal zone was initiated at the Coastal Imaging Laboratory of Oregon University in the eighties, and in 1992 a pioneering automated unmanned system called Argus was installed at Agate Beach (Holman et al.,

1993; Holman and Stanley, 2007). Since then, the Argus system was continuously improved and its applicability has been greatly extended through the capability of hydrodynamic forcing quantification which allows the system to be regarded not only as a surveying tool but also to be in the center of a processes based approach to understand coastal evolution.

Following the development of Argus, several similar coastal monitoring video systems have emerged, as the EVS (http://www. svm.it), the Kosta (http://kostasystem.com), the Horus (http:// www.horusvideo.com), the Beachkeeper (Dessy et al., 2008) and the SIRENA (http://medea.uib-csic.es/tmoos/sirena/). A recent comprehensive comparison of four video monitoring systems can be found in Archetti et al. (2008).

In 2007, the analysis of existing operational video monitoring systems suggested that their applicability and use by management organizations and the scientific community was not limited by their potential, which is unquestionably high as demonstrated, for example, by Davidson et al. (2007), but, essentially, by operational and financial constraints. In fact, system installation depended on the availability of adequate infrastructures (e.g., housing, electric power) and despite their high benefit–cost ratio (especially considering the wide range of tools offered) system hardware and software related costs were not insignificant.

From this background, it was decided to develop a new lightweight video monitoring system that would complement existing ones, specifically targeting simplicity. The objective of this work is twofold: (a) to describe the first operational version of the COaStal video MOnitoring System (COSMOS) and related software tools and (b) to discuss its range of applicability.

## 3.3. SYSTEM DESCRIPTION

COSMOS has been developed at the Lisbon University since 2007. System development aimed at several key characteristics including portability, low-cost, robustness and easy installation. To meet these objectives the following development strategy was applied:

- Detach the acquisition and image processing tasks so that the system can be camera independent. This makes it possible to use any type of camera (webcam, video-camera or still-camera), does not impose any constrains on camera optics or image resolution, allowing portability and easing installation costs.
- Decouple the post-processing tasks in two major phases: geometric correction (lens correction and rectification) and image processing and feature extraction (e.g., production time average and variance images or perform automatic shoreline

detection). This procedure encourages the use of existing commercial programs to make image analysis tasks with the advantage of reducing programming effort.

- Give special attention to the lens distortion procedure as the use of low-cost non-metric cameras could have a large influence on the results accuracy. This precludes the use of bundle approaches to compute internal and external camera parameters and requires careful camera calibration before field deployment.
- Develop a simple and friendly user interface that enables system use by non IT specialists.

The developed video system is composed of three major modules (Figure 3.1): image acquisition, geometric correction and image processing and feature extraction.

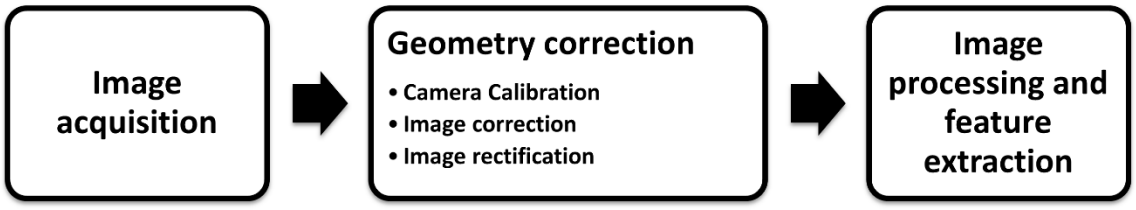


**Figure 3.1 - Main modules of the coastal video monitoring system (COSMOS).**

### *3.3.1. IMAGE ACQUISITION*

Image acquisition should be performed in locations with a good overview over the target beach, generally at a high place. In most cases, as in the selected areas, there are no infrastructures, the access to the power supply is difficult and, normally, there are serious housing problems. In the present system, this difficulty was overcome taking the advantage of its portability characteristics, which were achieved through the autonomization of the image acquisition procedure (i.e., the acquisition device is computer independent; a computer is only needed for archiving or post-processing tasks). So far, this decentralized concept has been implement using standard photographic cameras and state-of- the-art autonomous IP video cameras. While the first option only enables the acquisition of still images (which can be used, for example, in long term studies in sites with low waves, e.g., migration of tidal inlets), the latter is sufficiently flexible so that results are similar to the ones obtained using standard PC centralized schemes, easing, at the same time, the setting up in a wide range of coastal environments and conditions. Due to logistics constrains, up

to now, images have been recorded at an on-site hard disk. Notwithstanding, the use of data transfer technologies to allow remote access to the data is also a good option in case of available Wi-Fi or Ethernet access.

### 3.3.2. GEOMETRY CORRECTION

The transformation of image coordinates into world coordinates involves three main steps: (i) camera calibration, where the internal camera parameters are determined in the laboratory; (ii) image correction, which aims to correct the relatively large image distortions induced by camera optics; (iii) image rectification to transform oblique images into vertically equivalent images (rectified images). In the COSMOS system these tasks were accomplished using the Rectify Extreme program, a tool developed in Windows using C# and MATLAB® (release 2010a) programming languages, freely available at system website (http://cosmos.fc.ul.pt). Rectify Extreme can be royalty-free deployed to computers that do not have MATLAB installed, as the software was developed using MATLAB Builder$^{TM}$ NE to create dot NET components that were used within the Microsoft Visual Studio environment. In this case, the installation of the MATLAB Compiler Runtime (MCR), an execution engine made up of the same shared MATLAB libraries, is required.

#### 3.3.2.1. CAMERA CALIBRATION AND IMAGE CORRECTION

Camera calibration consists in the computation of camera internal parameters (focal length, position of the principal point, pixel skew and distortion coefficients) and is usually performed by computer applications that establish the geometric relation between a calibration object and its projection in the camera CCD. A detailed review of some most used calibrating techniques can be found in Salvi et al. (2002). In the developed system, internal camera parameters are measured in laboratory using the open- source computer application Camera Calibration Toolbox for MATLAB® developed by Vision Caltech (2009), in which images of a calibration object are recorded in laboratory from several camera orientations and positions.

Image distortions induced by camera optics were corrected using developed MATLAB® subroutines based on Heikkila and Silvén (1997) distortion model that accounts both for tangential and radial distortion components (Equations 3.1 to 3.3). This model can be described in matricial form as:

$$\begin{bmatrix} x_p \\ y_p \\ 1 \end{bmatrix} = KK \begin{bmatrix} x_d(1) \\ x_d(2) \\ 1 \end{bmatrix} \quad \text{where} \quad KK = \begin{bmatrix} fcx & alpha0 \times fcx & ccx \\ 0 & fcy & ccy \\ 0 & 0 & 1 \end{bmatrix} \qquad \textbf{Equation 3.1}$$

where $x_p$ and $y_p$ represent the coordinates of a point in the distorted coordinate system (metric), fcx and fcy the focal length (in x and y directions, respectively), ccx and ccy the image center (principal point) and alpha0 the skew coefficient defining the angle between the x and y pixel axes. The xd vector corresponds to the normalized point with radial and tangential distortion numerically defined as:

$$x_d = \begin{bmatrix} x_d(1) \\ x_d(2) \end{bmatrix} = (1 + kc(1)r^2 + kc(2)r^4 + kc(5)r^6)x_n + dx \qquad \textbf{Equation 3.2}$$

where r is the radial distance to the image center of the point defined by the vector xn = [x; y], which contains the coordinates of non-distorted points. Finally dx corresponds to the distortion tangential vector:

$$dx = \begin{bmatrix} 2\mathrm{kc}(3)xy + kc(4)(r^2 + 2x^2) \\ kc(3)(r^2 + 2y^2) + 2\mathrm{kc}(4)xy \end{bmatrix} \qquad \textbf{Equation 3.3}$$

The tangential component, related to "decentering'' or imperfect centering of the lens components, is characterized by kc(3) and kc(4) elements of the kc distortion vector, while the radial component corresponds to the kc(1), kc(2) and kc(5) elements.

Using the internal camera parameters computed in the laboratory calibration phase (Figure 3.2), undistorted images are created using inverse mapping techniques. The image center of undistorted images can coincide with the principal point (default), the center of the original image or be based on user defined values. The image correction procedure is found to be of vital importance because the video system is built upon standard non-metric cameras. In fact, in the cameras used so far by COSMOS, distortion is dominated by the radial component, being dislocation errors at image outermost locations of the order of tens of pixels. After correction, image errors are always substantially lower than a pixel.

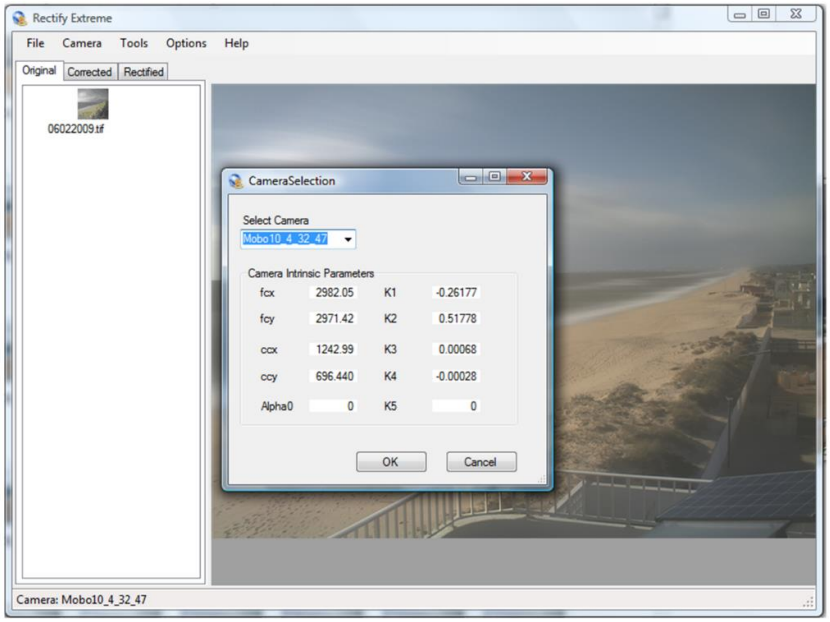


**Figure 3.2 - Rectify Extreme program window showing camera internal parameters (see definition in the text).**

### 3.3.2.2. IMAGE RECTIFICATION

Image rectification is the process that transforms an originally oblique image into a plan view equivalent image (rectified image), free from deformations induced by the camera obliquity.

The rectification procedure is supported on the collinearity conditions (Equations 3.4 and 3.5), which describe the physical model representing the geometry between the projection center, the image coordinates (xa, ya) and the ground coordinates (XA, YA, ZA). These equations can be easily solved from the knowledge of camera internal and external parameters, i.e., principal point and focal distance computed in the calibration procedure, camera position (XL, YL, ZL) and orientation.

$$x_a = ccx - f\left[\frac{m_{11}(X_A - X_L) + m_{12}(Y_A - Y_L) + m_{13}(Z_A - Z_L)}{m_{31}(X_A - X_L) + m_{32}(Y_A - Y_L) + m_{33}(Z_A - Z_L)}\right] \quad \textbf{Equation 3.4}$$

$$Y_a = ccy - f\left[\frac{m_{21}(X_A - X_L) + m_{22}(Y_A - Y_L) + m_{23}(Z_A - Z_L)}{m_{31}(X_A - X_L) + m_{32}(Y_A - Y_L) + m_{33}(Z_A - Z_L)}\right] \quad \textbf{Equation 3.5}$$

where $m_{nm}$ correspond to the parameters of the orientation matrices (Wolf and Dewitt, 2000).

Concerning external orientation (extrinsic parameters) a least squares solution is achieved using the classical non-linear space resection based on collinearity equations, given known 3-D control points (Figure 3.3A). External camera parameters inverse mapping techniques are used to create rectified images from undistorted images (corrected images). The use of such a method requires a definition of the output space, which, in COSMOS, is defined by the user (Figure 3.3B). In this process, regularly spaced pixels in the output image plane are projected into the input image plane and their values interpolated from the surrounding input image data. As in the resampling procedure a projected point does not coincide with the input image, spectral data is interpolated using the following methods: (1) bicubic interpolation computed from sixteen surrounding pixels; (2) bilinear function applied to the surrounding four points; (3) nearest neighbour (Figure 3.3B).

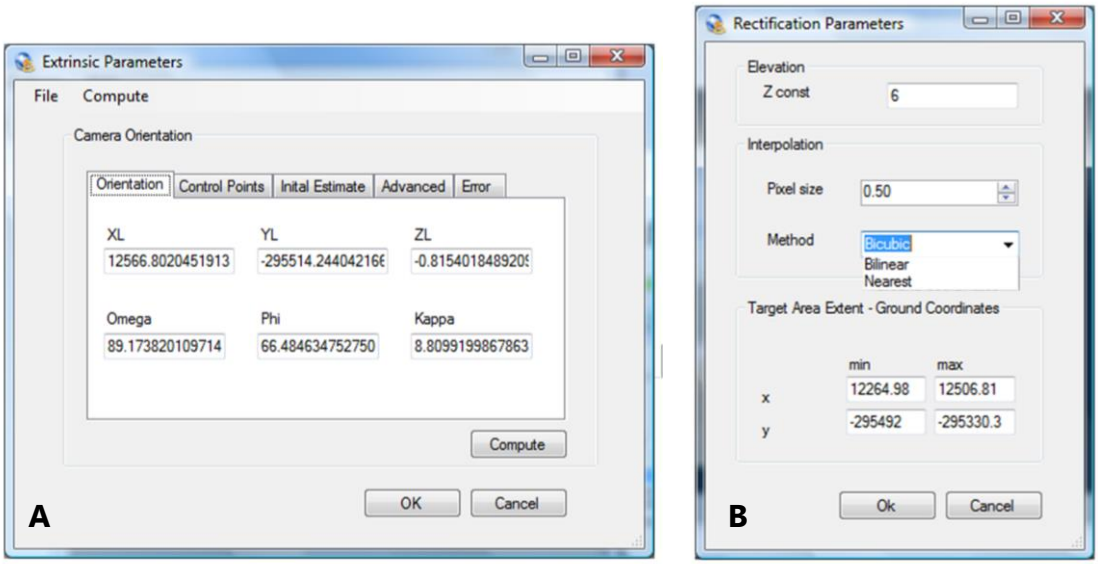


**Figure 3.3 - Rectification related dialog boxes: (A) computation of external orientation and (B) rectification options, the default initial estimates correspond to the extent of the GCP used in the rectification procedure**.

### *3.3.3. IMAGE PROCESSING AND FEATURE EXTRACTION*

At the present stage of the video-monitoring system development, specific routines concerning image processing are limited to the computation of time average (TIMEX) and

variance images (Holland et al., 1997). These procedures have been implemented in a tool named COSMOS IPT (image pre-processing routines).

After the completion of the rectification processes, the application automatically writes a Tiff World File (a six-parameter plain text file used in the affine transformation from image coordinates into map coordinates), so the rectified georeferenced images can be directly imported by standard GIS applications (either commercial or open-source). Therefore, other procedures, such as shoreline detection and computation of intertidal beach topography, can benefit from all GIS capabilities. An example of automatic coastline extraction over a TIMEX image, using the maximum likelihood method in commercial software application ESRI/ArcGIS®, is displayed in Figure 3.4.

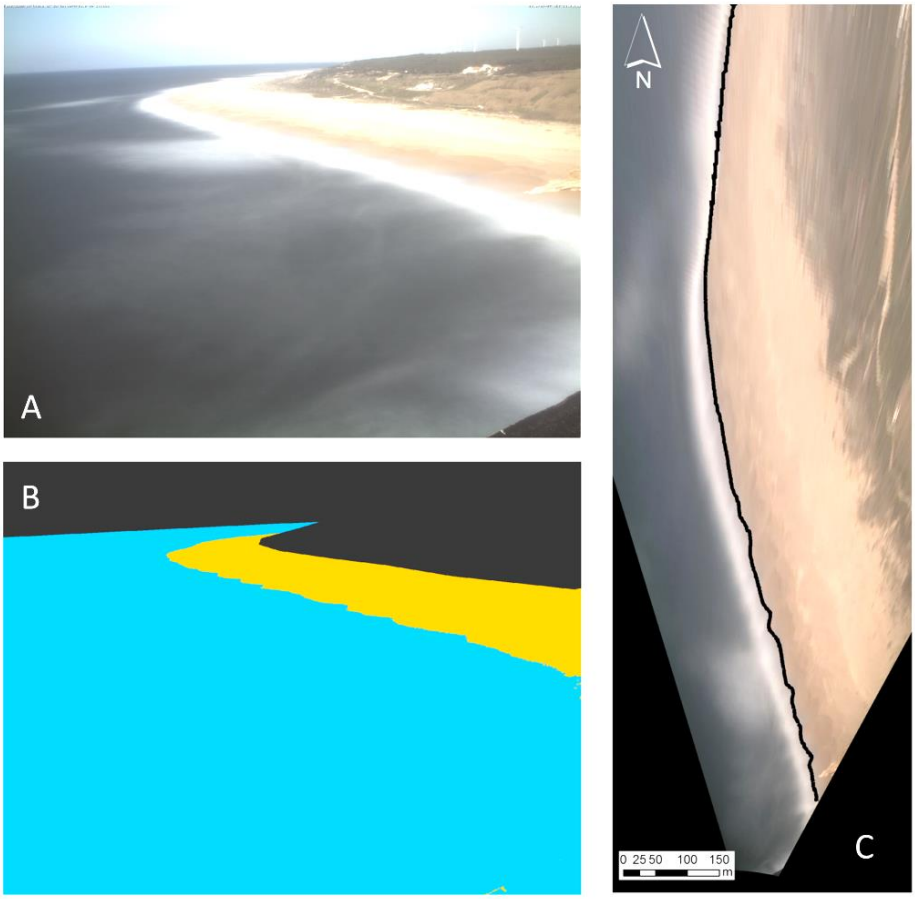


**Figure 3.4 - Example of coastline extraction using maximum likelihood classification: (A) original image; (B) classified image and (C) extracted coastline over a rectified image.**

### 3.3.4. SYSTEM APPLICATION

Due to the unprecedented flexibility and portability, COSMOS monitoring system has already been successfully tested in a considerable range of European coastal environments (Figure 3.5 and Figure 3.6). Monitoring objectives have been quite diverse and include: recording coastline variability, extraction of the intertidal digital terrain model (DTM) at fetch limited beach (Silva et al., 2009 - *Chapter 2 – Video Monitoring)*, study of inlet channel migration at a coastal lagoon, computation of salt marsh intertidal topography, evaluation of wave dissipation patterns, monitoring beach nourishment evolution and evaluation of wave induced morphological impacts (Table 3.1). The latter application, performed in the scope of the EU project MICORE (Morphological Impacts and COastal Risks Induced by Extreme Storm Events), are related to the record of morphologic evolution and identification of features generated by wave storms (dune breaches, overwash fans, erosional scarps, etc) as well as socio economic impacts.


**Figure 3.5 - Examples of system setup: (A) Alfeite; (B) Albufeira; (C) Dziwnow; (D) Aljezur and (E) Nazaré. See Table 3.1 and Figure 3.6 for details.**

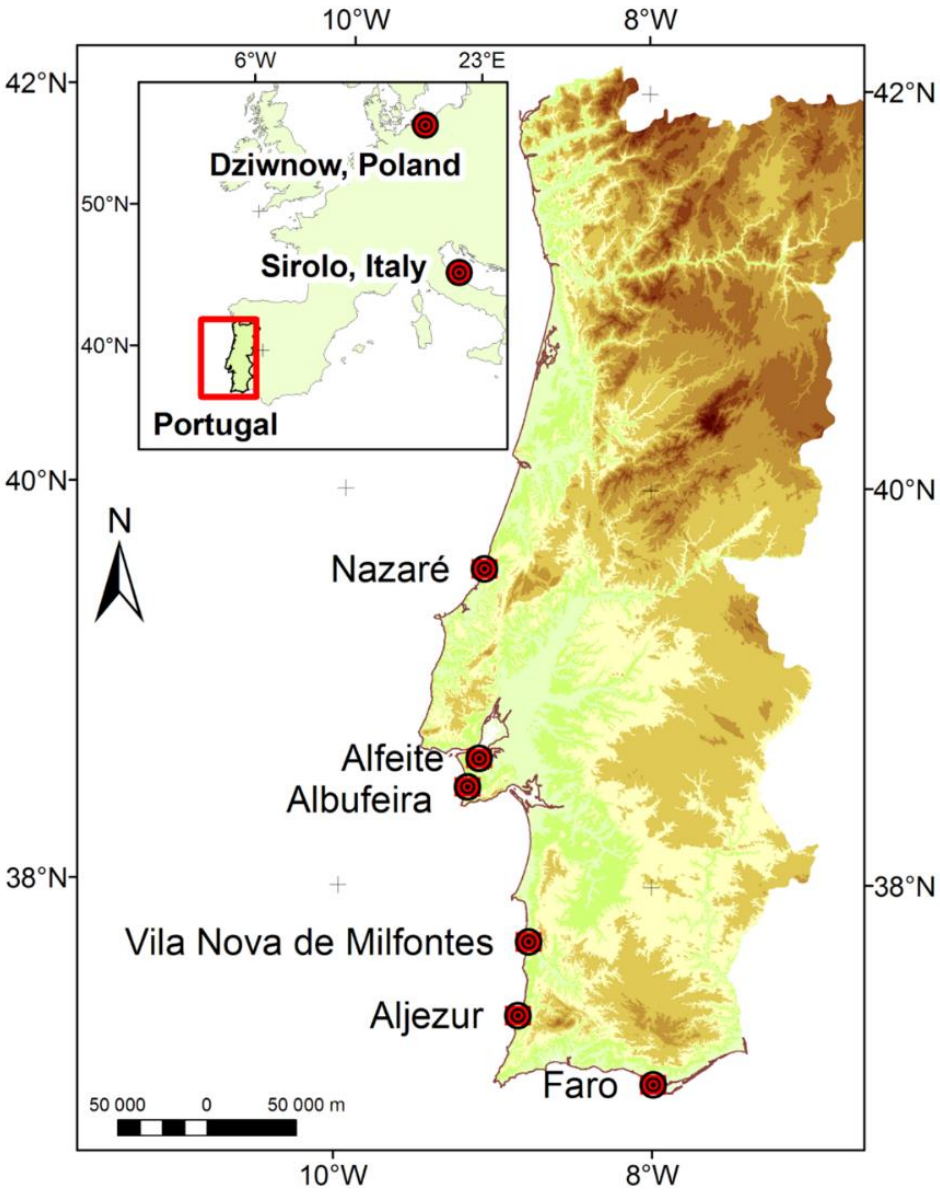


**Figure 3.6 - Sites where COSMOS system has been successfully employed.**

**Table 3.1 - Summary of COSMOS study sites.**

| | | | | | | | |
|---|---|---|---|---|---|---|---|
| ***Site*** | | | | | | | |
| *Country* | Portugal | Portugal | Portugal | Portugal | Poland | Italy | Portugal |
| *Beach* | Aljezur | Alfeite | Nazaré | Albufeira | Dziwnow | Sirolo | Milfontes |
| ***Main objective*** | | | | | | | |
| | Wave breaking and dissipation patterns | Intertidal topography | Coastline evolution | Inlet migration | Storm induced morphological changes | Beach nourishment evolution | Intertidal topography |
| ***Acquisition*** | | | | | | | |
| *Deployment timescale* | Days | Days | Months to years | Days | Months to years | Months to years | Days |
| *Camera type* | IP Video - MOBOTIX | IP Video - MOBOTIX | IP Video - MOBOTIX | IP Video - MOBOTIX | IP Video - MOBOTIX | IP Video - MOBOTIX | IP Video - MOBOTIX |
| *Camera installation* | Top of cliff | Top of electric pole | Lighthouse | Top of dune | Beach tower | Electric pole | Top of cliff |
| *Access to electric power* | No | No | Yes | No | Yes | Yes | No |
| *On site computer* | Yes / Laptop | Yes / Laptop | Yes / Desktop | Yes / Laptop | Yes / Desktop | No | Yes / Laptop |

An example of system results are shown with the study site of Norte beach (Nazaré). At this site, a MOBOTIX camera with fixed lens and 3.1 megapixel resolution (2048 × 1536) was installed at the Nazaré lighthouse facility, located approximately 50 m above mean sea level. Prior to installation, the camera was carefully calibrated in the laboratory using the procedure described in Section 3.3.2.1. As suggested by Sun and Cooperstock (2002), the sixth order term (kc(5)) was not included in the radial distortion model as it can degrade calibration performance. Results from the calibration procedure (which is camera specific) show that the lens deformation was dominated by the radial component, with dislocation errors larger than 50 pixels at the outer edge of the original image (the error related with the tangential component were always lower than 1 pixel). After calibration, computed standard error was reduced to approximately 0.15 pixels. This result shows the importance of modelling lens distortion, especially in case of low cost, non-metric, cameras

Camera external orientation was estimated using six ground control points (GCPs); the relation between undistorted image coordinates and ground coordinates was performed manually in the *Georref* tool, a component of the Rectify Extreme software (Figure 3.7).

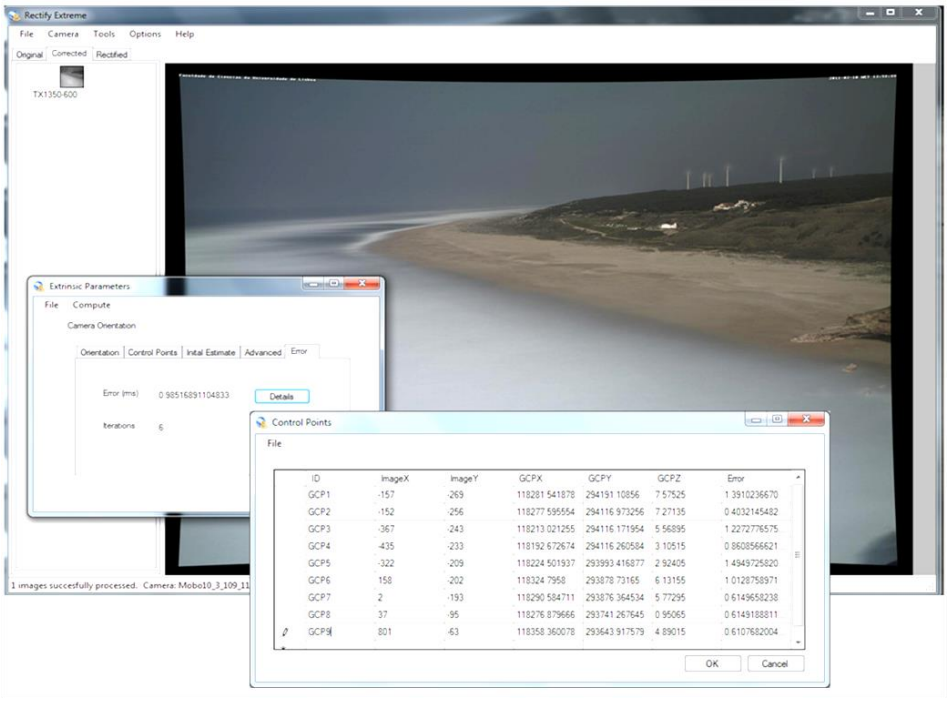


**Figure 3.7 - Examples of error computation in camera orientation: imageX, imageY undistorted image coordinates; GCPX, GCPY, GCPZ – ground control point coordinates.**

Pixel footprint, which represent the dimension of each pixel in the geographic space, shows the typical contrast between alongshore and cross-shore components (Figure 3.8).

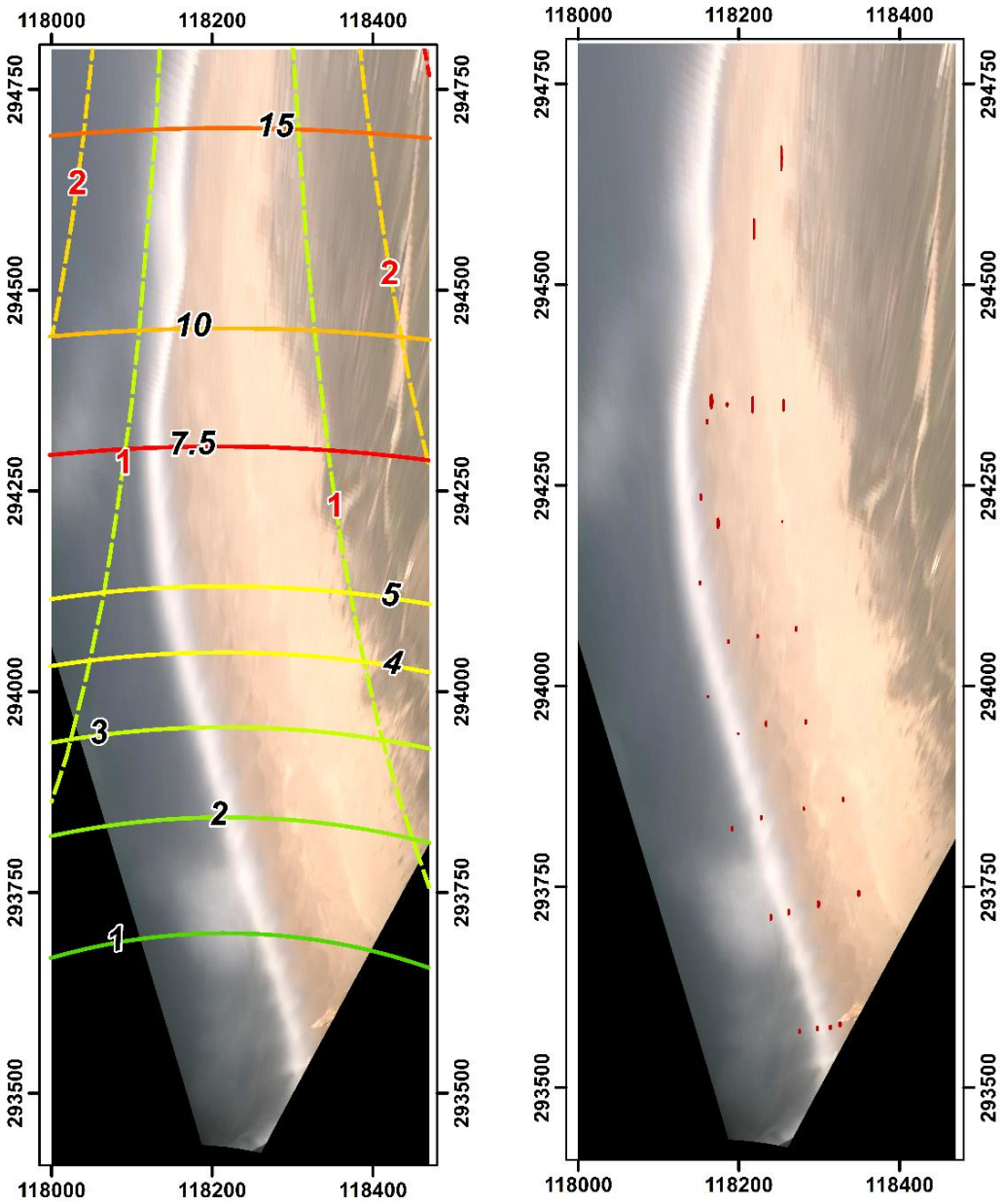


**Figure 3.8 - Pixel footprint (m) across Norte beach (Nazaré) study site. Solid lines: longshore component; dashed lines – cross-shore component. B) Longshore and cross-shore location error ellipses across the study site. Grid coordinates: ETRS89 PT-TM06 (EPSG: 3763).**

The alongshore footprint is more sensitive to the distance from the camera and range from a few decimetres to more than 10 m when the distance exceeds 1 km; on the other hand, the cross-shore component is generally lower than 2 m throughout the target area. As pixel footprint conditions the accuracy of the extracted beach features, it is expected that the positional accuracy will decrease when the distance from the camera increases. Nevertheless, and despite pixel footprint relevance, system accuracy also depends on the several other parameters such as camera optics, the image rectification software (the algorithm used and how it is implemented) and stability of the camera orientation over time. For that reason, to evaluate overall COSMOS positional accuracy, differences in the position of a set of 30 GCPs (acquire one year after camera orientation and not used to solve the geometry) were computed. Results, displayed in Figure 3.8 and Figure 3.9, show significant differences between cross-shore and longshore positional accuracy, with a root mean square error (rmse) of 1.18 m and 9.93 m, respectively.

As expected, the error is closely related with pixel footprint, with the longshore accuracy exhibiting a strong dependence with camera distance; while errors are generally lower than 10 m within a 1 km range of the camera, they reach up to 30 m at a distance of 1.3 km (Figure 3.9). The difference between the cross-shore and longshore components in the positional accuracy has strong implications when considering the extraction of coastal features as most of them are generally longitudinal (such has the coastline - water/land interface - or swash line - wet/dry interface) and therefore the error is dominated by the (lower) cross-shore component.

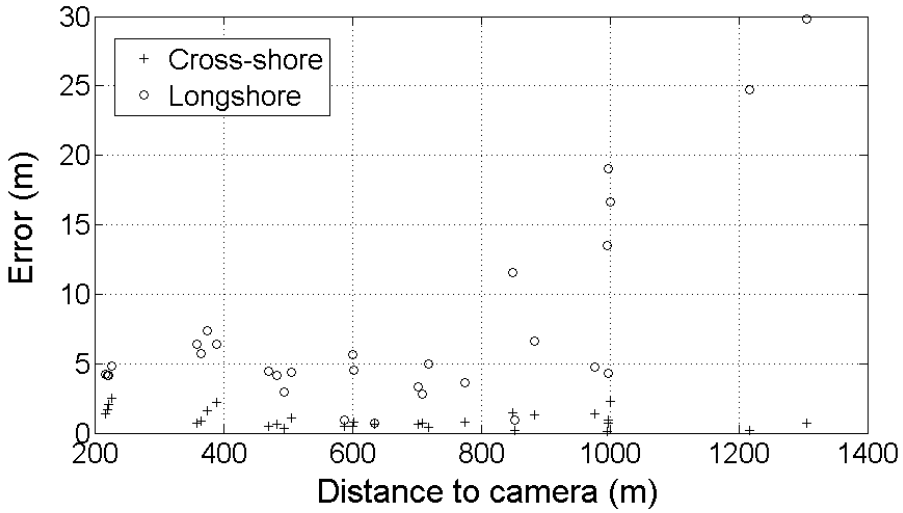


**Figure 3.9 - Variation of the cross-shore and longshore location error with distance from the camera.**

The positional accuracy of the extracted features can be illustrated in a practical example. For instance, when comparing the swash line position extracted from the rectified image (considering an adequate elevation, see for example Plant and Holman, 1997) and surveyed by a RTK-GPS the rmse of the swash line position was 1.4 m, which is in-line with the observed cross-shore rmse. When the system is used in the extraction of intertidal topography, the vertical error is further reduced as typical beach face slope is generally 0.1 or lower, translating in the reduction of the error by an order of magnitude. For example, using this system to extract a DTM of the intertidal beach at Alfeite, Silva et al. (2009 - Chapter 2 – Video Monitoring) found an overall vertical root mean squared error (VRMSE) of 0.08 m with a maximum of 0.15 m at 390 m of the camera. Using Argus system, Aarninkhof et al. (2003) obtained errors lower than 0.15 m along 85% of the 2 km beach studied; Plant and Holman (1997) reported 0.24 m VRMSE, latter corrected to 0.06 m when empirical corrections of water level were made and Vousdoukas et al. (2011), using an automated video system with two MOBOTIX cameras, found an VRMSE of 0.22 m for a five-month period of fully automation operation. These results are very encouraging in what concerns COSMOS application in the long-term monitoring of beach systems since the vertical precision obtained is similar to other systems and comparable to standard surveys methods.

## 3.4. DISCUSSION

This work presents a new coastal video monitoring system targeting portability, low-cost, robustness and easy installation. In order to meet these objectives, system development strategy followed the principles specified in the system description section and has greatly benefited from the use of autonomous IP video cameras and the development of the software tools described above.

For coastal monitoring purposes, the main advantage related to the use of this kind of IP camera is that all the acquisition procedure is controlled by the video camera thus dispensing the use of other acquisition software/hardware or even a computer. However, this advantage can also be regarded as its main weakness, as camera built-in software is generally not as flexible as specifically developed software. In fact, this feature can impose limits on acquisition rate (for example, in the used MOBOTIX cameras the acquisition rate of still images is limited to 1 Hz) and difficulties in precise camera synchronization can constrain system applicability especially for stereo-reconstitution techniques. Nevertheless, using this kind of system, image acquisition can be performed using only a camera and a standard portable computer or even with no computer at all, when recording is made on camera's internal storage devices (MicroSD card) or directly on a USB disk. If

the system is supported by a MOBOTIX camera or similar, portability is further enhanced by the low power consumption of the cameras (as they do not require heating/cooling even for a temperature range from -30° to + 60°) so that power can be supplied using standard PoE (Power over Ethernet) technology, which also simplifies installation process. The fact that the system depends on only a camera (with built-in cable protection and no mechanical moving parts) guarantees its robustness and the ability to operate under adverse atmospheric conditions without any specific waterproof housing. All these features make the system extremely portable as installation processes is limited to camera fixing at an appropriate location and connecting the Ethernet cable to the power supply (in case of short term deployments usually a battery) and a computer; for most cases this procedure only takes a few minutes.

Software is another key component of the system. In COSMOS software development targeted two main technical objectives: (1) correct the large image distortion induced by the use of non- metric cameras and (2) develop a user interface that enables system use by non IT specialists, while maintaining system costs as low as possible. In case of IP cameras, since image acquisition software is supplied within the camera and there are several open-source alternatives to perform camera calibration, software development was restricted to image correction and rectification (in the *Rectify Extreme* tool). As this software is freely available at COSMOS internet page (cosmos.fc.ul.pt), system cost is only linked with camera acquisition, computer and storage (which can start from less than 1k €); this approach assures that COSMOS is indeed a low-cost system.

The simplicity of COSMOS architecture adds for portability, low-cost, robustness and easy installation but at the same time, when compared to other systems, it constrains performance as, at the present stage of development, it delivers no image processing tools (with the exception of COSMOS IPT module that computes TIMEX and variance images) and has some limitations in relation to image acquisition (as previously discussed). In fact, considering a system classification where portability and low-cost are on one end and performance on the other, COSMOS will be on positioned at the former end while Argus system will be classified at the later, with all other video monitoring systems at different inter- mediate positions.

The number and diversity of COSMOS applications so far (Figure 3.6, Figure 3.5 and Table 3.1), clearly demonstrates system usefulness, especially considering that is a quite recent development.

Future system developments include the integration of routines for estimating beach state (e.g., van Dongeren et al., 2009) and the design a communication infrastructure that will

enable to use COSMOS in a real time coastal hazard warning system. This task will be eased by the use of standard IP surveillance cameras, a domain where most of communication operational constrains have already been sorted out.

## 3.5. CONCLUSIONS

This paper describes a new coastal video monitoring system (COSMOS) that has been developed since 2007. This system aims to complement existing ones specifically targeting portability, flexibility and low-cost. COSMOS has reached its operational stage and has already been successfully applied to monitor a reasonable range of coastal environments across Europe. Future progress includes the development of a reliable communication structure so that this system can be used to set up real-time warning systems in relation to coastal hazards.

## 3.6. ACKNOWLEDGMENTS

This work is a contribution to the European project MICORE— Morphological Impacts and Coastal Risks induced by Extreme storm events (Grant agreement no.: 202798), Fundação para a Ciência e Tecnologia (FCT) project B2C — Beach to Canyon Head Sedimentary Processes (PTDC/MAR/114674/2009) and Red CYTED TANGO (Teledetección Aplicada ala Prevención de Riesgos Geológicos Costeros). Ana Silva was supported by a PhD grant (SFRH/ BD/ 41762/2007) of FCT. This work has benefit from the constructive comments of two anonymous reviewers and fruitful discussions with João Catalão and Mafalda Carapuço.

## 3.7. APPENDIX A. SUPPORTING INFORMATION

Supplementary data associated with this article can be found in the online version at http://dx.doi.org/10.1016/j.cageo.2012.07. 013.

# CHAPTER 4

# Hydrodynamic and Morphodynamic Modeling

# CHAPTER 4 – HYDRODYNAMIC AND MORPHODYNAMIC MODELING

**This chapter is based on a manuscript published in the Journal of Coastal Conservation:**

Ana Nobre Silva and Rui Taborda, 2012. "*Integration of beach hydrodynamic and morphodynamic modelling in a GIS environment*". Journal of Coastal Conservation, Volume 17, Issue 2, pages 201-210. DOI: 10.1007/s11852-012-0212-5 EID: 2-s2.0-84878115623

## 4.1. ABSTRACT

This work describes a Beach Morphodynamic Model tool (BeachMM) that integrates state of the art wave/morphological numerical models (SWAN and XBeach) within a standard GIS platform (ArcGIS), aiming to streamlining the process related with the beach morphodynamics modelling. The BeachMM tool interface was developed using Python scripting language, taking advantage of its object-oriented and cross platform capabilities as well as its flexibility and strong integration with ArcGIS. In this work, we discuss the merits of this approach through an application example, where the tool was applied to the morphodynamic modelling of an exposed beach located at the Portuguese western coast. This tool has proven its applicability as it greatly simplifies dataflow effort, reduces the human error and provides a dynamic visualization of the modelling results.

## 4.2. INTRODUCTION

Since the beginning of the 20$^{th}$ century the coastal zone has been subjected to an increasing human occupation which conflicts with its intrinsic dynamic behaviour. For that reason, coastal hazards are nowadays achieving more and more importance in coastal management policies that can only be handled by a wider understanding of the complex coastal processes. This, knowledge based, approach should rely upon predictive models (numerical and/or analytical) firmly supported by field observational data. Field data generally has a spatial context which nowadays is mostly managed in a geographical information system (GIS) environment, taking advantage of its capability to capture, store, manage, analyse and display all forms of data that has a geographic reference.

Predictive models present the opportunity to simulate and understand the physical processes that affect the littoral and give decision makers valuable quantitative information about a wide range of coastal state indicators. Nevertheless, the link between the GIS and the predictive models is not always a trivial task mostly because of the diverse data format

requirements, but also because of the models complexity and non-user friendly interfaces that difficult the modelling by non-IT (non-information technology) experts.

Considering that contemporary GIS applications often include tools to develop customizations that can extend the capabilities of the system, emerges the opportunity to link the GIS with even more powerful analytical modules (Crossman et al., 2007). The integration of the predictive models with a GIS system rises like a natural solution with vast operational advantages. A GIS coupled with an environmental model provides a tool to run a simulation and to interpret the results in a spatial context (Pullar and Springer 2000).

Considerable work has been reported in this matter with different levels of coupling or interoperability between the programs, for example the work of Pullar and Springer (2000) or Crossman et al. (2007) integrates external models/software's by calling them within the GIS code while, in contrast, Cheng et al. (2010) or Winterton and Livermore (2004) add the mathematic functions into the GIS system using the development environment VBA (Visual Basic for Applications). In the literature is reported a few different categorizations of methods for integrating models with GIS (Brandmeyer and Karimi 2000). In the work of Cheng et al. (2010) and Di Luzio et al. (2004) we can find the classification for these integration methods in three classes: "loose", "close" and "tight" coupling (initially proposed by Liao and Tim, 1997): 1) the loose coupling usually involve only data exchange between programs, the GIS is used to generate model input files (pre-processor) and display model output data (post-processor), in this case the interchange data files are both stored using a database (in GIS) and ASCII formats; 2) close coupling passes information between the GIS and the model via memory-resident data models rather than external files and 3) tight coupling where the model integration focuses on incorporating the functional components of one system within the other (i.e. the model within the GIS program) (Liao and Tim 1997). In this later kind of solutions, data flow GIS-model and the return of the results to GIS are accomplished by routines that are addressed directly by the interactive tools customized in the GIS environment (Di Luzio et al., 2004).

Regarding the specific field of coastal hydro-morphodynamic modelling this integration is generally either absent or supported by proprietary data management procedures. The latter solution is used in reference coastal modelling packages (e.g. SMS, Zundel 2000 and DELFT3D, Delft 2005) which have addressed this issue through the development of specific, non-standard, spatial data management interfaces. In these solutions all the geovisualizations, data input and output are handled within the same software. While this approach eases all data management processes, the use of non-standard GIS platforms reduces their potential in what concerns spatial data analyses and integration with other systems and significantly increases the software related costs.

Notwithstanding, in most cases integration is performed "loosely" as the available coastal modelling tools do not support any spatial data management module and each component (e.g. wave generation, wave propagation and sediment transport) is an independent variable that, generally, inputs/outputs data in specific non-standard formats. While this approach can be considered flexible, it also increases data management and exploitation effort as it imposes the development of specific data/model/GIS interfaces, deviating the effort from the physical problem.

The objective of the present work is the development of a tool that eases the hydrodynamic and morphodynamic modelling of a coastal stretch, trough "tightly" coupling of two of the most powerful coastal models within a GIS environment: the SWAN wave propagation model (Booij et al., 1999) and the XBeach morphodynamics model (Roelvink et al., 2007). This objective was accomplished through the development of a geoprocessing tool for ArcGIS (ArcMap 10.0) using the Python programming language (ESRI 2010; Python Software Foundation 2010). The developed tool aims to simplify the simulation procedure, automate the data flow between predictive models and GIS and graphically display the results with minimal user interaction.

ArcGIS software was chosen because of its proven skills in geospatial analyses like the raster surface modelling capability and for including scripting support for many of today's most popular scripting environments, such as Python, VBScript among others. Python scripting language is characterized to be object-oriented programming language, open-source, platform independent and most of all for having a clean syntax and simple, clear concepts that makes it easy to learn and use by non-programming experts. Developing Python-based geoprocessing tools for ArcGIS is easy: all tools share a common graphical user interface provided by ArcGIS, and developers must implement only the geospatial analysis tasks performed by the tool (Roberts et al., 2010), which in the present work, corresponds to the wave/morphological model run.

## 4.3. SWAN MODEL

The correct assessment of the wave behaviour along the shore is fundamental for a valid characterization and prediction of the coastal dynamics where wave predictive models, regardless of its complexity, provide an enormous contribution. In the present work it was decided to use the wave hydrodynamic model SWAN as it represents the state of art in the wave propagation model for nearshore waves.

The SWAN Model is a third-generation wave model for obtaining realistic estimates of wave parameters in coastal areas, lakes and estuaries from given wind, bottom and current

conditions. The SWAN model propagates the oceanic waves from deep water to the surf zone by solving the spectral action balance equation. This equation takes into account several physical processes and represents its effects on spatial wave propagation, refraction, shoaling, generation, dissipation and non-linear wave-wave interactions. The SWAN model is a freely available predictive model developed at Delft University of Technology that has been widely used by government authorities, research institutes and consultants worldwide (SWAN, 2009).

The model inputs include one, or more, spatial input grid(s): one (essential) bottom grid where the ocean floor is characterized, generally, by a rectangular grid; and others (optional) spatial grids as water level and/or the wind input. All physical processes, wave initial condition and additional (e.g. grid extent and cellsize) information is defined in a parameters file through some lines of code, followed by the request for outputs and its formats.

To increase the computational efficiency of the model, SWAN users commonly use nestage grids i.e. first the model computes the waves on a coarser grid for a larger region and then uses the simulation results along a finer grid boundary to re-run the model for the nested finer grid that represent a smaller region. Nesting can be repeated on over decreasing scales with the only condition to use the same type of coordinates in the coarser and nested computational grids. In these simulations the wave output is generally in form of density wave spectrum along the nested grid boundaries, and act as an input file for the following model run that simulates the waves along the nested/finer grid.

An essential request for the successful run of SWAN in nesting is the correct agreement of the grid characteristics (for example the origin, extend and cellsize) defined in the SWAN parameters file, simultaneously in the outputs of the regional grid and in the characterization of the nested grid. For instance, a small difference between both parameters can prevent the model to run. Hence, the programming of this kind of tasks, particularly in a GIS context, can be more productive as it saves time and removes the margin of error intrinsic to any manual process (Crossman et al., 2007).

## 4.4. XBEACH MODEL

The morphological variations that occur along the littoral are strongly connected with the forcing mechanisms that act on the shore. In fact, the wave action is the foremost factor that contributes for the coastal morphodynamics.

The XBeach is a, recently developed freely available, numerical model for nearshore processes intended as a tool to compute the natural coastal response during time-varying storm and hurricane conditions, including dune erosion, overwashes and breaching (Roelvink et al., 2010). A more comprehensive description of the model is given by Roelvink et al. (2009).

The XBeach model was chosen for its proven prediction skills in wide morphologic contexts, for instance, good results have been accomplished in the prediction of the coastal profiles (Van Dongeren et al., 2009), in simulating runup and inundation overwash over longshore-varying terrain (McCall et al., 2010). XBeach also have a good performance in different situations including dune erosion, overwash and breaching with specific emphasis on swash dynamics, avalanching and 2DH effects (Roelvink et al., 2009).

More recently, intensive testing and validation of the XBeach coastal erosion modelling was performed for various European coastal sites in the scope of the European project MICORE (www.micore.eu/). Model results at Italy, Portugal, Spain, France, UK, The Netherlands, Belgium, Poland and Bulgaria where validated through field data collection contributing to test the model under a wide range of environmental conditions (Deltares, 2011).

Minimal model requests are bathymetric information, in a grid format, and wave forcing. Similarly to SWAN model, the information regarding model inputs, physical parameters and outputs is defined in a text file, which is accessed when the model XBeach executable is employed.

For a simple simulation with stationary waves the wave parameters (wave height, wave period and wave direction) can be entered directly in the parameters text file. Nevertheless, more advanced options are possible, namely the definition of time/space varying wave boundary conditions. The XBeach model also allows, as input, the definition of density wave spectrums which represents the statistical wave parameters variation in time. SWAN spectrum results can be directly introduced in the XBeach model which converts the input spectral data into boundary condition time series. In this mode, XBeach uses the boundary condition until the simulation is complete.

As expected, for an error free data exchange between models, a perfect match between the configurations of the input/output grids is required, as well as a compatible parameter definition. This requirement can be easily accomplished through the development of an integration tool that automates data and parameters transfer between models and GIS.

## 4.5. BEACHMM INTEGRATION TOOL

This section focus on the technical and methodological aspects related to the development and application of the Beach Morphodynamic Modelling tool (BeachMM tool), which integrates SWAN and XBeach modelling capabilities within the ArcGIS environment. This topic targets operational aspects of tool application and does not discuss either SWAN or XBeach physical background. It must be stressed that the use of BeachMM tool should be preceded by a careful validation phase in order to evaluate model adequacy and applicability to each particular coastal zone. It is only after successful model validation, that BeachMM can be used as operational tool, providing useful data to the understanding of coastal morphodynamics.

### 4.5.1. TOOL DEVELOPMENT

The developed tool, freely available at http://disepla.fc.ul.pt/Micore/Micore.html, is a Python-based geoprocesing script for the ArcGIS 10.0. Phyton scripting was chosen due to its strong integration within the ArcGIS environment, providing excellent facilities for interoperating all the geoprocessing functions available within ArcGIS and, at the same time, offering access to external modules and programs. The graphical user interface (GUI) customization of the BeachMM tool was built within ArcGIS 10.0 as it entirely provides all the necessary interfaces (text boxes, check boxes and list boxes).

The BeachMM Python tool implements four main tasks, namely: 1) conversion between different bathymetric raster formats; 2) automatic creation of model input parameter files according to user input and bathymetric grid properties; 3) save model output in ArcGIS compatible formats; and 4) call the external models to run within the ArcGIS. The processing time is constrained by the time required to run each model simulation, being the time expended in data exchange and configuration negligible.

The BeachMM tool architecture is illustrated in Figure 4.1. Modelling strategy follows a simple but effective scheme, where SWAN and XBEACH models are automatically fed with data and driven from a GUI that runs within ArcMap. The modelling process starts with the definition of bathymetric and oceanographic forcing; bathymetric data is prepared using standard raster creation procedures, and involves the design of SWAN and XBeach domains; offshore wave data is inputted directly on the interface, using either spectral or significative wave parameters.

The main loop starts with the creation of SWAN compatible bathymetric file (bottom grid.bot) and the command file (parameters file.txt, a file containing the instructions of the

user to SWAN), then the SWAN model is run and waves are propagated over the domain. The BeachMM tool user can repeat the SWAN wave propagation in nested domains (optional nesting loop), until the resolution is considered adequate for use in the morphological (XBeach) domain. In this case offshore boundary waves are characterized using a spectral file automatically created in the previous run (nestage.nst file). After this step, SWAN results are exported to a XBeach compatible format (swan results.txt) and the morphodynamic modelling phase is initiated. The XBeach is driven with parameters defined in the GUI (parameters files.txt) and over a domain defined by the file bottom grid.grd. After XBeach modelling completion, the tool converts the result of each selected output variable, at each time step, into an ArcGIS compatible raster file.

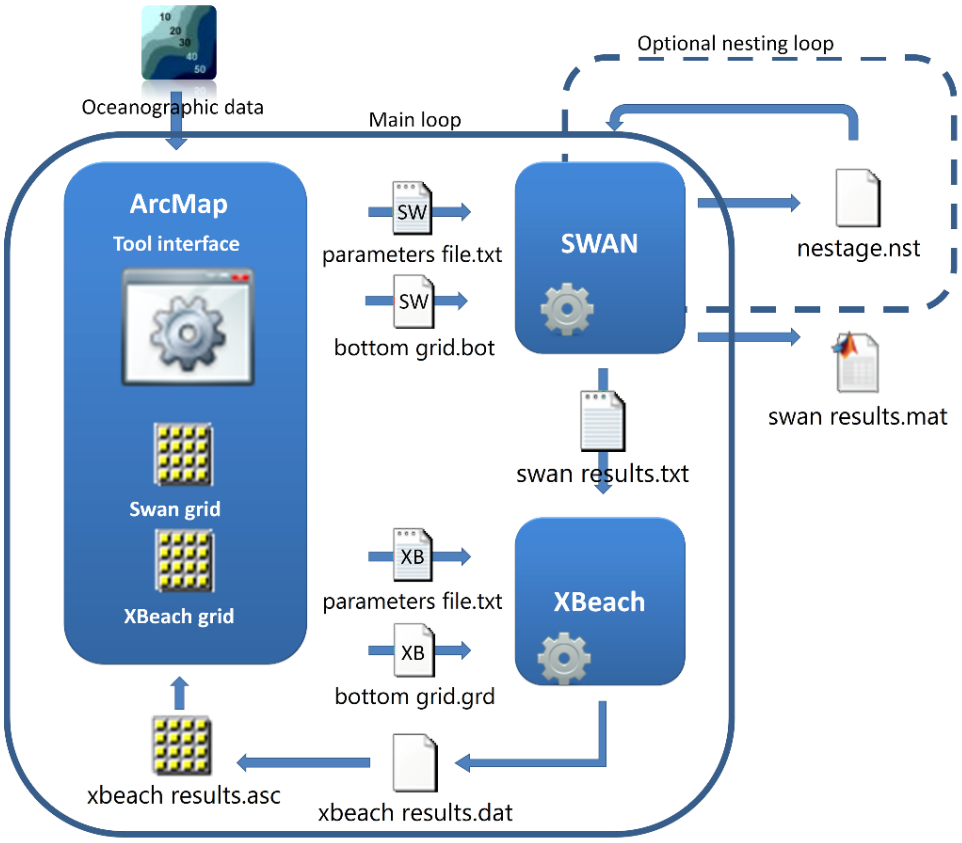


**Figure 4.1 - Schematics of the BeachMM tool architecture (arrows represent the data flux managed by the developed tool).**

The modular nature of the BeachMM tool, supported by independent components, presents a clear advantage in the sense that the tool can be considered to have longer live

cycle as it is version independent i.e. the actualizations of both SWAN and XBeach software do not, necessarily imply changes in BeachMM tool.

### 4.5.2. TOOL GRAPHICAL USER INTERFACE

The BeachMM run is supported by a GUI that defines model input and output parameters related with SWAN and XBeach models. For SWAN simulation (Figure 4.2a) the GUI considers the following parameters: 1) the path for the bathymetric Input SWAN Raster File; 2) the vertical reference of the SWAN raster, downward positive or negative; 3) the SWAN Model workspace path, where the parameters file template and the executable are stored; 4) the option for saving SWAN simulation results into a MATLAB file; 5) the Operation Mode: results can either be saved in a SWAN nesting file (SWAN Nestage) or in XBeach compatible format (default) (SWAN to XBEACH) ; 6) and, the path for the nested raster file (in case of an operation mode in nesting).

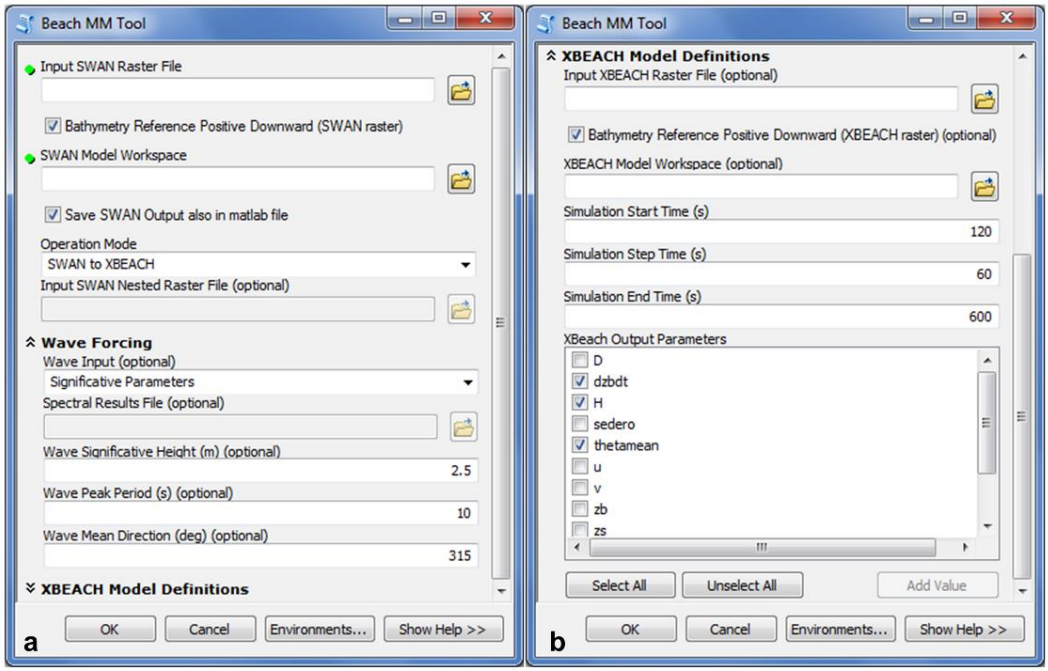


**Figure 4.2- BeachMM tool user interface in ArcGIS environment (a – Inputs for the SWAN simulation and wave forcing options; b – Inputs for XBeach definitions).**

A second block of information is related to the wave forcing (Figure 4.2a). Here, the user can choose between two boundary offshore wave options: the use of a single

representative wave, using significative parameters (default), or a spectral wave representation. If the first option is selected the user has to define the Wave Significative Height, Wave Peak Period and Wave Mean Direction while if the latter option is selected the user must define the path to a "Spectral Results File" specific for the boundaries of the SWAN raster .

Finally, in the third block of information, required only if the tool is run in SWAN to XBEACH operation mode, the user must define the XBeach Model Definitions. These definitions appear at the bottom of the interface (Figure 4.2a and Figure 4.2b) and include: 1) the path to the XBeach bathymetric raster file; 2) if the bathymetric information is downward positive or negative; 3) XBeach model workspace path, where the executable and template parameters file are stored; 4) the start, step and ending time of the XBeach simulation; and 5) morphodynamic variables to be modelled and saved.

Every input required by the BeachMM tool includes a small description only visible when the "Show help" (bottom right of Figure 4.2a and Figure 4.2b) of the ArcGIS tool interface is selected. This information is particularly relevant for the XBeach Output Parameters selection as it describes each parameter, including required input units.

## 4.6. EXAMPLE APPLICATION: MORPHODYNAMIC MODELLING AT NORTE BEACH

### 4.6.1. STUDY SITE

Norte beach is located in the west coast of Portugal, more precisely in the southward limit of the littoral cell that extends from Douro river mouth and the Nazaré Canyon head (Figure 4.3). This coastal stretch is exposed to the North Atlantic wave regime characterized by a predominant swell from the NW quadrant superimposed with a generally less energetic local wind sea with a wider directional spread. The nearshore wave propagation in this area is strongly disturbed by the presence of the Nazaré submarine canyon, which interrupts the net southward longshore sediment transport (Dias et al., 2002). It is one of the largest submarine canyons of the world, cuts the full width of the continental shelf and slope, with an approximate E-W orientation, and has been reported in the literature as the major active sediment conduit to the abyssal plain (Oliveira et al., 2007). The canyon head is located very near the shore and reaches 20 m depth in few meters distance of the beach.

These regional setting raises the difficulties for the morphodynamic characterization of the Norte beach, as is immediately located northward of the submarine canyon where the waves suffer intense refraction processes.

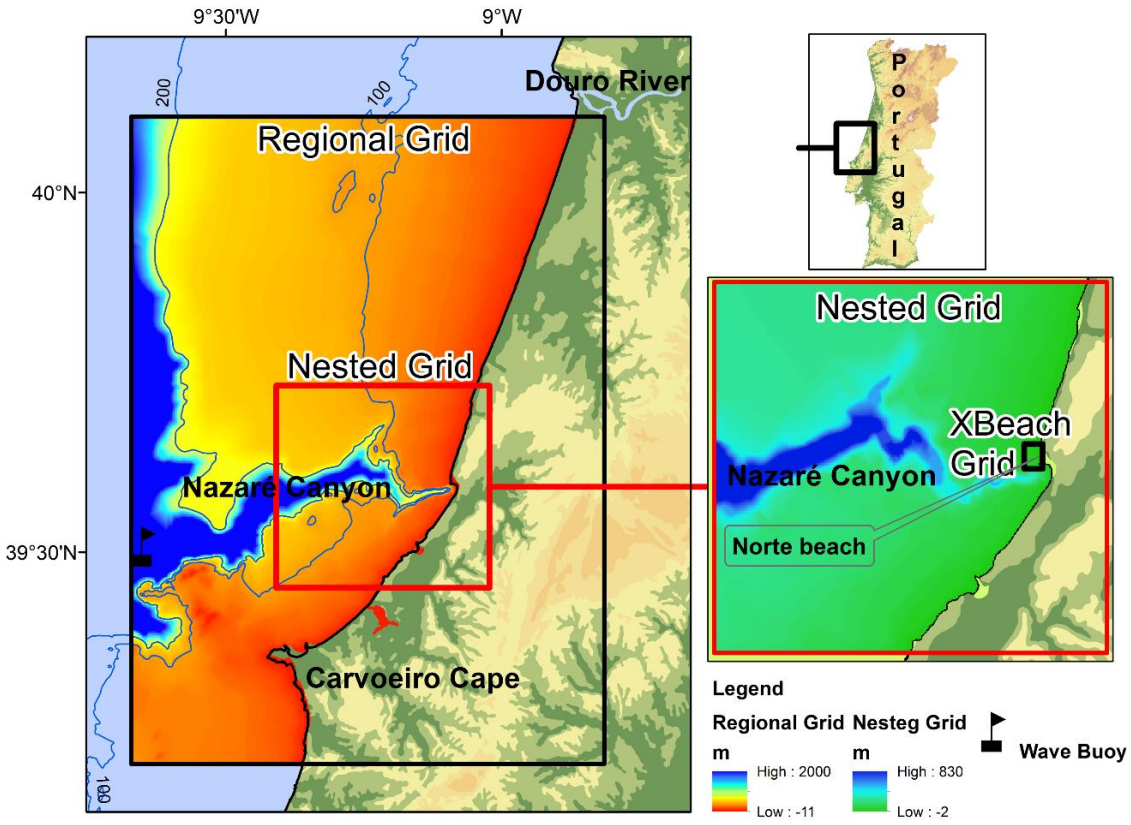


**Figure 4.3 - Norte beach location and spatial coverage of the bathymetric grids used in the morphodynamic modelling.**

## 4.6.2. METHODS

The morphodynamic modelling of Norte beach was performed, through the application of the BeachMM tool. Wave propagation modelling was performed over two domains, one regional coarser grid and one finer nestage grid, using the nesting loop option in the BeachMM tool. The regional grid extends roughly between Douro river mouth and a few km south of Carvoeiro cape, is 71 km × 100.2 km wide, with a cellsize of 200 m. The nestage grid covers the Nazaré canyon head and Norte beach nearshore with 30.1 km × 30.1 km and a cellsize of 100 m (Figure 4.3).

Model was driven with measured wave conditions at one point along the offshore regional grid boundary. Wave conditions represented the average conditions for the tree days prior to 23rd July 2011 (2.8 m significant height, 8.15 s peak period and a 350º of mean direction) as an unusual (roughly decadal recurrence) sediment accumulation had occurred around the Nazaré headland.

Using the spectral wave data generated by SWAN along the nestage described above, the BeachMM tool was again used, in this case with the SWAN to XBeach operation mode (main loop). Using this mode, the SWAN simulation was automatically followed by the XBeach simulation (Figure 4.4) over Norte beach area. SWAN raster file corresponds to the previous described Norte beach nestage grid. In this case, the wave input was defined as the density spectrum file obtained by the run in nestage wave grid. Regarding the XBeach model definitions, the input XBeach raster file is a grid that covers the Norte beach (Figure 4.3) with 1.51 km × 2.01 km wide and a cellsize of 10 m. In both cases, it was chosen to also store the results from the SWAN simulations in Matlab compatible format.

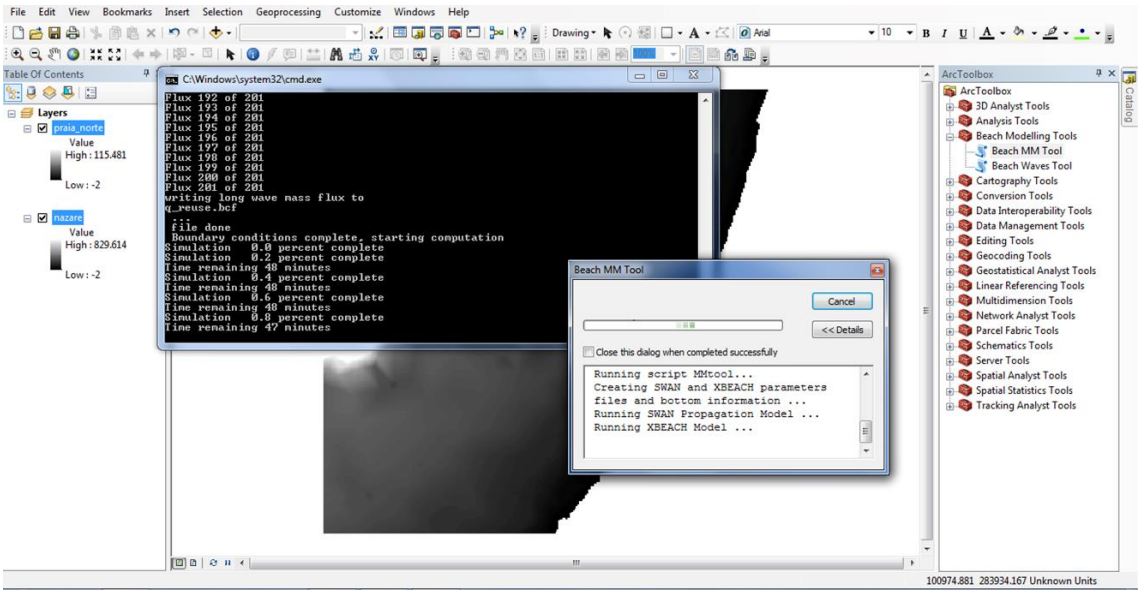


**Figure 4.4 - General aspect of the BeachMM tool in execution. The command window in second plan shows the XBeach simulation in progress.**

## 4.6.3. RESULTS

The results of the application of the BeachMM tool, at the study site, are represented in form of spatial variation of the hydrodynamic and the morphodynamic parameters requested (examples in Figure 4.5 to Figure 4.8). As described above, the tool enables not

only to display final model results but also to save intermediate results. This feature, allows the user to verify model results during all the modelling processes. For example, the analysis of the spatial distribution of the nearshore wave height in the two SWAN computational domains (Figure 4.5) shows the expected refraction pattern considering waves coming from NW.

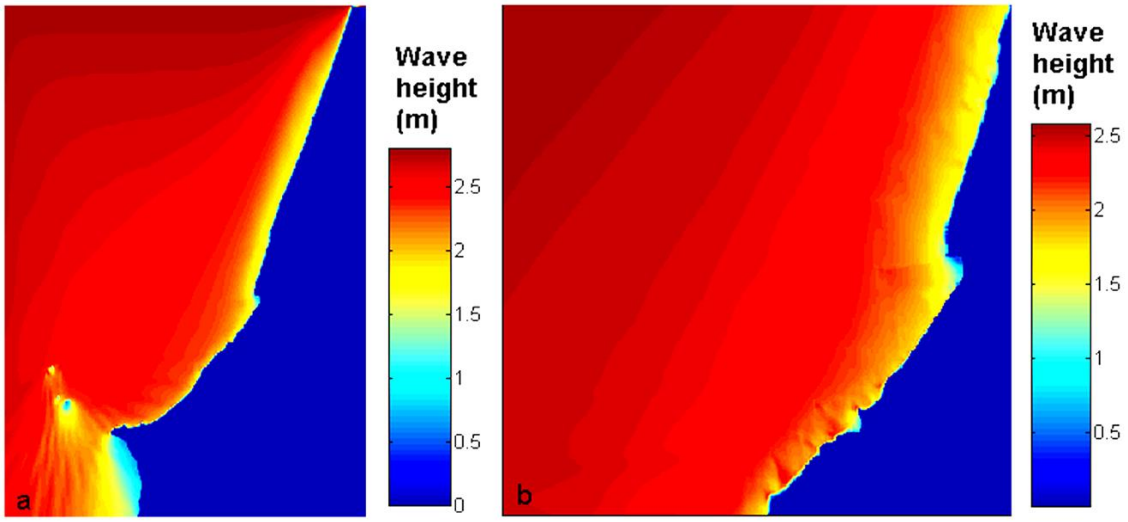


**Figure 4.5 - SWAN model wave height outputs example (a – results for the regional grid and b – results for the nestage grid).**

As an example of the XBeach results, the spatial variation of the wave energy dissipation is displayed in Figure 4.6. The dissipation pattern reveals the presence of a submarine sand bar roughly parallel to the coast which is located further offshore at the northern section of Norte beach. Model results (Figure 4.7a) match the observations performed by a video monitoring system (COSMOS) (Silva et al., 2009) located at Nazaré headland lighthouse (Figure 4.7b).

Modelled nearshore velocity pattern agrees with the uncommon development of a beach that surrounded the headland at that time, reaching Pedra do Guilhim (Figure 4.8). Results, show a southward sediment transport along the Norte beach; at Pedra do Guilhim the sediment transport pattern is W-E directed presenting the ideal conditions for a sediment accumulation around the headland.

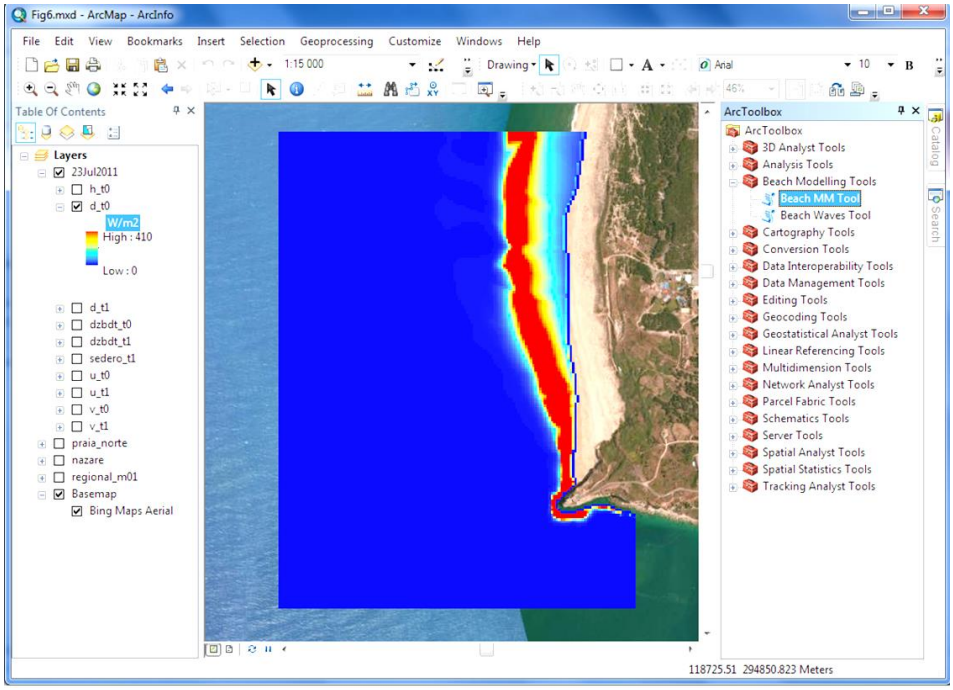


**Figure 4.6 - Modelled energy wave dissipation along the study area.**

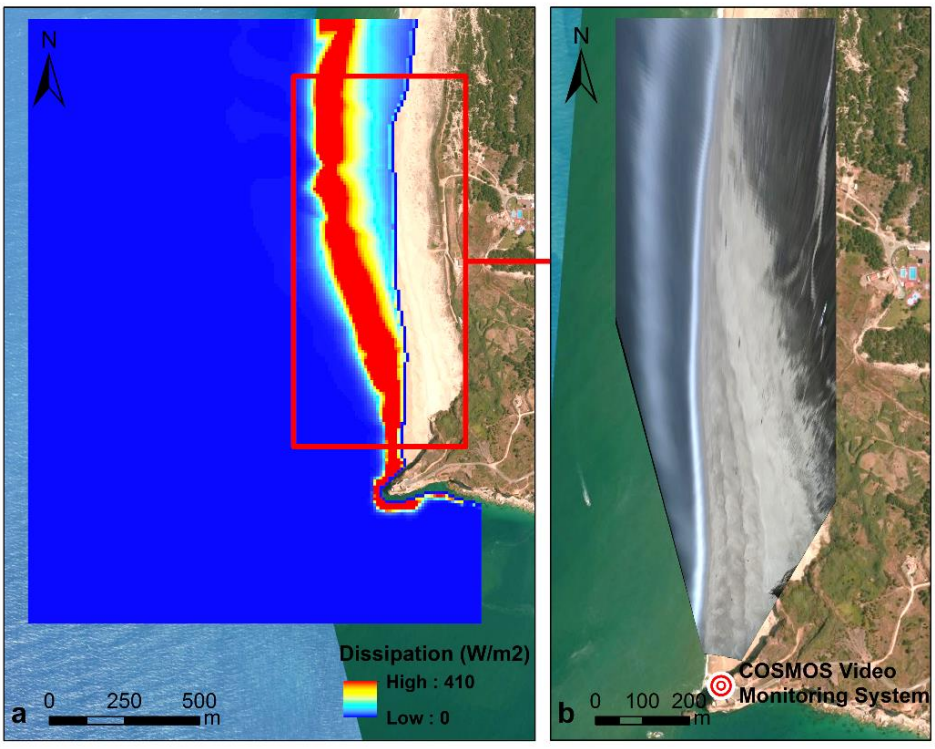


**Figure 4.7 - Dissipation modelled using the BeachMM tool (a) and rectified time averaged image (TIMEX) of the Norte Beach obtained from COSMOS monitoring system (b) showing the wave dissipation.**

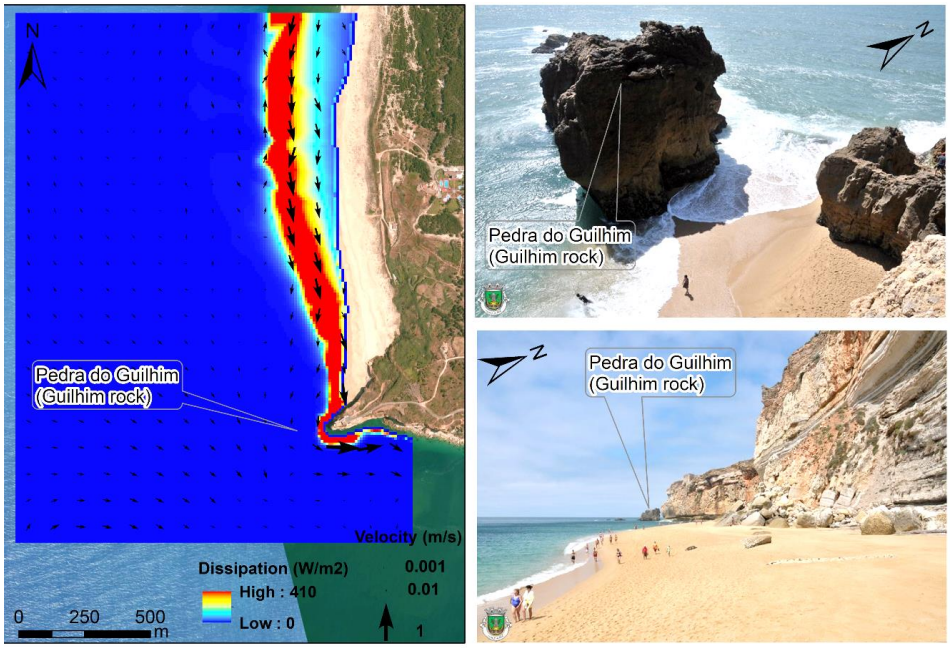


**Figure 4.8 - XBeach velocity pattern (left) and photographs showing the unusual beach formation around the Nazaré headland, reaching Pedra do Guilhim (Images obtained from Nazaré Municipality website).**

## 4.7. DISCUSSION

The integration of state of the art wave/morphological numerical models (SWAN and XBeach) within a standard GIS platform, proved to be a useful tool in beach morphodynamics modelling, as it eases some of the most time-consuming tasks in the modelling processes as it provides: i) seamless integration of geospatial data in the existing numerical models, ii) model chain automation, iii) powerful visualising and analysis tools for the exploitation of model results. The ability to integrate model results with georeferenced raster and vector data such as shoreline, remote sensing data and human occupation proved to be an important advantage of this approach.

The BeachMM tool, included in the ArcToolbox of ArcMap, provide to a regular ArcGIS user a recognizable tool as the requested input for the tool are comparable to any other ArcToolbox tool. This friendly use of the tool permits any ArcGIS user to be able to manage and operate the Beach Morphodynamic Modelling tool.

Nevertheless, this approach can have some drawbacks, which are related to the misuse of a powerful, yet complex, tool that must be careful verified before the exploitation of the results. The likelihood of model misused was reduced by including in the user interface

only the parameters needed for the operational use, being the calibration parameters included in a concealed file only handled by SWAN or XBeach experienced users.

## 4.8. CONCLUSIONS

The main objective of this work was to develop a user-friendly tool that simplifies the procedures related to morphological modelling of the coastal zone, using state of art numerical models (SWAN and XBeach). The development of this tool benefited from the data management tools available in ArcGIS and the flexibility of customization given by the Python scripting. Model integration was built upon a user friendly interface that efficiently automatize the data exchange between GIS and the models with minimum user action. This tight coupling permits to ease the modelling procedures and, at the same time, minimize the errors induced by the manual processes related to the meticulous models configurations.

The freely available BeachMM tool is believed to increase the potential of the morphodynamic modelling of the coastal zone as it automated functioning within ArcGIS reduces time and operational costs and allows the user to focus on the exploitation of modelling results.

## 4.9. ACKNOWLEDGMENTS

This paper is a contribution of Red Tango (Red Iberoamericana en Teledetección Aplicada a la Prevención de Riesgos Geológicos Litorales), the European project MICORE – Morphological Impacts and Coastal Risks induced by Extreme storm events (Grant agreement no.: 202798) and the Portuguese foundation for Science and Technology (FCT) project B2C - Beach to Canyon (PTDC/MAR/114674/2009). The first author is financially supported by the FCT through PhD grant (SFRH / BD / 41762 / 2007).

# CHAPTER 5

# Longshore Sand Transport Variability at the Northwest Coast of Portugal

# CHAPTER 5 – LONGSHORE SAND TRANSPORT VARIABILITY AT THE NORTHWEST COAST OF PORTUGAL

**This chapter is based on a manuscript published in the Journal of Waterway, Port, Coastal, and Ocean Engineering:**

Ana Nobre Silva, Rui Taborda, Xavier Bertin and Guilaume Dodet, 2012. "*Seasonal to Decadal Variability of Longshore Sand Transport at the Northwest Coast of Portugal*". Journal of Waterway, Port, Coastal, and Ocean Engineering, Volume 138, Number 6, pages 464-472. DOI: 10.1016/j.margeo.2007.02.009 EID: 2-s2.0-34247588614.

## 5.1. ABSTRACT

Longshore sediment transport (LST) is a major driver of coastal evolution. However, despite the recognition that it presents an unsteady behavior at seasonal scale, the variability at longer term scales (interannual and decadal) is still far from being properly acknowledged. The present work contributes to the understanding of the seasonal to decadal variability of the LST, benefiting from recent developments in wave hindcast modelling. This work was developed for the northwest coast of Portugal, which is fully exposed to the highly energetic wave regime generated it the Northeast Atlantic Ocean that induces unusually large LST rates. Hindcast offshore waves, between 1953 and 2010, were used as offshore forcing to deduce LST estimates.

The mean annual LST, between 1953 and 2010, shows an irregular and non-cyclic pattern. Computed mean annual LST, for this coastal stretch, is around one million cubic meters directed to the south, with yearly averages ranging from 108,000 $m^3$ $year^{-1}$ to 2,240,000 $m^3$ $year^{-1}$ always directed to the south. The maximum observed annual LST magnitude exceeds the mean magnitude by more than 100%. The variability in LST magnitude was found to be mainly related to LST magnitudes of autumn/winter months in response to the wave regime seasonality. Results show that to estimate the long-term LST within an error about 20%, a period of about 10 years of data/observations is required.

Interannual variability in the magnitude of the LST was found to be correlated ($R^2$ = 0.55) with the annual North Atlantic Oscillation (NAO) index. In the years where the NAO index was higher, the mean annual LST was generally greater than the long-term average, while negative NAO index corresponds to lower than average LST estimates.

## 5.2. INTRODUCTION

Longshore sediment transport (LST) plays a major role in the sedimentary dynamics of the coastal zone and long-term shoreline evolution; its quantification remains essential for the assessment of sedimentary budget and for the understanding of coastal zone dynamics.

The coastal stretch between Espinho and Cape Mondego, Portugal is characterized by a considerable LST induced by highly energetic northwest swells combined with a relatively narrow continental shelf and steep beaches. The coastal development that took place in the 20th century, which included port structures and groin constructions, has disturbed the sedimentary budget, inducing large LST gradients along this coastal stretch with severe socio-economic impacts. The large LST gradients are not only responsible for severe coastline retreat, reported to reach up to 200 m, between 1958 and 1998, in the northern sector (Taveira-Pinto et al., 2009), but they also hinder the development and implementation of adequate management policies.

The LST along this littoral stretch presents a highly unsteady behavior related not only to seasonality but also with longer term fluctuations (interannual and decadal). For example, coastal erosion data from Baptista (2006), although not directly translated into LST, suggests that the magnitude of the transport has a strong interannual variability that can exceed 100% of its average value. When coastal management policies are being developed, this variability should be considered by decoupling the seasonal, interannual and, long-term components. As recognized by Schoonees (2000), to estimate long-term LST rate, it is necessary to account also for the interannual variation. According to this author, long-term LST estimates should rely on 5 - 8 years to achieve an accuracy of less than 10%. However, the applicability of these results to this coastal stretch has not been verified, and because there are no long-term sediment flux estimates, the uncertainties related with seasonal to decadal variability in LST rates are presently unknown.

The present work aims to improve our knowledge on the seasonal to decadal variability of the LST. This objective will be achieved through the use of an empirical LST formula coupled with long-term simulated wave information. The recent advances in wave modelling together with the availability of wind field reanalyzes data for the last 60 years (e.g. Kalnay et al., 1996) has enabled the study of the wave climate variability in the Northeast Atlantic Ocean since 1953 (Dodet et al., 2010; Pilar et al., 2008). Such wave hindcasts provide a unique opportunity to characterize the interannual LST variability along the Portuguese coast.

## 5.3. STUDY AREA

The study area, located between the mouth of the Mondego River and Nazaré Canyon, is within Douro - Nazaré littoral cell on the Portuguese west coast (Figure 5.1). This littoral cell comprises about 160 km of linear sandy coast, only interrupted by the inlet of Aveiro lagoon, the mouth of the Mondego River, and Cape Mondego, with similar characteristics of the LST behavior throughout because similar wave exposure and shelf morphology. Although the aforementioned interruptions correspond to natural barriers bypassed by the sediments, some artificial structures (like the jetties of the Aveiro inlet and the groin fields at the south of Aveiro) strongly disturb the sediment supply downdrift and induce severe erosion problems with high socioeconomic impacts (Andrade et al., 2002; Taborda et al., 2005; Taveira-Pinto et al., 2009).

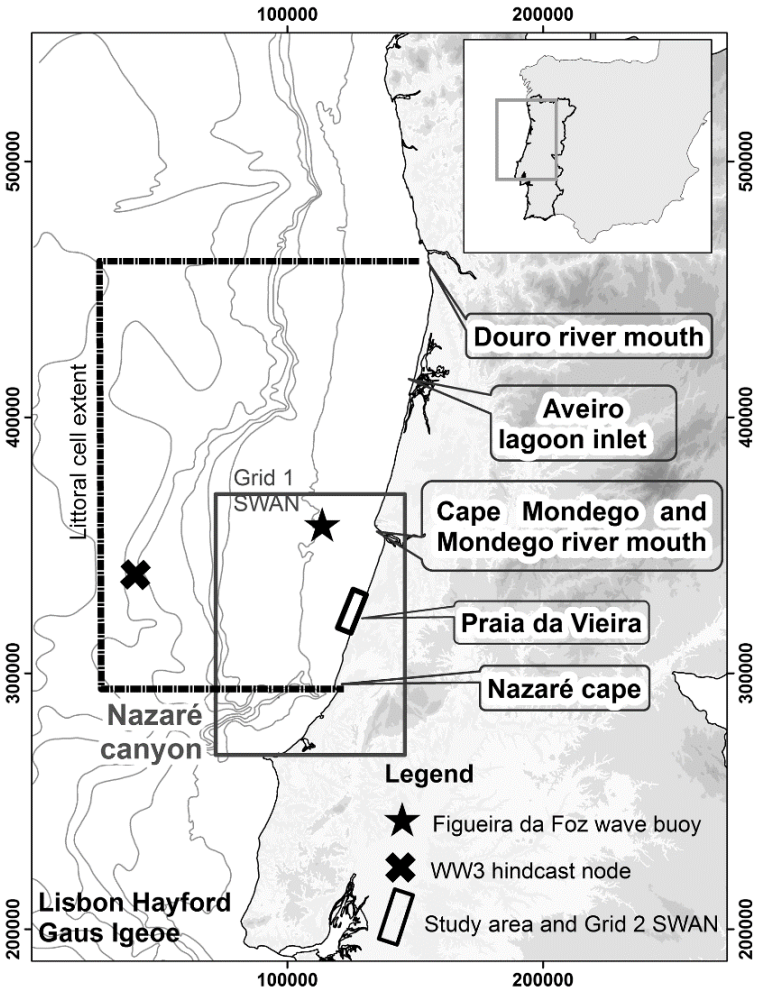


**Figure 5.1 - Location map with the position of observed and modeled waves and the extent of the regional and the nested rectangular grids used by SWAN model.**

This coastal stretch is limited to the south by the presence of the Nazaré submarine canyon, which interrupts the net southward LST. The Nazaré Canyon cuts the full width of the continental shelf and slope, with an approximate east-west orientation, is referenced in the literature as the major active sediment conduit to the abyssal plain, and has been the object of many studies since 1937 (Freire de Andrade 1937; Oliveira et al., 2007). Its head is located very close to the shore and reaches 20 m depth within a few meters distance of the Nazaré beach.

Within the study area, a small coastal section in the vicinity of Praia da Vieira beach was selected as representative of the coastal stretch because of its geomorphologic characteristics: an alongshore uniform, NNE-SSW, linear coastal ribbon with linear and parallel contours, without sediment sources or sinks, no rocky outcrops, and insignificant anthropogenic perturbation. For these reasons, this beach has already been used as representative of the coastal stretch between the mouth of the Mondego River and Nazaré Canyon in other coastal dynamic studies (Oliveira et al., 2004; Silva et al., 2005). Praia da Vieira beach is characterized by an intermediate beach profile (subaerial beach slope = 0.02) composed of coarse grain-size sediments (d50 = 0.71 mm) backed by small-height dunes. Additional information on the field site can be found on Larangeiro et al. (2004) and Silva et al. (2005).

The study site is fully exposed to the North Atlantic wave regime characterized by a predominant swell from the northwest quadrant superimposed with a generally less-energetic local wind sea with a larger directional spread. Recent developments in wave hindcast modelling enabled the calculation of extended, high-quality, continuous-wave time series, improving the knowledge of long-term wave regime along the western Portuguese coast (Dodet et al., 2010). In that study, integrated wave parameters, namely the significant wave height (Hs), the peak period (Tp) and the mean wave direction (Mwd), were computed with the third-generation spectral wave model WAVEWATCH III (WW3; Tolman 2009), and very good agreements were presented with measurements made at Figueira da Foz (Figure 5.2). Statistical errors between modeled and in-situ data are presented in Table 5.1.

**Table 5.1 – Validation Parameters and Wave Statistics for Significant Wave Height ($H_s$), Peak Period ($T_p$), and Mean Wave Direction ($M_{wd}$).**

| | Validation parameters for wave hindcast | | | | Wave statistics | | | | |
|---|---|---|---|---|---|---|---|---|---|
| ***Wave parameters*** | **Bias** | **RMSE** | **NRMSE** | **Number of obs.** | **Mean** | **P25** | **P75** | **Max.** | **Number of obs.** |
| ***$H_s$ (m)*** | -0.14 | 0.45 | 20.49% | | 2.03 | 1.26 | 2.45 | 13.00 | |
| ***$T_p$ (s)*** | -0.38 | 1.60 | 14.20% | 2,491 | 10.47 | 8.58 | 12.2 | 22.68 | 81,816 |
| ***$M_{wd}$ (°)*** | 0.93 | 14.98 | - | | 307.2 | 293.7 | 323.1 | 360.0 | |

Note: Validation parameters for wave hindcast: bias, root-mean-square error (RMSE), root-mean-square error normalized by the mean of observed values (NRMSE), and number of observations (Number of obs.; adapted from Dodet et al., 2010); and main statistics: mean, 25th and 75th percentiles, and maximum (Max.), for the period 1953-2008 at a 6-h interval record.

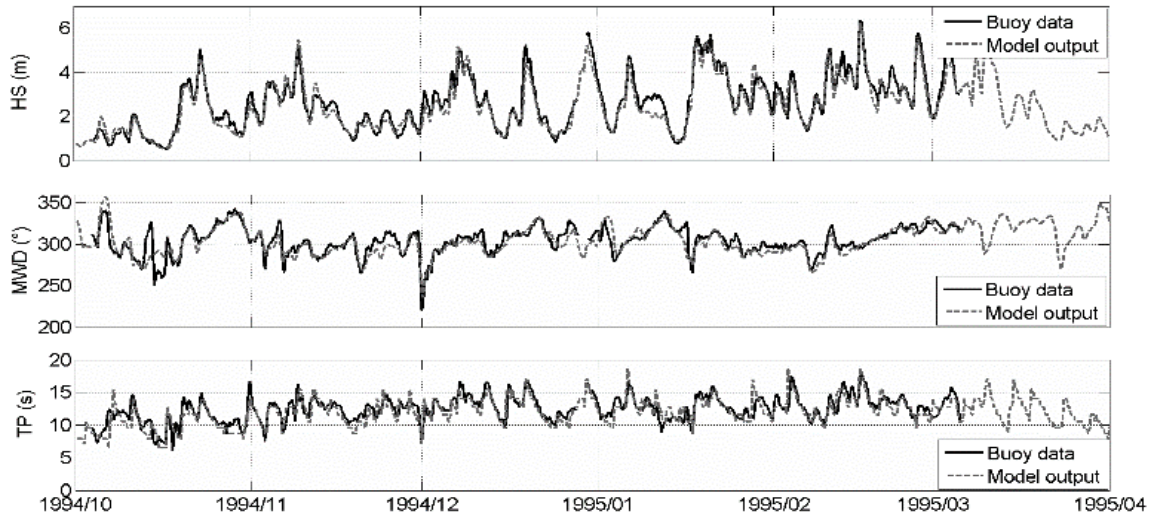


**Figure 5.2 - Comparison between 6-h interval modeled and measured waves at Figueira da Foz buoy from October 1, 1994, to April 1, 1995; (top) $H_s$ ;(middle) mean wave direction; and (bottom) $T_p$.**

The wave data set used in the present work was obtained from the aforementioned work at node 40ºN, 10ºW (Figure 5.1) and extends from 1953 to 2008 (56 years) with a 6-h interval.

The offshore wave climate is characterized by a mean significant wave height of 2.0 m with a maximum value of 13 m, the mean peak period is 10.5 s with a maximum of 22.7 s, and the average mean wave power direction is 307º (Table 5.1).

**Table 5.2 – Validation Results for the Modeling Strategy (Including the WW3/SWAN coupling).**

| ***Wave parameters*** | **Bias** | **RMSE** | **NRMSE** | **Number of observations** |
|---|---|---|---|---|
| ***$H_s$ (m)*** | -0.17 | 0.39 | 0.18% | |
| ***$T_p$ (s)*** | -0.28 | 1.48 | 0.13% | 2,514 |
| ***$M_{wd}$ (°)*** | -0.05 | 12.10 | - | |

The LST estimates reported in literature for this coastal stretch were made through different techniques from cartographic comparison with mathematical modelling, whose results led to a wide range of values from 200,000 (Abecasis 1955) to 3.5 million $m^3$ $year^{-1}$ (Teixeira 1994), although most values converge towards a mean value of around 1 million $m^3$ $year^{-1}$ (Taborda et al., 2005). Even using the same mathematic formulations, previous studies have shown relatively large discrepancies, which can be related to bathymetric data,

coastline orientation, and wave refraction modeling and, additionally, can also be attributed to the interannual variability of the offshore wave regime.

## 5.4. METHODS

The nearshore wave regime was modeled using the SWAN wave model (version 40.72), which is based on the wave-action balance equation (Booij et al., 1999). The model was run in stationary mode. The geographical space was discretized using two grids: (1) a first rectangular grid, with a 2-km resolution, which extends from the Berlengas Islands to the north of Cape Mondego and (2) a nested curvilinear grid, starting around 50 m water depth and with a resolution ranging from 300 m offshore to 20 m in the cross-shore profile where wave parameters at the breaking point were extracted (Figure 5.1). These grids were interpolated on bathymetric data resulting from a compilation of the available data for the northwest Portuguese continental shelf. The inner grid (Grid 2) was based on an alongshore smoothed profile, with contours parallel to the coastline, with a constant N22ºE orientation. The spectral space was discretized using 24 regularly spaced directions and 24 frequencies having a logarithmic distribution. The model was forced along its open boundary with time series of energy spectra originating from the WW3 hindcast of Dodet et al. (2010) at the node (40ºN, 10ºW; Figure 5.1). The model was set to account for wave breaking according to Battjes and Janssen (1978) bore-based model, bottom friction using Madsen et al.'s (1988) method with a physical roughness of 0.05 m, and triad wave-wave interactions. Because SWAN was only used to propagate offshore-generated waves, all wind-wave related processes (whitecapping and quadruplets) were switched off.

This modeling strategy (including the WW3/SWAN coupling) was validated through the comparison of SWAN outputs with available buoy data from Figueira da Foz (Figure 5.1). Results, displayed in Figure 5.2 and Table 5.2, show a good agreement between both data sets. The significant improvement of wave predictions compared to a direct comparison with WW3 outputs can be attributed to a better representation of the shelf bathymetry in the SWAN model.

Wave parameters at the breaking point were computed from January 1953 to December 2010 using a 6-h time step (over 80,000 runs). The breaking point was defined as the point where the rate of energy dissipated by breaking exceeded 5% (Bertin et al., 2008).

Bulk LST estimates (total rate across the beach profile) were computed with the recognized Coastal Engineering Research Center (CERC) formula (Rosati et al., 2002), where the volumetric sand transport rate (Q in $m^3/s$) is related to the breaking significant wave height ($H_{s,\,b}$) and direction ($\alpha_b$), assuming standard values for the water and sediment density

(1.025 and 2.650 g/cm$^3$, respectively) and porosity (0.4), through the following expression (Equation 5.1):

$$Q = k \times 0.233 \times H_{S,b}^{5/2} \times \sin(2\alpha_b) \qquad \textbf{Equation 5.1}$$

where K = dimensionless empirical constant, generally taken as 0.39, and 0.233 is a dimensional empirical coefficient (m$^{1/2}$/s). Annual and monthly net LST estimates were computed through the sum of the 6-h interval LST values obtained using this expression.

While the use of the so-called CERC approach to compute long-term LST is presently widely accepted, it is important to realize that the rates computed by this method still are subject to a considerable degree of uncertainty [e.g. Kamphuis (2000)]. In this work the use of the CERC approach was validated using tracer data acquired at Praia da Tocha beach (Taborda et al., 1994), located within the same sediment cell. Data obtained in this tracer experiment, performed in high-energy conditions and morphodynamic characteristics similar to those of the study area, validated the use of the CERC approach albeit with a slightly higher coefficient (K = 0.45) than the recommended one (0.39). Considering the uncertainties related to this coefficient and that the use of a K equal to 0.39 provided net annual LST estimates similar to the ones reported in previous studies for this coastal stretch (≈1 million m$^3$ year$^{-1}$), this latter value (0.39) was chosen. To get a sense of the uncertainties related to the adoption of this approach to access LST temporal variability, the same computations were performed using different empirical constants in the CERC formula and other bulk LST formulas [e.g. Kamphuis (1991)]. Results show an obvious influence of the chosen approach on the magnitude of LST estimates but very limited impact on the temporal LST variability pattern, which is the aim of the present work.

## 5.5. RESULTS

The interannual variability of the deep water wave climate was evaluated by the analysis of mean annual values of the wave hindcast. The computed statistics (Table 5.3) show that the mean annual significant wave height ranges from 1.76 to 2.26 m, with a median value of 2.02 m. The mean annual peak period ranges from 9.82 to 10.99 s with a median peak period of 10.45 s. The direction from which waves approach is 307.7º (median) and ranges from 299.4 to 314.8º. The evaluation of the interannual variability magnitude, measured by the coefficient of variation (ratio between the SD and the average), shows that wave height

displays the higher variability. In the study area, the time series of average annual wave height does not exhibit any obvious periodicity or long-term trend (Dodet et al., 2010).

**Table 5.3 – Main Statistics for Mean Annual $H_s$, $T_p$, and $M_{wd}$ between 1953 and 2008.**

| *Wave Parameters* | Min. | P25 | Median | P75 | Max. | SD | COV |
|---|---|---|---|---|---|---|---|
| $H_s$ *(m)* | 1.76 | 1.94 | 2.02 | 2.14 | 2.26 | 0.11 | 0.0561 |
| $T_p$ *(s)* | 9.82 | 10.36 | 10.45 | 10.61 | 10.99 | 0.21 | 0.0202 |
| $M_{wd}$*(°)* | 299.4 | 305.0 | 307.7 | 309.0 | 314.8 | 2.97 | - |

The month-based analysis of the time-series (Figure 5.3, Figure 5.4 and Figure 5.5) shows that the biggest part of the interannual variability is related to the variability observed during the maritime winter months, which correspond to the months with a higher difference between the minimum and maximum month average result. In fact, the summer months (April to September) are significantly less variable than the maritime winter months (October to March) in the significant wave height, peak period, and also wave direction. In addition to the established seasonal behavior of the wave parameters presented in the following figures in which the higher values for the wave height and wave period tend to occur during the winter months, there is a remarkable wide range between maximum and minimum values during the winter. Moreover, the wave height is the most variable parameter governing the seasonal variability; for example, mean July values for wave height vary between nearly 1m to 1.5 m, while in December, the mean value observed ranges from about 1.7 to 4.3 m (Figure 5.3).

Comparatively, the wave peak period has a less remarkable seasonal variability for the maximum and minimum range, but has also a seasonal character for the median value (Figure 5.4).

The seasonal behavior of the wave direction follows the acknowledged clockwise rotation during the summer, while the westernmost directions occur in the winter months. Despite this rotation, the monthly mean wave direction is persistently from the northwest quadrant with only a few exceptions occurring in January and December, where the minimum value observed is less than 270º. Likewise, the interannual variability is larger in the winter months, where the range between extreme values is significantly higher than in the summer months (Figure 5.5).

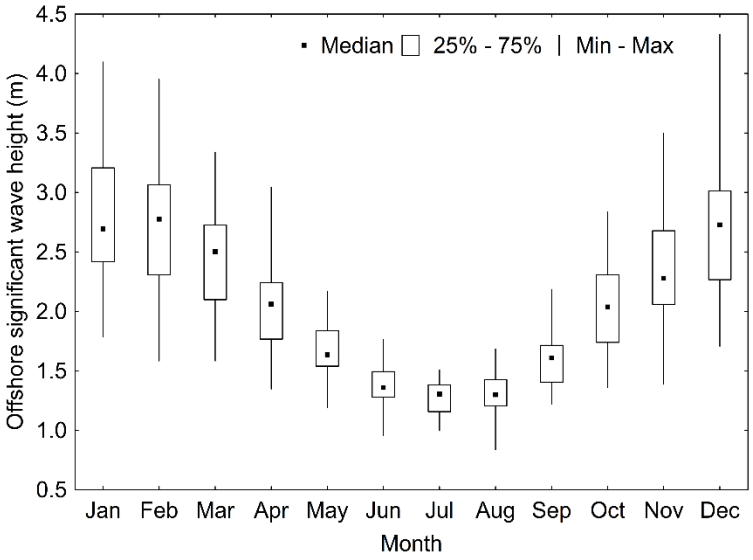


**Figure 5.3 – Monthly average of the offshore significant wave height for the 56 years of wave hindcast.**

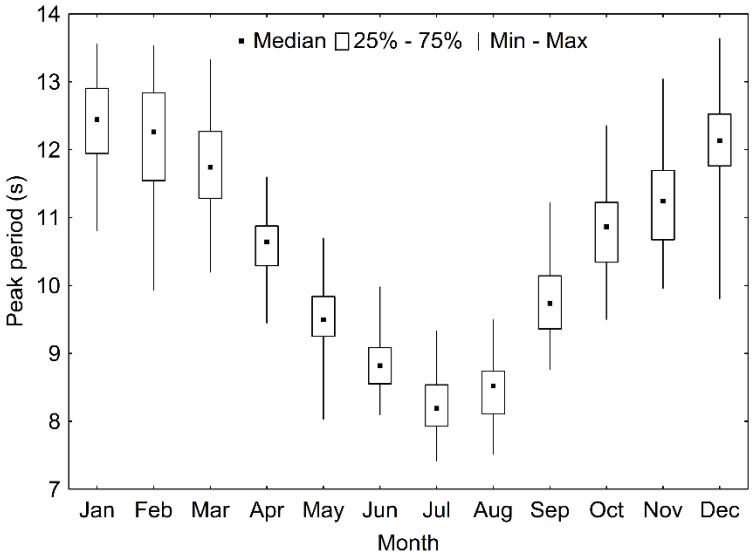


**Figure 5.4 - Monthly average of the peak period for the 56 years of wave hindcast.**

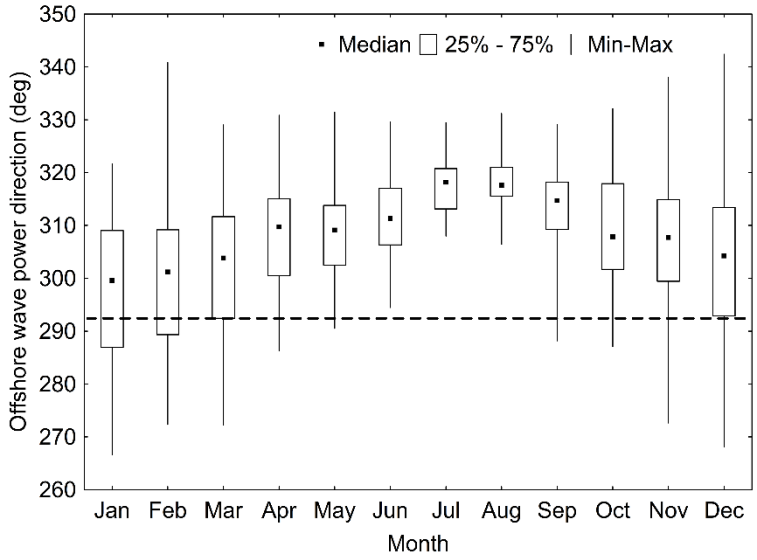


**Figure 5.5 - Monthly average of mean offshore wave direction for the 56 years of wave hindcast (the dashed line represents the coastline orientation).**

The temporal variability of the littoral LST was investigated at a cross-shore profile (along the middle of nested SWAN grid, Figure 5.1) that was considered representative of the potential LST along the study site. The results from every 6-h period wave were integrated in a yearly base to provide mean annual LST values and investigate the interannual LST variability. The results (Table 5.4) show a mean annual magnitude of LST that slightly exceeds one million cubic meters directed to the south, which is in agreement with previous estimates for the Portuguese northwest coast (Andrade et al., 2007; Coelho et al., 2009). Annual littoral LST values exhibit a large variability with a maximum of 2.24 million $m^3$ $year^{-1}$, which exceeds the long-term mean magnitude by 105%, and a minimum, 108,000 $m^3$ $year^{-1}$, 10 times less than the mean value. The time series of mean annual values between 1953 and 2010 shows an irregular pattern with a clear predominance of net LST directed to the south (Figure 5.6). The southward-directed maxima, characterized by annual LST magnitudes larger than 2 million $m^3$ $year^{-1}$ were observed during the years 1984 and 1986. The LST minima (less than 200,000 $m^3$ $year^{-1}$) are not only related with atypical small southward components, like during the years 1955 and 1985, but also to a very strong northward component as observed in 1966, the year where the maximum northward LST component occurred (Figure 5.6).

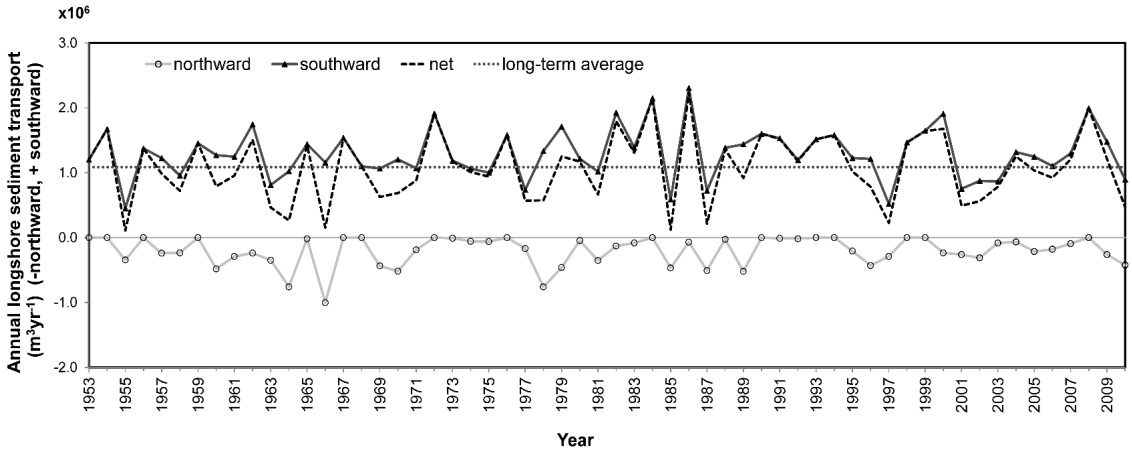


**Figure 5.6 – Components of LST for the 58 years**.

The LST seasonality was also studied based on 58-year monthly averages (Figure 5.7). The seasonal behavior, expressed in the long-term median monthly values, presents an annual cycle with maximum values in winter and minima in summer. This analysis also reveals that the larger variability occurs during autumn/winter months (October to April), with an interannual range higher than 200,000 $m^3$, while the spring/summer months exhibit a more consistent LST pattern. Figure 5.7 also shows that the northward-directed LST occur more frequently between December and April, while during the period between May and September, the monthly average LST is always directed southwards.

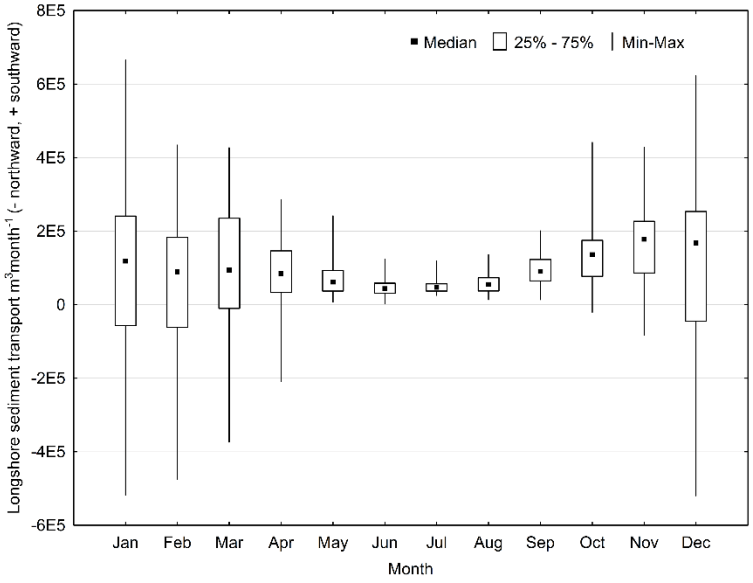


**Figure 5.7 – Monthly average LST for the 58 years.**

## 5.6. DISCUSSION

Long-term, high-resolution, LST estimates for the northwest Portuguese coast revealed a relatively large temporal variability at a wide range of timescales. Monthly average results ranged from about -520,000 to 670,000 $m^3$ $month^{-1}$ (Figure 5.7), while annual values ranged from 108,000 to 2.24 million $m^3$ $year^{-1}$ (Table 5.4). This behavior is connected to the temporal variability of the offshore wave regime, mainly in what concerns wave height and direction.

**Table 5.4 –Mean Annual Potential Longshore Sediment Transport Statistics ($m^3$ $year^{-1}$) at the Study Area.**

| *LST statistics* | Average | Minimum | Maximum | COV |
|---|---|---|---|---|
| ***Potential LST ($m^3year^{-1}$)*** | $1.09x10^6$ | $1.08x10^5$ | $2.24x10^6$ | 0.48 |

The analysis of variance (ANOVA) for the monthly average magnitudes of the forcing mechanisms during the 58 years of wave hindcast shows that the seasonal component clearly dominates the wave climate variability. Results for the wave height show that the seasonal component accounts for 67% of the data variability contrasting with the 30% and 3% of the subseasonal and interannual components, respectively. Similar results were achieved for the peak period where 85% of variation is associated with the seasonal component and only 13% and 2% related to the subseasonal and interannual ones. Monthly averaged wave direction is dominated by subseasonal perturbations (68%), while the other components show a secondary role (seasonal component 23%; interannual component 9%). The LST is also dominated by the subseasonal perturbations (84%), while the seasonal and interannual components are responsible for 6% and 10%, respectively. This behavior, represented in figures Figure 5.3, Figure 5.4, Figure 5.5 and Figure 5.7, shows that, despite the strong seasonality of the wave forcing, the opposing behavior of wave height and direction (i.e. in summer, the lower waves generally have a higher than average angle of incidence, while in winter these two variables display an opposite behavior) strongly reduces the seasonal component of the LST.

Notwithstanding these results, the interannual variability component still plays an important role in the evaluation of the coastal sedimentary budget, as its mean annual value can more than double in magnitude (Table 5.4). This variability, represented in terms of a coefficient of variation (COV) of 0.48, is within the range of results found by Schoonees (2000) at three South African study sites (COVs between 0.19 and 0.88). According to the

same author, the most intense annual net LST rate obtained exceeded by 149% the mean annual transport for the 14-yr data set. In a similar analysis, Shi-Leng and Teh-Fu (1987) found a 1.31 maximum-to-mean ratio for 7 years of LST estimates, at Mauretania, which is comparable to the 2.06 ratio obtained in this work.

Considering that LST estimates are frequently based on a few years of data, it was considered relevant to assess these uncertainties through the analysis of maximum-to-mean (max r) and minimum-to-mean (min r) ratios computed using different time windows (ranging from 1 to 20 consecutive years). As expected, increasing the time window decreases the variability (Table 5.5 and Figure 5.8); for example when, when only 1 year is considered, the LST magnitude can more than double the long-term mean value, while when a time window of 10 years is considered, the estimates are roughly within 20% of the long-term value. To ensure that the deviation from long-term mean is of the order of 15%, a period of about 20 years is necessary, which contrasts to 8 to 9 years obtained by Schooness (2000). This difference might be related to the presence of long-term (> 10 years) weather oscillations at decadal time scales in the study site.

**Table 5.5 – Variability Factors in Each Time Window.**

| ***Window (years)*** | **1** | **2** | **3** | **4** | **5** | **…** | **10** | **…** | **20** |
|---|---|---|---|---|---|---|---|---|---|
| ***Max. r*** | 2.04 | 1.59 | 1.61 | 1.36 | 1.40 | … | 1.22 | … | 1.15 |
| ***Min. r*** | 0.10 | 0.34 | 0.56 | 0.53 | 0.70 | … | 0.79 | … | 0.88 |

Note: Min. r = Minimum r; Max. r = Maximum r.

The high magnitude of the interannual component of the LST variability should be related to a low-frequency component of the wave regime variability, which in turn, is known to be linked to the North Atlantic Oscillation (NAO - a meteorological phenomenon in the North Atlantic Ocean represented by the difference of atmospheric pressure at sea level between the Icelandic low and the Azores high; Bauer 2001; Dodet et al., 2010; Woolf et al., 2002). This behavior suggests that a relation between the LST and the NAO index could also exist. To investigate this relationship, the annual LST estimates for this coastal stretch, between 1953 and 2009, were compared with the annual NAO index [the NAO index data is provided by the Climate Analysis Section, National Center for Atmospheric Research, Boulder, CO (Hurrell 1995)].

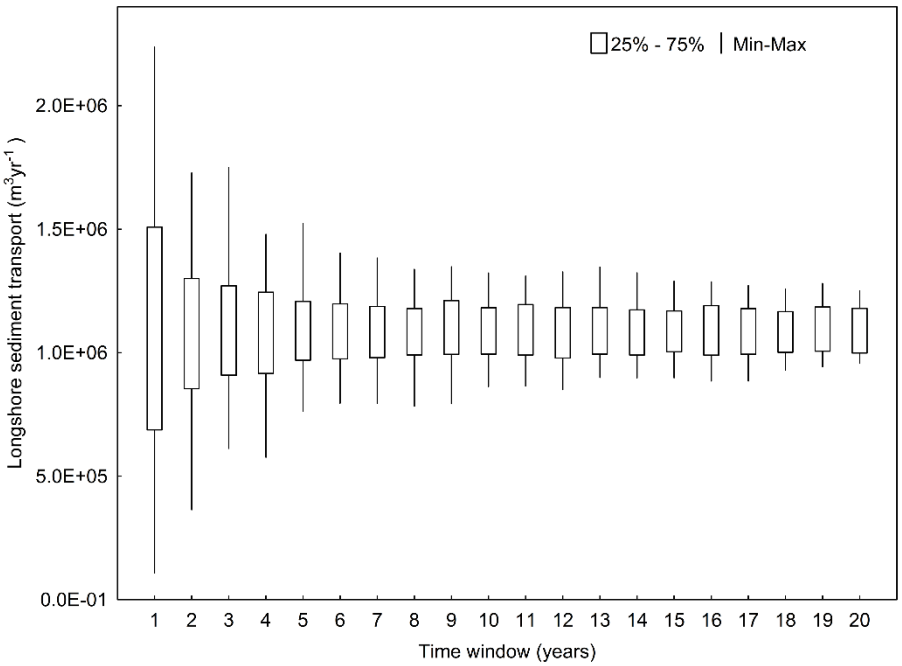


**Figure 5.8 – Variability associated with each time window considered.**

Results, displayed in Figure 5.9, show a reasonable agreement ($R^2$ = 0.55): in the years where the NAO index was higher, the mean annual LST was generally greater than the long-term average, while negative NAO index corresponds to lower than average LST estimates. This agreement is particularly good for the period between 1953 and 1961 and between 1981 and 1988, with an almost perfect correspondence between data sets. Positive NAO years correspond to higher-than-normal sea level pressure gradients, which at the study-site latitude, induce long-period waves coming from a very narrow northwest direction (Dodet et al., 2010), resulting in a higher-than-average southward LST. Negative NAO years, with a larger westward component, induce a larger-than-average northward LST component, resulting in a lower-than-average net (southward) LST. The correlation between the NAO index and LST estimates, obtained for the study site, primarily depends on the relationship between this index and wave climate, which as shown by Dodet et al. (2010), exhibits a marked spatial variation across the Northeast Atlantic. Because this variation is expected to be translated in the quality of the correlation between these variables (LST and NAO), the extrapolation of correlation results to other sites is not straightforward. However, considering the spatial pattern found by Dodet et al. (2010) a higher correlation is expected across the coastlines of the Iberian Peninsula and northern Africa compared with northern European ones. Further research should be made to confirm this hypothesis and extend these findings to other sandy coasts. Notwithstanding,

the exploration of this link can significantly enlarge the time frame for a quantitative explanation of past coastal evolution, as the NAO index can be extended back to the 16th century (Luterbacher 2002).

Mean Annual Potential Longshore Sediment Transport Statistics ($m^3$ $year^{-1}$) at the Study Area.

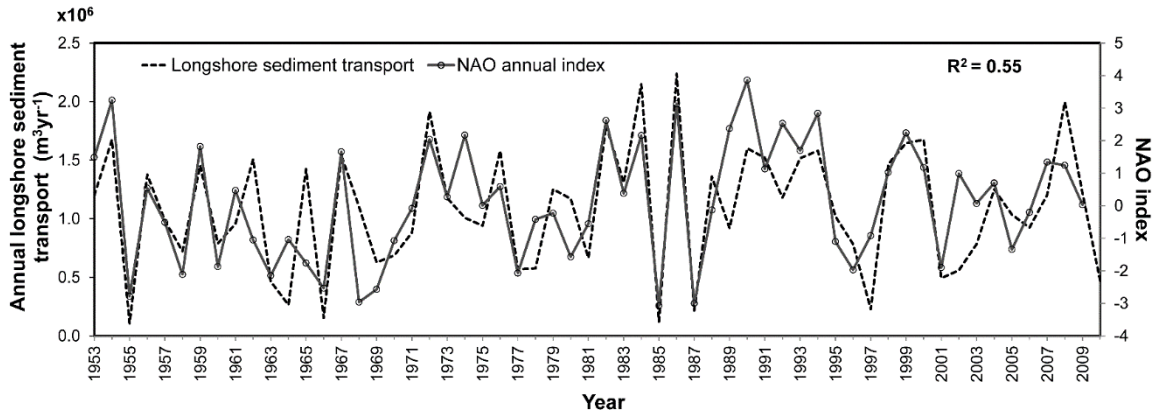


**Figure 5.9 – Annual LST and NAO index variability between 1953 and 2009.**

## 5.7. CONCLUSIONS

The analysis of 58 years of wave hindcast, and derived LST rates revealed a strong seasonal and interannual variability. Although LST is directly related to the wave forcing, the non-linear relationship between these variables induces considerable changes in the signal frequency for subseasonal, seasonal, and interannual components.

Variations in the magnitude of annual LST were found to exceed the long-term mean value by more than 100%, which has strong implications in the time extent that should be used to support a sedimentary budget analysis. For the study site, to obtain an estimate that is within ±20% of the long-term average LST, a minimum of 10 years data/observations is required.

Interannual variability in the magnitude of the LST was found to be highly related with the annual NAO index.

This work benefits from recent advances in wave modeling hindcast studies, providing for the first time, a long-term perspective of LST variability at decadal timescales. The long-term LST variability can be connected with periods where the coast has exhibited higher-than-average rates of shoreline evolution/retreat that could be described as hot periods.

These results contribute to a broader understanding of long-term coastal behavior and can help relate recent shoreline changes not only to anthropogenic causes but also to decadal climatic variability.

## 5.8. ACKNOWLEDGEMENTS

The first author was conferred a Ph.D. grant (Grant No. SFRH / BD / 41762 / 2007) by the Portuguese Science and Technology Foundation (FCT). This work is also a contribution to the European project Morphological Impacts and Coastal Risks induced by Extreme storm events (MICORE; Grant No. 202798) and the FCT project Beach to Canyon Head Sedimentary Processes (B2C; Grant No. PTDC/MAR/114674/2009). The final version paper has benefit from valuable comments of three anonymous reviewers.

# CHAPTER 6

# Shoreline Variability at the Norte Beach

# CHAPTER 6 – SHORELINE VARIABILITY AT THE NORTE BEACH

**This chapter is based on a manuscript published in the Journal of Coastal Research:**

Ana Nobre Silva, Rui Taborda, Carlos Antunes, João Catalão and João Duarte, 2013. "*Understanding the coastal variability at Norte beach, Portugal*". Journal of Coastal Research, Special Issue 65, pages 2173-2178. DOI: 10.2112/SI65-367 EID: 2-s2.0-84883820540.

## 6.1. ABSTRACT

Norte beach stands in a coastal stretch fully exposed to the high energetic North Atlantic wave regime. The beach is located updrift of the Nazaré submarine canyon head, a sedimentary sink that captures the southward directed longshore drift. Systematic monitoring of Norte beach has been conducted by a coastal video monitoring system since 2008. A total of 31 monthly coastlines were extracted and analyzed in the period between December 2008 and May 2012. Results show a rare high seasonal coastline variability which exceeds 160 m in the southward sector (adjacent to the headland) and 70 m at the central and north sectors. These coastline variations are related with modifications in the planform beach configuration: beach oscillates between a straight (generally from June to August) and an arcuate configuration (during the remaining months of the year). Results suggest that Norte beach variability depends mainly on longshore drift gradients rather than with cross-shore sedimentary transfers. The intense wave refraction over the canyon head, associated with the westerly swell waves, generates a sedimentary convergence at the centre of the beach promoting the increase of the beach curvature, while, northern and/or short waves (more frequent in summer) tend to linearize the beach. This work contributed with valuable information about the sedimentary dynamics of the Norte beach and showed that this site is a suitable candidate to evaluate longshore drift from shoreline changes.

## 6.2. INTRODUCTION

Understanding beach morphological variability is essential to support coastal risk assessment and help in the decision making process, especially in what concerns the implementation of mitigation measures in response to erosive events reported worldwide.

It is now well established that shoreline erosion is closely related to longshore drift gradients, so the quantification of this process is essential to understand and predict coastline evolution.

The quantification of longshore sediment transport goes back to the middle of last century, and was accomplished by the evaluation of the sediment blocked in artificial structures, or by the inverse process i.e. by the quantification of the erosion rates downdrift of the blocking structure. This method was developed in the pioneering work of Watts (1953), and followed by numerous authors during the XX$^{th}$ century (see Komar, 1998 for a critical review of this theme). However, this method is prune to errors, such as the local effects of the structures on local wave and currents, sand bypassing in front of the structures, and the time needed to retain enough sediment that can induce shoreline changes that are unequivocally higher than the uncertainties of the measurement techniques.

Naturally, the quantification of sediment retention and associated longshore drift can also be performed in natural structures such as headlands, sand spits, inlets and estuaries. In the former, the sand retention processes and coastline evolution are similar to the ones observed in artificial structures. However, in headland settings it is not generally possible to define neither the conditions where the retention process began nor the transposing processes (time and magnitude). Yet, in some cases the coastline evolution related with the retention process can be identified; this generally occurs where the downdrift boundary of a littoral cell only allows one way sediment transposition (e.g. related to the existence of a submarine canyon). In these cases longshore drift inversions lead to a sedimentary depletion of the updrift beach adjacent to the headland; if the longshore drift inversion is persistent enough to retreat the coastline to a minimum the subsequent infill of the beach can be used to access longshore drift. This method is only suitable when the magnitude of coastline variations in relation to longshore processes clearly dominates the cross-shore component.

The use of video-monitoring techniques has already been established as an efficient tool for coastal monitoring providing high-resolution data both in the spatial and temporal domains (Holman and Stanley, 2007; Davidson et al., 2007 and Van Koningsveld et al., 2007). Since the works of Plant and Holman (1997) and Davidson et al. (1997) video monitoring has been widely used in coastline evolution studies (e.g. Aarninkhof et al., 2003; Alexander and Holman, 2004; Armaroli et al., 2007; Conley et al., 2007, Silva et al., 2009). Generally coastline detection is performed trough the location of the water/land interface in time average images (TIMEX) where the swash effects are eliminated.

The present study aims to understand the shoreline variability, using video monitoring techniques, at a headland restricted beach located updrift of the Nazaré submarine canyon head, ultimately targeting its relationship with the longshore drift processes.

### 6.2.1. STUDY AREA

The study site, Norte beach, is located at the Portuguese west coast, which is exposed to the high energetic NW North Atlantic swell and the locally generated sea that is characterized by a wide directional spreading (from N to SW octants). Offshore incident wave regime is characterized by significant wave height of about 2 m and average peak period of 11 s (Dodet et al., 2010). It is characterized by a mesotidal regime with an amplitude that ranges from 1.5 at neap tides and 3.5 at spring tide. The wave propagation over the complex canyon morphology is responsible for one of the largest wave height surf spots in the world (with waves that exceed 20 m).

Norte beach is located at the southern limit of the littoral cell that extends from Espinho to Nazaré canyon (Figure 6.1). The beach, composed of -2.6 ϕ to 1.79 ϕ (mean value 0.18 ϕ) quartzic sand (Cascalho et al., 2012), is characterized by a wide berm and a steep beach face.

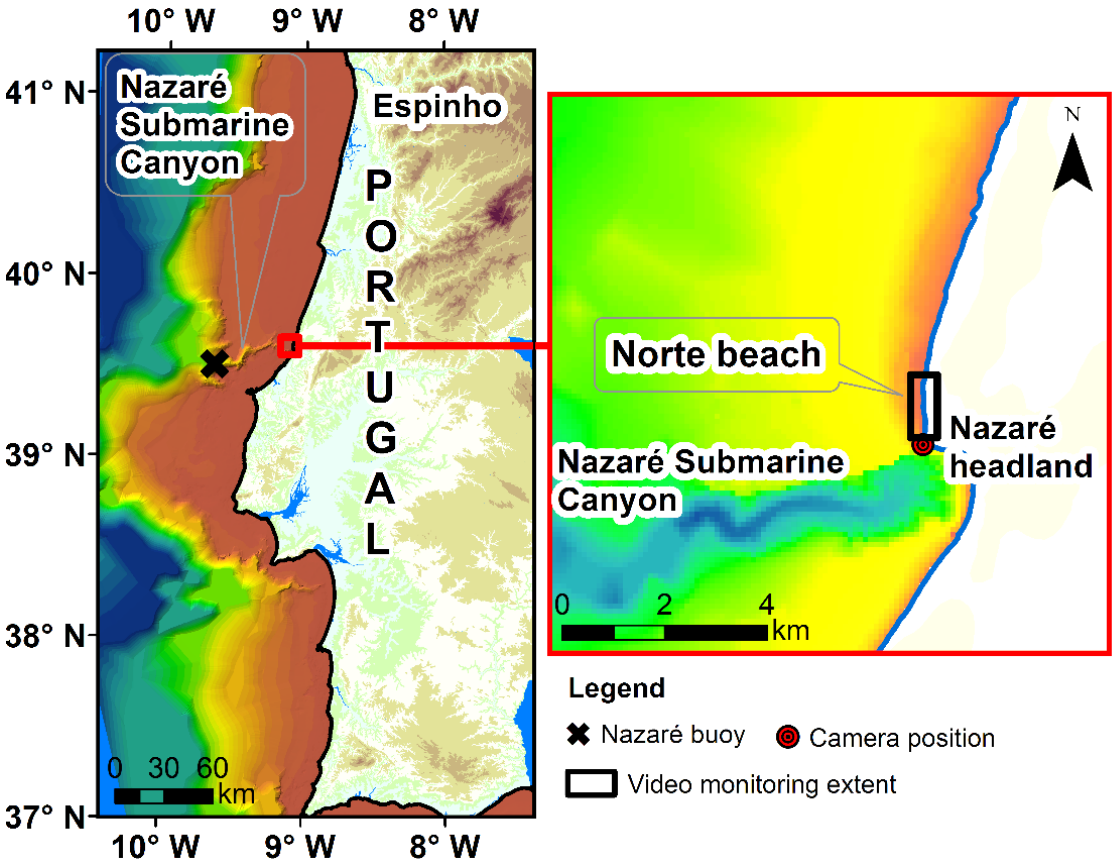


**Figure 6.1 - Norte beach and Nazaré submarine canyon location.**

## 6.3. METHODS

For 3.5 years, shoreline evolution at Norte beach was assessed through a combination of monitoring techniques (video monitoring and DGPS topographic surveys), data acquisition procedures (wave and tide measurements), modeling (tide and waves) and processing tools (image analysis and Principal Component Analysis – PCA), described below.

### 6.3.1. VIDEO MONITORING

Systematic monitoring of Norte beach has been conducted by COSMOS coastal video monitoring system (Taborda and Silva, 2012) since December 2008. The video camera is installed in the Nazaré headland, about 50 m above mean sea level and is looking obliquely to Norte beach (Figure 6.1). Image acquisition was performed at 1 image per second, during 20 minute intervals each daylight hour. TIMEX images were created for each 10 minutes image block to eliminate the swash effects.

Despite some time gaps, due to technical failures, a total of 31 monthly Timex images of the beach were carefully chosen in the period between December 2008 and May 2012. Images were chosen based on a predefined total water level (TWL); this value -2 m above mean sea level (MSL) - was defined in order to restrain the maximum run-up level to the beach face (therefore minimizing the horizontal error) and assure comparable conditions.

Each of the 31 monthly images was rectified using the 2 m height as the level for the rectification, following the procedures described in Taborda and Silva (2012). Camera laboratorial calibration and camera extrinsic parameters were estimated following the methodology described in Silva et al. (2009) and in Taborda and Silva (2012).

During the monitoring period a total of 20 topographic field campaigns were performed at Norte beach in order to orientate, calibrate and support the video monitoring. The campaigns involved DGPS surveys of ground control points for the external orientation of the camera (5 campaigns), of 14 cross-shore beach profiles (20 campaigns) and the survey of the run-up reach (8 campaigns).

### 6.3.2. SHORELINE ELEVATION

The quantification of the shoreline elevation includes three main components: 1) astronomical tide; 2) storm surge; and 3) run-up. The astronomical tide was estimated, at 10 min. interval, for Peniche harbour, located about 40 km southward of Norte beach. This tide model was estimated through harmonic analyses from the data of 2010, collected by

the national hydrographic institution (IH – Instituto Hidrográfico), with 20 harmonic constituents and an estimated precision of 10 cm (Antunes, 2007). A short tide elevation record acquired by IH, at Peniche and Nazaré gauges, show small differences, in height and time, which are in the order of the model precision.

To compute the run-up component several empirical models available in the literature (e.g. Guza and Thorthon, 1981; Holman, 1986; Nielsen, 1989; Aarninkhof et al., 2003; Stockodon et al., 2006 and Hughes et al., 2010) were tested against field measurements of maximum run-up levels (Rmax). Results showed the inadequacy of existent empirical models to predict run-up magnitude at Norte beach. This can be explained by the high wave deformation induced by the presence of the canyon, which inhibits the direct application of most empirical models that rely on the offshore wave. For this reason, an empirical site specific run-up formula was developed in the scope of the present work. The development of this expression was based upon the best linear fit between offshore wave and tide parameters with field data.

### 6.3.3. WAVE DATA

The offshore wave data was provided by the MONICAN project from the Portuguese Hydrographic Institute (http://monican.hidrografico.pt/) particularly by the buoy MONICAN01, located in the oceanic domain c.a. 2000 m depth and about 50 km offshore the Norte beach (Figure 6.1). The gaps of the buoy data (about 8% of the record) were filled with NOAA (National Oceanic and Atmospheric Administration) hindcast wave data for the nearest point (3 h interval between each record). Error statistics from the data comparison between measured data and hindcast are presented in the Table 6.1. From the above procedure, a continuous offshore wave time series from December 2008 to May 2012 with 3 h interval between records was obtained.

The wave offshore conditions associated for each of the analyzed month were estimated based on the average of the wave parameters (Hs – Significative height, Tp – Peak period and Dir - Direction) of the previous 30 days.

**Table 6.1 - Error statistics of the comparison between MONICAN wave buoy data and NOAA wave hindcast. $H_s$ = significant wave height; $T_p$ = peak wave period and Dir W = direction of waves approaching from west.**

| *Wave Parameter* | Bias | RMS | correlation coefficient | N. Observations |
|---|---|---|---|---|
| ***$H_s$ (m)*** | -0.036 | 0.386 | 0.946 | 7479 |
| ***$T_p$ (s)*** | 0.036 | 1.821 | 0.745 | 7487 |
| ***Dir W(°)*** | -9.885 | 23.814 | 0.722 | 7333 |

### 6.3.4. COASTLINE DETECTION

Coastline detection was performed on 31 rectified TIMEX images using the maximum likelihood supervised image classification method within ArcMAP software. The spectral signature for both water and sand areas was defined on representative timex images and were used to classify the other rectified TIMEX images. Due to variable lighting conditions and the irregular extent of the breaking zone, a total of 4 different spectral signatures were used. Image classification results were visually validated and about 6% of the initially images were discharged and replaced by similar ones.

The georeferenced interface between the water and the sand at 2 m above MSL, herein defined as coastline, was converted into vector format.

An estimation of the error related to the coastline detection was investigated through the comparison between the 2 m height points surveyed during the field campaigns and the coastline detected by the video monitoring system. The horizontally and vertically components of the displacements were investigated along the surveyed area whenever simultaneous video and topographic data existed.

### 6.3.5. SHORELINE CHANGES

The coastline variability at Norte beach was investigated through the analyses of the 31 coastlines using equally spaced, 100 m, transects. A total of 14 transects where considered along the 1400 m of the monitored beach.

The coastline changes were investigated through the use standard statistical parameters and principal components analysis (PCA) in order to extract the significant modes of the shoreline variability (Miller and Dean, 2007).

## 6.4. RESULTS

### 6.4.1. SHORELINE ELEVATION

The best fit between maximum run-up levels (Rmax) and a combination of offshore wave and tide forcing was found to be given by (Equation 6.1):

$$Rmax = 0.58 \times H_S + 0.32 \times \cos(270 - Dir) + 0.69 \times AT \qquad \textbf{Equation 6.1}$$

where Hs is the offshore significant wave height, Dir is the offshore wave direction and AT the astronomical tide. This relationship revealed a very high determination coefficient of 0.95 (Figure 6.2A). The 270 cosine argument is related to the average coastline orientation and the AT component empirically accounts for the greater wave dissipation at low tide.

In order to estimate the shoreline elevation extracted from the TIMEX images it was necessary to deduce the run-up exceedence level ($R_{x\%}$) detected by the image classification algorithm and the corresponding elevation. These values were found in a specific field measurement where a systematic topographic survey of the level attained by each wave during a period of 10 minutes (the equivalent of the respective TIMEX image composition) was performed. Results shown that the coastline extracted from TIMEX image (Figure 6.2B) corresponds to R75% which is equivalent to 32% of the maximum run-up.

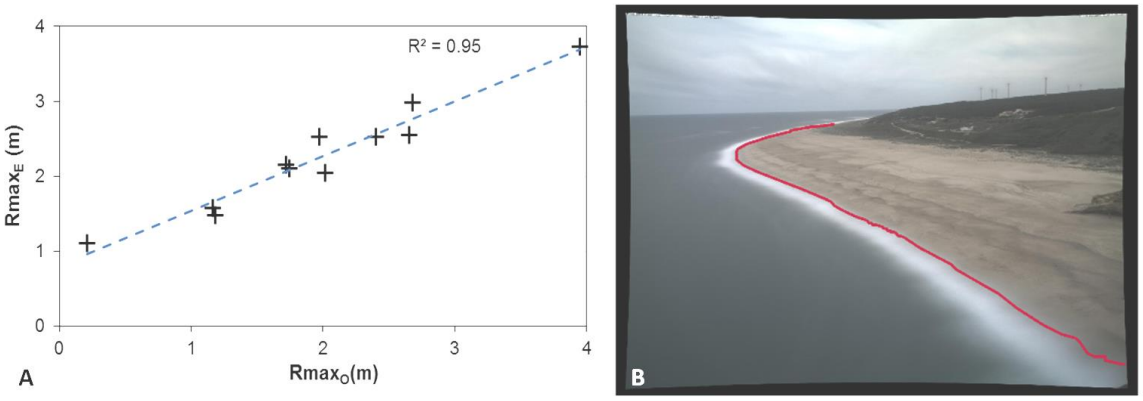


**Figure 6.2 - (A) Relation between measured water level at Norte beach and the water level estimated based on empirical formula (B) Timex (10 minute image) acquired during the water level survey with the coastline detected using maximum likelihood classification.**

Using the aforementioned relationships, TWL was computed using the following expression (Equation 6.2):

$$TWL = 0.32 \times Rmax + AT \qquad \textbf{Equation 6.2}$$

Representative monthly shorelines were extracted from TIMEX images where TWL was within 2 ± 0.15 m, resulting in 31 georeferenced coastlines.

A total of 54 points where used to estimate the horizontal and vertical components of the displacement between the coastline detected by the video monitoring and the 2 m height contour level measured in the Norte beach during several field surveys. The results (Figure 6.3) revealed that the vertical uncertainties are in the order of a few tens of centimetres (mean -0.29; root mean square 0.72 m). In what concerns the horizontal displacement, the most relevant component for shoreline positioning, the displacements are of few meters (mean -2.41m; root mean square 5.30 m).

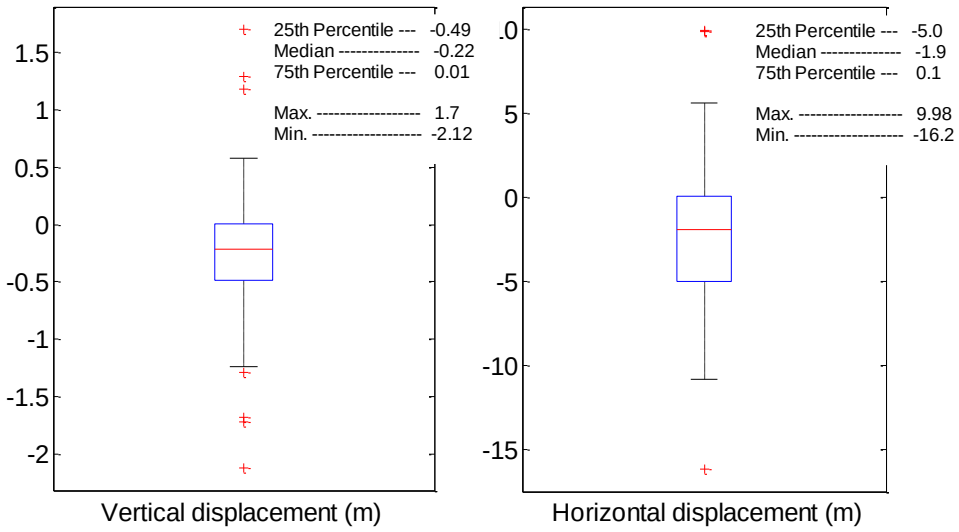


**Figure 6.3 - Vertical and horizontal uncertainties related to the video monitoring coastline detection.**

## 6.4.2. SHORELINE CHANGES

The coastline position during the monitoring period, which extends from December 2008 to May 2012, reveals that the Norte beach presents a huge coastline variability, with an amplitude that exceeds 160 m (Figure 6.4A). The spatial distribution of these changes is

clearly asymmetric, with a northern sector less variable than the southern one. The larger amplitudes are found at transects 2 and 3, progressively decreases up to the transect 7 (about 800 m northward of the headland), where the amplitude of shoreline variation attain a magnitude of about 70 m; northward of this transect it remains approximately constant (Figure 6.4A and Figure 6.5). The apparent particular behaviour at transect number 1 is related to the smaller number of coastlines that extents to the vicinity of the Nazaré headland (only in 10 out the 31 coastlines there was a beach at transect location).

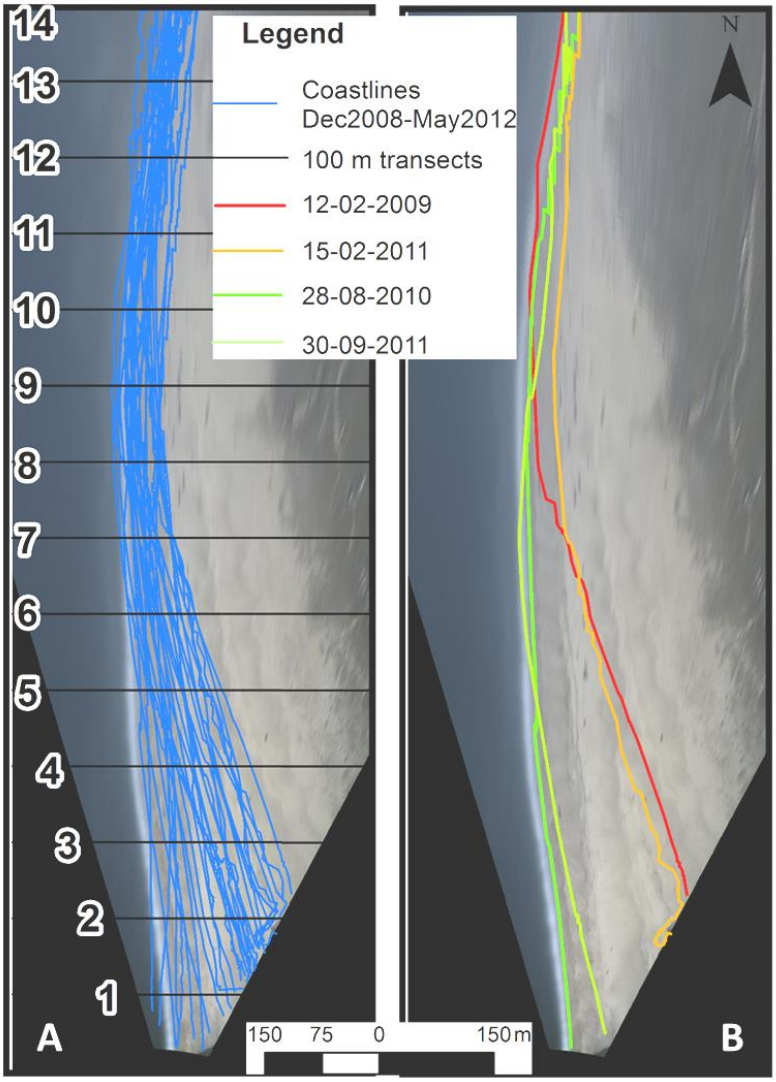


**Figure 6.4 - (A) Coastline positions during the video monitoring period and (B) examples of typical summer and winter coastlines at Norte beach.**

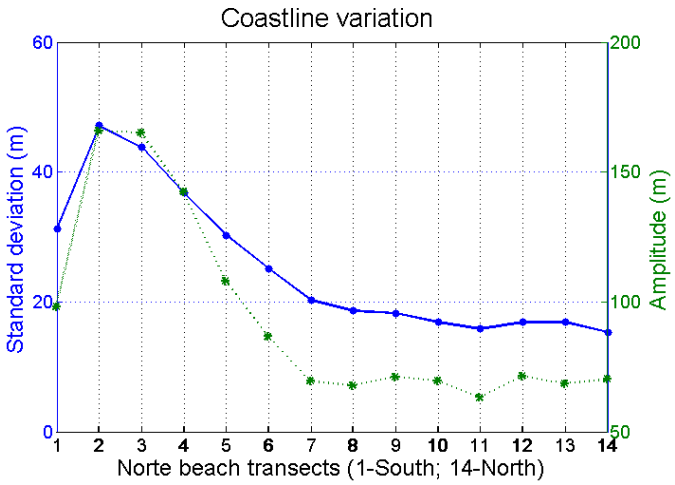


**Figure 6.5 - Norte beach coastline variation along the 14, 100 m spaced, transects.**

The variability of shoreline position at each transect was also investigated through the computation of the standard deviation of the coastline position (Figure 6.5). This parameter revealed a similar pattern, with the higher values in the southern sector of the beach, up to the 7th transect.

The beach behaviour also presents a high seasonality that in the summer periods is characterized by a very large beach, particularly in the southern sector up to the 7th transect, with a straight configuration (generally from June to August) while in the winter the beach presents an arcuate configuration (more typical of the remaining months of the year) (Figure 6.4B).

The deviation of the beach relating to its mean position during monitoring period (Figure 6.6A) also presents a very different pattern between the northern and southern sections of the beach. The transect located northward (14) do not show a clear evidence of seasonality effects, the higher beach accretion occurred during the March 2009, July 2009 and during December 2011 and January 2012.

At the southern section (represented by transect 3), the beach displays a strong seasonal signal (Figure 6.6A) with a huge beach advance during the months between July and October that sometimes reach about 60 m (in relation to its mean position). On the opposite the maximum beach retreat occurred during February and March

Despite the video monitoring gaps in the early 2009 (absence of data in April, May, July, August and September) the coastline position of June 2009 displays the beach advance in the summer of 2009.

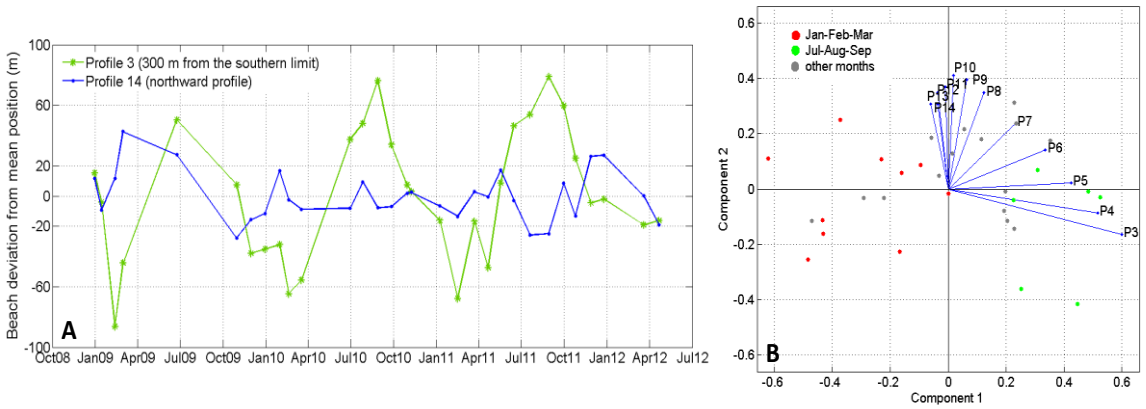


**Figure 6.6 - (A) Norte beach coastline variation during the monitoring period on transects number 3 and number 14 (B) and principal component analysis (PCA) of the Norte beach variability.**

## 6.5. DISCUSSION

The characteristics of coastline variability at Norte beach were investigated using PCA. This analysis was applied to the coastline variation time-series along the 14 transects, the derived components represent modes of longshore variability and an associated set of temporal coefficients (cf. Miller and Dean, 2007).

Results showed that the variability can be explained by two major components which explain 90 % of the system variability. Although results or components should be considered a mathematical abstraction with no direct physical significance they provide a simple and objective description of the system behaviour.

The first PCA component, which by itself accounts for 68 % of the shoreline variability, is connected to the behaviour of the southernmost transects particularly transects 3 to 5 (Figure 6.6B), representing therefore the beach width at the southern section of the Norte beach. The shoreline variability mode related with component 1 progressively fades out northward, while component 2 starts to increase its influence; at transect 9 the shoreline variability is essentially correlated with component 2, related to the beach width at the northern section particularly visible at transect 10.

Considering the time-series of the two main modes of shoreline variability at Norte beach (Figure 6.7) it can be seen that:

1) Component 1 have the highest positive values during the months of July, August and September, while negative values are observed in January, February and March (Figure 6.4 and Figure 6.6). This evident seasonal behaviour is linked with seasonality of incident wave regime, with beach accretion rotated northwards, inducing a southward longshore drift

that progressively infill the southern section of the beach until the headland retention capacity is exceeded. During winter months the waves approaching more southerly than average invert the typical longshore drift direction resulting in the retreat of the shoreline near the headland. This process is responsible for the complete erosion of the beach at transect 1 and, sporadically, at transect 2.

2) Component 2 apparently does not have any seasonality with maxima at October/November 2010 and March 2009 minima at January/February 2011 and July/August 2011. This apparent lack of seasonality seems to be related with the time lag between the wave forcing and the shoreline response of the northern, less variable, sector of the beach.

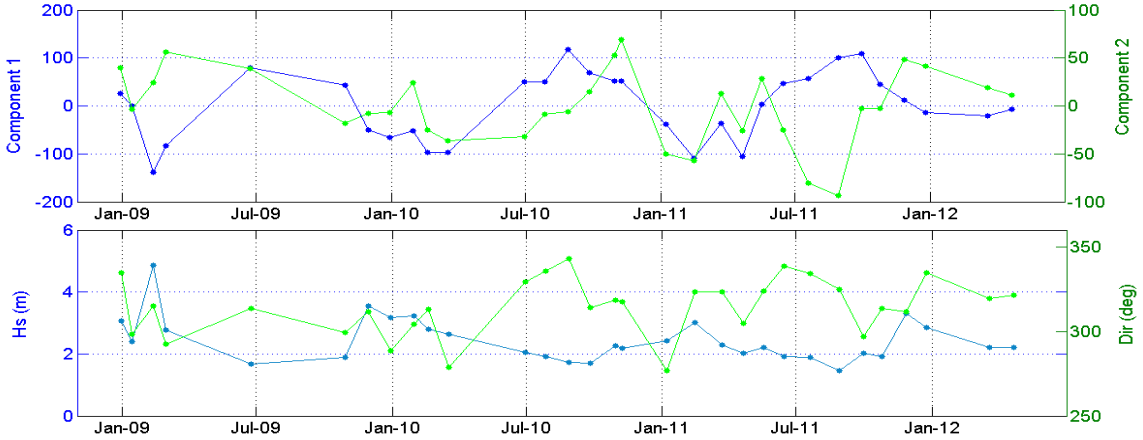


**Figure 6.7 - Temporal variability of the two first non-normalized PCA scores (top), and time of monthly average wave significative height (Hs) and direction (Dir) (bottom).**

## 6.6. CONCLUSIONS

This work describes the shoreline variability at Norte beach, Portugal. Results show a rare high seasonal coastline variability which exceeds 160 m in the southward sector (adjacent to the headland) and 70 m at the central sector and northern sectors (transect 7 to 14).

Coastline variability was related with modifications in the planform beach configuration: beach oscillates between a straight (generally from June to August) and an arcuate configuration (during the remaining of the year).

Results suggest that Norte beach variability depends mainly on longshore drift gradients rather than with cross-shore sedimentary transfers. The intense wave refraction over the canyon head, associated with the westerly swell waves , generates a sedimentary

convergence at the centre of the beach promoting the increase of the beach curvature, while, northern and/or short waves (more frequent in summer) tend to linearize the beach.

This work, supported on video monitoring techniques, contributes with valuable information about the sedimentary dynamics of the Norte beach. Results show that the shoreline changes, in what concerns magnitude and time of response, make the Norte beach a suitable location to estimate the magnitude of the longshore drift and its relation with the oceanographic forcing.

## 6.7. ACKNOWLEDGEMENTS

This work is a contribution and is funded by the project MOWADI - 3D MOrphodynamic modelling of WAve Dominated Inlets (PTDC/ECM/103801/2008), supported by FCT (Foundation for Science and Technology). It benefits from a contribution of the project B2C - Beach to Canyon Head Sedimentary Processes (PTDC/MAR/114674/2009), supported by FCT.

The first author was conferred a PhD grant by FCT (ref. SFRH / BD / 41762 / 2007).

# CHAPTER 7

# Norte Beach Morphodynamics – Long-term perspective through video monitoring

# CHAPTER 7 – NORTE BEACH MORPHODYNAMICS – LONG-TERM PERSPECTIVE THROUGH VIDEO MONITORING

**This chapter is based on a manuscript (in press by Springer) as a chapter contribution for the Book "Remote Sensing and modeling: Advances in Coastal and Marine Resources"**

Ana Nobre Silva and Rui Taborda, 2014 (in press). "Advances in Video Monitoring of the Beach and Nearshore: The Long-Term Perspective", In: Remote Sensing and modelling: Advances in Coastal and Marine Resources, Coastal Research Library 9, Finkl, C.W. and Makowski, C. [Eds.], Springer International Publishing, Switzerland. DOI: 10.1007/978-3-319-06326-3_11.

## 7.1. ABSTRACT

It is widely recognized that video monitoring systems are excellent tools in coastal morphodynamic studies as they can capture, simultaneously, beach morphological changes and the forcing mechanisms. Over the last years this remote sensing technique has experience huge developments related not only to technology advances but also to the success of numerous applications reported by the scientific community.

Since the first steps of video monitoring of the coastal zone, made by the Coastal Imaging Laboratory of Oregon University in the 80's, several years have passed by enabling the existence of long-term imagery records. The existence of extended high-resolution time-series make possible to broaden typical video application studies from short-term studies to annual (or longer) time scales as morphological inter-annual variability of the coastal systems is still largely unknown.

This work summarizes recent developments on the use of video systems in the under-standing of yearly to decadal beach morphological changes and describes the application of a video system deployed at Nazaré, Portugal. The system, operational since December 2008, allowed a detailed description of the coastal evolution at a pluriannual timescale. Results, which are in agreement with previous works, indicate that system variability depends not only on the forcing characteristics that occur at different time-scales (storm, seasonal and inter-annual) but also on antecedent morphology. The use of video systems arises as an optimal data acquisition method to capture this variability and thus support the fully understanding of beach morphodynamics at these wide range of spatio-temporal scales.

## 7.2. INTRODUCTION

Beaches are, by nature, extremely dynamic systems. The processes acting on these environments range from short spatio-temporal scales, as waves or storm events, to longer ones, related to beach seasonality, interannual variability or even long-term coastal evolution. In order to understand this dynamics (including those related with climate change effects), and to support adequate management policies, it has been long recognized the importance of developing long-term monitoring programs.

Until recently, long-term data sets typically consisted of low frequency and spatially limited topographic surveys that aimed to characterize beach seasonality and evolution, but often fail in the characterization of high-frequency events such as storms effects or post-storm recovery because of its low temporal resolution. This could have strong consequences in the understanding and interpretation of system dynamics as the continuous interaction between the forcing mechanisms and the morphology is added to system complexity. In fact "snapshot" monitoring approach can be of little added value in the understanding of beach dynamics, as system behavior depends on the antecedent morphology (Wright and Short, 1984; Alegria-Arzaburu and Masselink, 2010; Quartel et al., 2008) and on the non-linear system dynamics that can lead to chaotic behavior (Vriend and Capobianco, 1993; Southgate et al., 2003; van Enckevort and Ruessink, 2003b). Thus, beach dynamics cannot be fully understood using only low-frequency data.

Currently the importance of developing long-term high-resolution monitoring pro-grams is rather consensual (Larson et al., 2003; Larson and Kraus, 1994; Smit et al., 2007; Southgate et al., 2003; Harley et al., 2011). A review of multi-decadal and high resolution coastal monitoring programs is presently in (Harley et al., 2011).

Long-term monitoring can be supported by a wide range of techniques that, over the last years, have experienced large developments. From the plethora of available methods, video monitoring has emerged as one of the most effective techniques. Video monitoring is supported on the fact that most of the nearshore phenomena that can be visually discerned can be quantified thought video image processing techniques (Holman et al., 1993, Holland et al., 1997; Aarninkhof, 2003; Holman and Staney, 2007). Considering these features and the ease and safety of operation (only minor logistic and financial commitments is needed compared to in situ measurements in a hostile surf zone environment). These characteristics makes video systems adequate to serve long-term monitoring programs with high-resolution in time (Smit et al., 2007).

The main objective of this work is to summarize recent developments on the use of video systems in the understanding of long-term (yearly to decadal) beach morphological

changes and to demonstrate the use of such a video-monitoring system deployed at Nazaré (Portugal).

## 7.3. PLURIANNUAL VIDEO MONITORING PROGRAMS

Since the first steps of video monitoring of the coastal zone, made by the Coastal Imaging Laboratory (CIL) of Oregon University in the 80's, several years have passed by enabling the existence of long-term imagery data that relates the oceanographic pro-cesses with the beach response.

The existence of extended high-resolution time-series makes possible to broaden typical video application studies from short-term studies to annual (or longer) time scales, which is a major improvement for coastal region planning and management (e.g. Liu et al., 2012; Davidson et al., 2007), for the correct formulation of conceptual behavior models (e.g. Kroon et al., 2008) and even for better understand the processes and improve the modelling strategies (e.g. Siegle et al., 2007, Southgate et al., 2003 and Larson et al., 2003).

Despite the importance of pluriannual studies, the number of published works that have been supported in more than three years video data still is relatively small (Table 7.1). Most of the references found in literature refers to ARGUS monitoring system, the pioneer system from CIL, even though nowadays several similar coastal monitoring systems exists (see (Taborda and Silva, 2012)).

The first long-term work (Holland, 1998) refers to the study of the timing of cusps formation and its relation with the environmental forcing from nearly 9 years of daily video images.

Soon after, new long-term studies started to develop mainly focusing the study of sand bars and/or nearshore morphology where 10 and 9 years period of daily sandbars monitoring can be found (Konicki and Holman, 2000) amongst several other authors that investigate bar dynamics in a less continuous approach (e.g. Siegle et al., 2007; Armaroli and Ciavola, 2011) quantifying particular episodes occurring during the time span of the video monitoring.

For instance, Siegle et al. (2007) use the video images to extract the intertidal morphology which supports the morphological modelling at a frequency that is dependent on the model required resolution, whereas (Armaroli and Ciavola, 2011) propose a morphological classification of outer bars based on its plan shape visible on TIMEX images spanning from February 2004 to May 2007.

Almar et al. (2008) performed a long-term study analyzing beach cusps through discrete episodes by selecting 24 beach cusps episodes (from 1999 to 2001) and analyzing its evolution.

The shoreline pluriannual evolution and variability is also a theme starting to rise in video monitoring searches by means of the shoreline response to storm events (Alegria-Arzaburu and Masselink, 2010) or to address the interannual coastline tendencies and behaviors (Smit et al., 2007; Foster, 2012 and Silva et al, 2013).

## 7.1. CASE STUDY

In order to demonstrate the applicability of a video system in the understanding of long-term of beach morphodynamics, a case study of a pluriannual monitoring program, at Nazaré (Portugal), is presented. It is clear that the coastline position and the beach volume are ultimately related to a fragile balance between relative sea-level positioning, sediment supply and wave forcing, acting at different time scales. Masselink and Pattiaratchi (2001) classify the beach change into two categories the "seasonal" that comprehend the winter/summer characteristic beach behavior and the "cyclic" where the main changes are related to the storm and post-storm changes on the beach, nevertheless in both cases the morphological change is primarily due to changes in incident wave energy. A "chaotic" category can be added into this list, where the beach behavior is also deeply dependent on the antecedent morphology of the beach (cf. Wright and Short, 1984; Wright et al., 1985; Quartel et al., 2008 and Alegria-Arzaburu and Masselink, 2010).

The join contribution of these three beach behaviors can led to an extremely high dynamic system that is often difficult to fully understand.

The presented case study aims to describe and interpret video-derived beach volume variations along nearly three and half years of monitoring and investigate its relation with incident waves, in order to contribute to the understanding of beach behavior at different temporal and spatial scales.

**Table 7.1 - Pluriannual monitoring programs based on more than 3 years of video data.**

| *Aim* | Video monitoring | | Reference |
|---|---|---|---|
| | Time span (years) | System | |
| ***Beach cusps*** | 8.9 | Argus | (Holland, 1998) |
| ***Transverse sandbars*** | 10 | Argus | (Konicki and Holman, 2000) |
| ***Sandbar morphology*** | 3.4 | Argus | (van Enckevort and Ruessink, 2003a) |
| ***Nearshore sandbars*** | 3.4 | Argus | (van Enckevort and Ruessink, 2003b) |
| ***Sandbar location; shoreline location*** | - | Argus | (Alexander and Holman, 2004) |
| ***Outer sand bar migration*** | 9 | Argus | (Haxel and Holman, 2004) |
| ***Nearshore morphodynamics*** | ~4 | Argus | (Ranasinghe et al., 2004) |
| ***Sandbar morphodynamics*** | 3.2 | Argus | (Siegle et al.,, 2007) |
| ***Shoreline evolution*** | 4.5 (with video) | Argus | (Smit et al.,, 2007) |
| ***Rips*** | 3 | Argus | (Turner et al.,, 2007) |
| ***Beach cusps*** | 3 | - | (Almar et al.,, 2008) |
| ***Beach users*** | 4 | Argus | (Guillén et al.,, 2008) |
| ***Nearshore bars*** | 4 (with video) | Argus | (Kroon et al.,, 2008) |
| ***Storm response beach morphology - shoreline*** | 3 | Argus | (Alegria-Arzaburu and Masselink, 2010) |
| ***Outer bar*** | 4.5 | Argus | (Armaroli and Ciavola, 2011) |
| ***Sand bars*** | 4.3 | Argus | (Ojeda et al.,, 2011) |
| ***Nearshore morphology*** | 4.3 | - | (Liu et al.,, 2012) |
| ***Shoreline variability and beach rotation*** | 3 | Cam-Era | (Foster, 2012) |
| ***Shoreline variability*** | 3.4 | Cosmos | (Silva et al., 2013) |

### 7.1.1. STUDY SITE

Norte beach (Nazaré) is located at the west Portuguese coast (Figure 7.1), is roughly N-S oriented and subject to a high energetic wave regime, generated at the Northeast Atlantic.

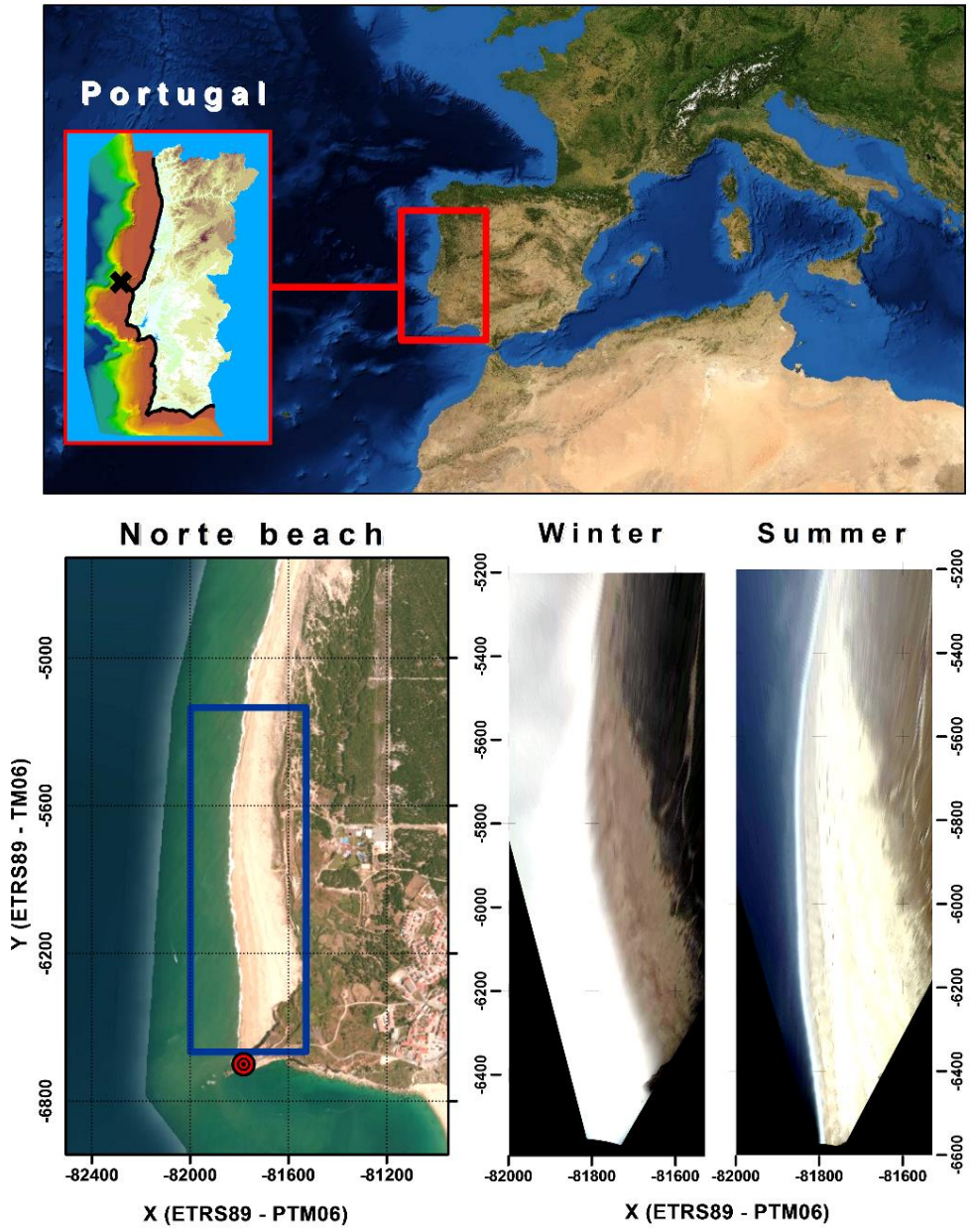


**Figure 7.1 - Study site with reference to the position off the offshore wave buoy (black cross), the video monitoring extent (blue rectangle) and video camera position (red circle) (Imagery Source: Esri, DigitalGlobe, GeoEye, i-cubed, USDA, USGS, AEX, Getmapping, Aerogrid, IGN, IGP, swisstopo, and the GIS User Community); The bottom right images represent examples of video derived rectifyed images of Norte beach in winter and summer condition.**

Wave propagation over the Nazaré canyon head is responsible for unusual high waves (that can exceed 20 m) near the beach. Norte beach is a reflective beach characterized by a wide berm (or multiple wide berms at summer) and a steep beach face. It is subject to a mesotidal regime, with tidal amplitudes ranging from 1.5 m to 3.5 m, at neap and spring tides, respectively. Average offshore wave regime, obtained by 56 years hindcast data for the northwest Portuguese coast (Dodet et al., 2010) can be described by 2 m significant wave heights, 11 s of average peak period and mean wave direction approaching from ENE-NE (308°). Sediments are characterized by quartzic sand with dimensions variable from -2.6 $\phi$ to 1.79 $\phi$ and mean value 0.18 $\phi$ (Cascalho et al., 2012).

In what concerns morphodynamics, Norte beach can be individualized into two main sectors, one in the vicinity of the Nazaré headland where the seasonal variability, expressed through the position of the shoreline, is extremely high (seasonal changes exceed 160 m); and one sector less variable and less seasonal imprinted where the amplitude of coastline changes do not exceeds 75 m (Silva et al., 2013).

## 7.1.2. METHODS

### 7.1.2.1. VIDEO MONITORING

A video monitoring system has been operational in Norte beach since December 2008. The COSMOS coastal monitoring system (Taborda and Silva, 2012) installed at Forte S. Miguel Arcanjo, Nazaré, consist of a 3.1 megapixel resolution camera mounted at about 50 m high relatively to MSL which is acquiring snapshot images at 1Hz, during 20 minutes interval each daylight hour. The geometric correction of the images, including the correction of the image distortions and image rectification, followed respectively the Heikkila and Silvén (1997) distortion model and the collinearity condition (Wolf and Dewitt, 2000), a detailed description of these procedures can be found in Taborda and Silva (2012) and Silva et al. (2009).

TIMEX images were computed using 10 minute block of snapshot imagery. To access shoreline changes between December 2008 and May 2012, a monthly TIMEX image was carefully chosen based on the same total water level (TWL). The 2 m value was selected in order to constrain the run-up level to the high slope beach (therefore minimizing the horizontal errors) and to assure comparable conditions. Despite some gaps, due to technical failures, a total of 31 images where analysed during the 3.5 years of monitoring presented in this study.

The shoreline herein defined as the 2 m height contour line was detected through image processing and analysis on the selected TIMEX images. Sand and water where automatically classified using the maximum likelihood method. Due to different image luminosity conditions, related to atmospheric conditions and the high variable extent of the breaking zone, four different spectral signatures were used. Shoreline detection results were visually validated and about 6% of the initially selected images were rejected and replaced by similar ones.

The estimation of the shoreline elevation (or total water level), comprehensively de-scribed in (Silva et al., 2013), was done adopting an empirical site specific formula which estimates the run-up height in function of the offshore significative wave height (Hs), the offshore wave direction (Dir) and the astronomical tide (AT).

#### *7.1.2.2. BEACH VOLUME*

To estimate the beach volume from the shoreline position it was necessary to assume a representative beach profile configuration along the study area. This profile model was based on the fact that the configuration of the surveyed transverse beach profiles was found to be highly uniform in what concerns the beach face and backshore slope (beach profile terms follows Shore Protection Manual;  CERC, 1984).

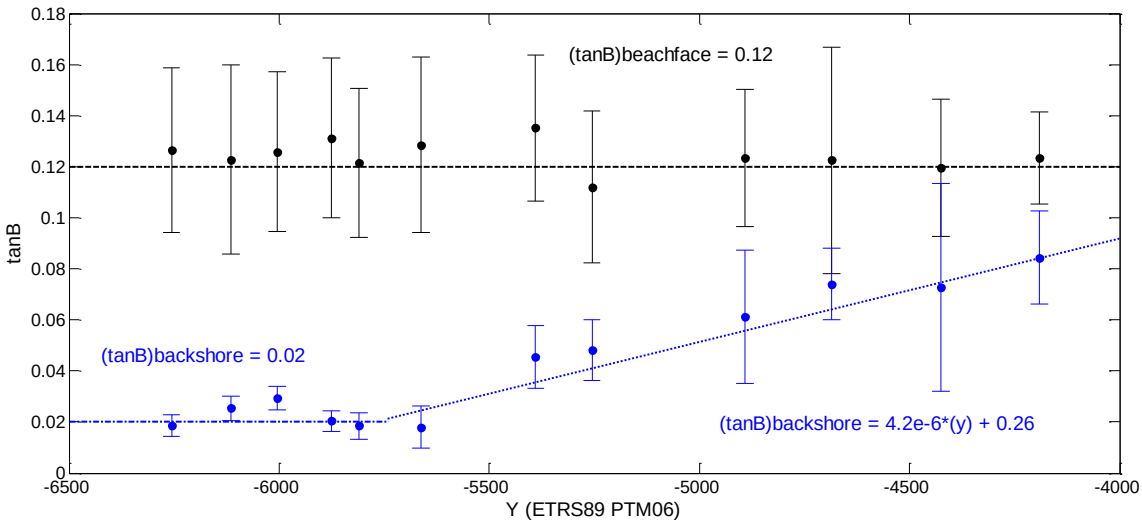


**Figure 7.2 - Alonsghore beach face slope (black) and backshore slope (blue) variability (the equation represent the model fitted to the alongshore backshore slope (Y coordinate of the ETRS – PTM06 coordinate system).**

The mean beach face slope (tanβ) was found to be spatially uniform, ranging from 0.10 to 0.16, with an average value of 0.12 along the entire surveyed stretch. The backshore slope exhibits longshore variations that enables to individualize the beach in two sec-tors: a southern sector where the backshore slope is rather mild and uniform (0.02); a northern sector where this slope increases northward from a value of 0.02 up to 0.08 at about 2 km north of Nazaré headland (Figure 7.2).

The profile model, represented in Figure 7.3, was developed considering two fixed points: one that represents the maximum seaward extent of the profile (the shoreline position, i.e. 2 m MSL contour line) and another that is the landward limit of the beach (the dune base represented by the 8 m MSL contour line). Below the 2 m contour and up to the closure depth the profile was extended using the equilibrium Dean profile (Dean, 1991; with an A parameter that best fitted the submarine profile data acquired from LiDAR data).

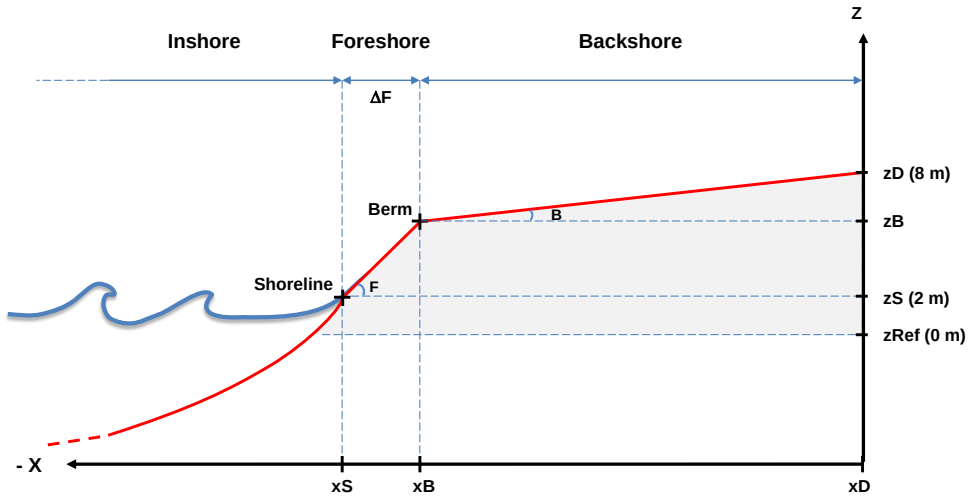


**Figure 7.3 - Schematics of the Norte beach profile model.**

From the knowledge of shoreline position (xS(y,t) acquired by video), dune foot coordinates (xD(y), zD acquired by a GPS survey and considered steady), representative foreshore slope (tanF) and backshore slope (tanB(y)), the berm position (xB(y,t); zB(y,t)) along Norte beach at given time (t) can be estimated from simple geometric considerations using Equation 7.1 and Equation 7.2.

$$xB(y,t) = xS(y,t) + \Delta F(y,t) \qquad \textbf{Equation 7.1}$$

$$zB(y,t) = zS + tanF \times \Delta F(y,t) \qquad \textbf{Equation 7.2}$$

where

$$\Delta F\,(y,t) = \frac{(zD - zS) - tanB(y) \times (xD(y) - xS(y,t))}{tanF - tanB(y)} \qquad \textbf{Equation 7.3}$$

and ΔF(y,t) is the foreshore width and zS the shoreline elevation (2 m) (Defined by Equation 7.3; Figure 7.2).

The comparison of the above profile model and the surveyed profiles is exemplified in Figure 7.4, using winter and summer profiles at two Norte beach sites. Both profiles extend between the dune foot and the 0 m contour. The profile model seems to be a good estimator of the real profile area even when the beach presents a multiple berms system (Figure 7.4).

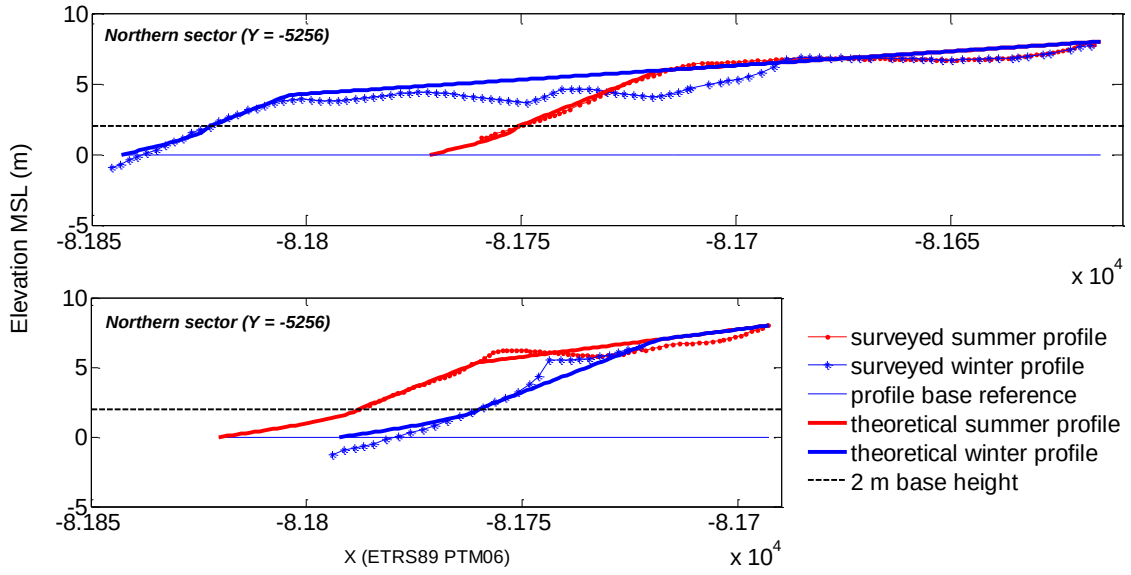


**Figure 7.4 - Comparison between theoretical and surveyed profiles at two different locations at Norte beach (top and bottom).**

Using the profile model and the video-derived shoreline, the beach volume was estimated, at a monthly basis, from December 2008 and May 2012. Total volume estimation, for the investigated area (between -6350 and -5210 coordinates, Y ETRS89-PTM06), was based on trapezoidal numerical integration with a longshore discretization of 5 m.

Normalized beach volume (VD (y, t)) was computed at each transect (y) by (Equation 7.4):

$$VD(y,t) = V(y,t) - \overline{V(y)} \qquad \textbf{Equation 7.4}$$

where V(y, t) is the volume estimated for each alongshore position (y) at a given time (t) and $\overline{V(y)}$ the average volume for the y alongshore position.

#### 7.1.2.2.1. MODEL VALIDATION

The beach volume model validation was performed by comparing the results with the ones obtained from methods that allow complete beach coverage: airborne LiDAR (Light Detection And Ranging) data, four-wheel all-terrain vehicle RTK-DGPS topographic surveys and aerial photogrammetry-derived digital terrain models (DTMs) (Table 7.2).

**Table 7.2 - Digital terrain models (DTMs) used in volume validation.**

| *Date* | DTM description | Scale/resolution | Credits |
|---|---|---|---|
| ***2001*** | Aerial photogrammetric-derived | 1:2000 | INAG – Instituto da Água |
| ***2008*** | Aerial photogrammetric-derived | 2 m | IGP – Instituto da Água |
| ***2011 (May)*** | RTK-DGPS topographic survey-derived | 5 m | Beach to Canyon Project |
| ***2011 (Jun-Dec)*** | Topo-bathymetric LiDAR-derived | 2 m | IGP– Instituto Geográfico Português |

Due to some inconsistencies found in LiDAR data, particularly in the area where the bathymetric and terrestrial LiDAR data was merged, beach volumes were only estimated up to the 2 m height reference. The same height reference was adopted for the May 2011 DTM because the survey did not reached the 0 m (MSL). Beach volume was estimated,

using ArcMap© surface volume tool, for the four DTMs, above 2 m height and above the 0 m height plane for the DTMs of 2001 and 2008 (Table 7.3).

The comparison between model and measured volumes show a maximum overestimation lower than 7 % and an underestimation that does not exceed 4 %. These results, which also depend on the quality of the measured data, validate the volume model used in the present work.

**Table 7.3 - Results for validation of the North beach model volume.**

| *MDT* | Reference height (MLS) | Volume $m^3$ | | Difference (%) | Length of beach compared (m) |
|---|---|---|---|---|---|
| | | Beach volume model | Measured | | |
| ***2001*** | 0 m | $11.99\times10^5$ | $1.12\times10^5$ | 6.67 | 1140 |
| | 2 m | $7.11\times10^5$ | $7.36\times10^5$ | -3.32 | |
| ***2008*** | 0 m | $11.56\times10^5$ | $10.88\times10^5$ | 6.29 | |
| | 2 m | $7.02\times10^5$ | $7.21\times10^5$ | -2.67 | |
| ***2011 (May)*** | 2 m | $6.01\times10^5$ | $5.66\times10^5$ | 6.10 | 1010 |
| ***2011 (Jun-Dec)*** | 2 m | $6.33\times10^5$ | $6.36\times10^5$ | -0.47 | 1140 |

#### *7.1.2.3. WAVE FORCING*

The characterization of the wave regime during the monitoring period was performed based on offshore wave data acquired by MONICAN01, an oceanographic buoy deployed by the Portuguese Hydrographic Institute (MONICAN Project – http://monican.hidrografico.pt/) at c.a. 2000 m depth (Figure 7.1). The gaps in the wave data record (about 8% of the records) were filled with NOAA (National Oceanic and Atmospheric Administration) hindcast for the nearest node, and wave time series was resample to meet the NOAA resolution (3 h interval between samples). In result, a continuous offshore wave time series of the main wave statistics (Hs – Significant wave height; Tp- Peak period and Dir – wave direction), at a 3 h interval was obtained, for the monitoring period. An improved description of the comparison between hindcast and buoy data can be seen in Silva et al. (2013), whereas the root mean square error is 0.39 m, 1.82 s and 23 ° for Hs, Tp and Dir, respectively.

The characterization of high energetic events during the monitoring period, was performed through the description of storms events (defined by a significant wave height threshold of 5 m - if two consecutive storm occurrences were spaced less than 24 hours they were

merged into a single storm). Total storm wave energy (E) was estimated using Dolan and Davis (1992) approximation (Equation 7.5):

$$E = \int_{t1}^{t2} Hs^2 \, dt, \;\; Hs > H_{threshold} \qquad \textbf{Equation 7.5}$$

where t1 and t2 are the start and end times of the storm event and $H_{threshold}$ the significant wave height threshold (5 m).

## 7.1.3. RESULTS

### 7.1.3.1. WAVE FORCING

The reconstructed wave record extends from 1 st December 2008 to 1 st May 2012, and can be characterize by mean significant wave height of 2.36 m, mean peak period of 11.05 s and mean wave direction of 319 °, for the overall wave series (Table 7.4 and Figure 7.5A). The seasonality of wave regime was also analyzed by the individualization of winter months (December, January and February; DJF) and summer months (June, July and August; JJA). Winter is characterized by 3.00 m height waves, mean peak period of near 13 s and waves approaching from 310°, although a wider direction spreading is visible at those months (see Figure 7.5A). Summer months have mean significant wave height of 1.77 m, mean peak period around 9 s and mean wave direction of 334°, with a narrower direction spreading (Table 7.4 and Figure 7.5A).

**Table 7.4 - Offshore wave parameters during the monitoring period (overall), and discretization of winter and summer conditions.**

| | Hs (m) | | Tp (s) | | Dir (°) | |
|---|---|---|---|---|---|---|
| | **mean** | **maximum** | **mean** | **maximum** | **mean** | **mean power** |
| ***Annual*** | 2.36 | 10.25 | 11.05 | 21.90 | 319 | 316 |
| ***Winter (DJF)*** | 3.00 | 9.10 | 12.59 | 21.30 | 311 | 310 |
| ***Summer (JJA)*** | 1.77 | 4.51 | 8.76 | 14.40 | 328 | 334 |

The offshore wave conditions synoptically related to each beach volume estimation were also investigated through the directional distribution of Hs (Figure 7.5B); each plot includes

the waves that occurred in the time interval between two consecutive dates of volume estimation (the represented date refers to the end of the interval).

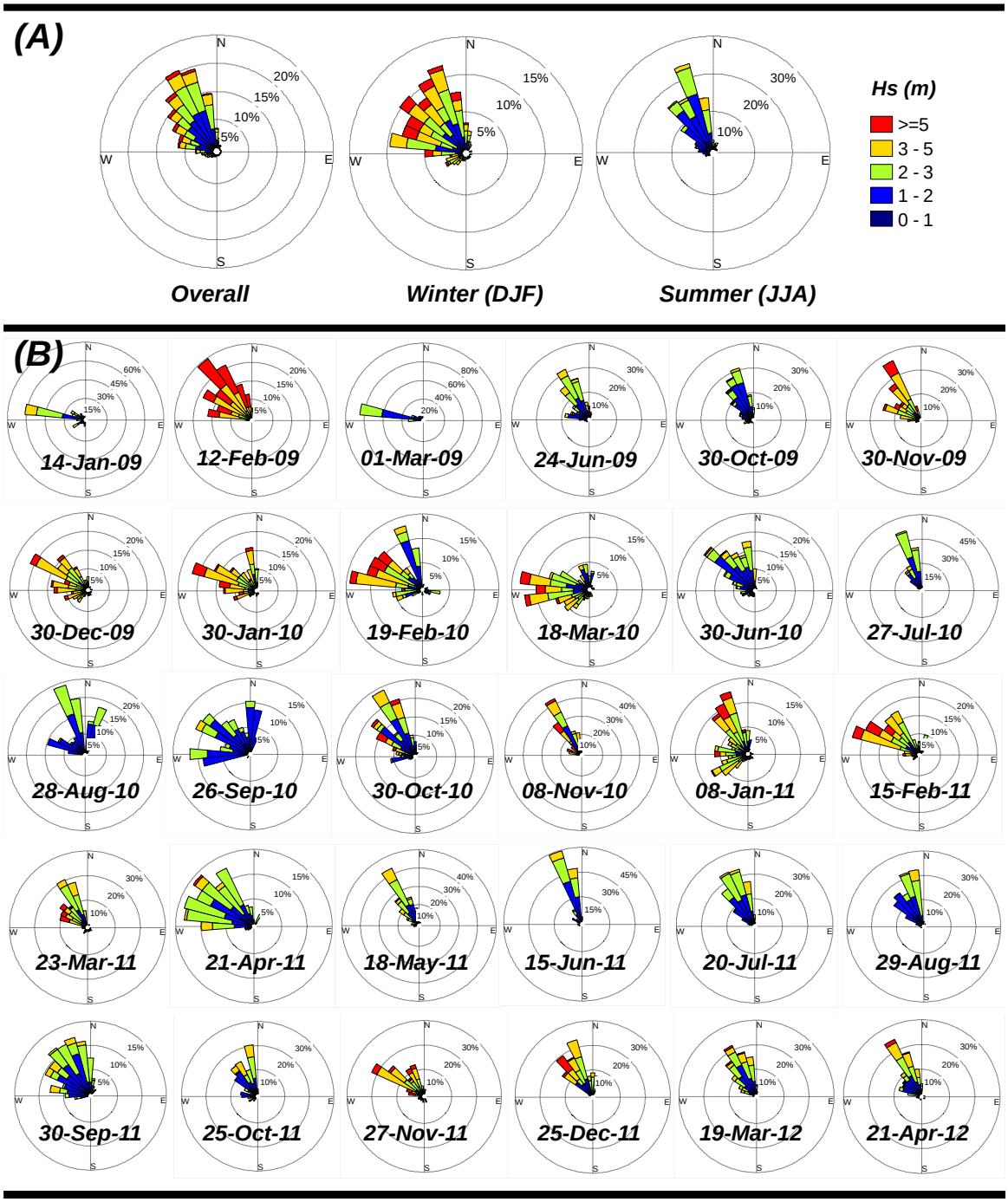


**Figure 7.5 - Offshore wave conditions during the overall monitoring period, winter and summer months (A) and offshore wave conditions between each beach volume estimation (B). (The dates refer to the date of the shoreline from which the volume was estimated).**

These data depicts the seasonal wave energy modulation: summer is dominated by low energetic north-northwest waves with small directional spreading, while in winter the higher energetic waves have a much wide directional spreading. Amongst these directional wave plots some events stand out due to its high waves and wide directional spreading: 12-Fev-09, 19-Fev-10, 18-Mar-10, 08-Jan-11 and 15-Fev-11.

A total of 44 storm events were recognized over the 3.5 year of wave data, the average parameters of the storm conditions is expressed in Table 7.5. The average duration of the storms is slightly longer than a day (1.37 days) with a mean wave direction of 310°.

**Table 7.5 - Average characteristics of the 44 identified storm events.**

| Hs (m) | | Tp (s) | | Dir (°) | Duration (days) | Energy ($m^2h$) | |
|---|---|---|---|---|---|---|---|
| **mean** | **maximum** | **mean** | **maximum** | **mean** | **mean** | **mean** | **maximum** |
| 5.67 | 6.54 | 14.90 | 19.32 | 310 | 1.37 | 1204 | 6201 |

### *7.1.3.2. BEACH MORPHODYNAMICS*

During the monitoring period, total beach volume (above 0 m MSL) ranged from 0.88 × $10^6$ to 1.22 × $10^6$ $m^3$; the amplitude of volume variation was circa 3.4 × $10^5$ $m^3$ which represents about 27% of the total volume above mean sea level.

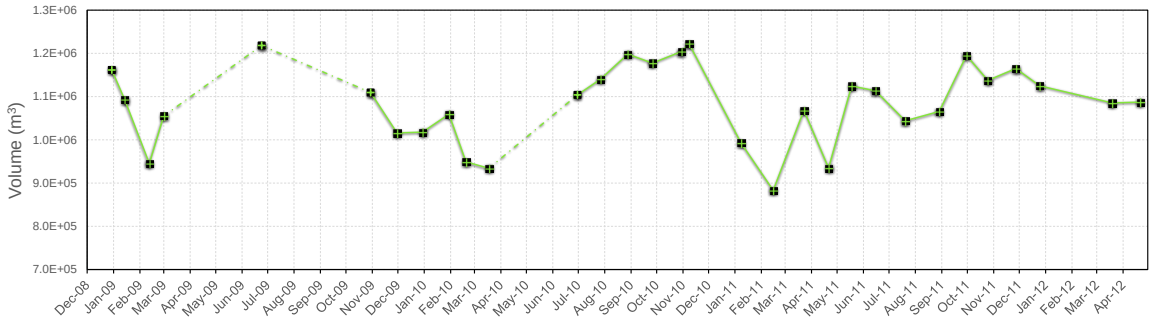


**Figure 7.6 - Total beach volume time series (dashed lines represent monitoring interruptions longer than 2 months).**

Minima values were found to occur in late winter months, Feb/09, Mar/10 and Feb/11, while annual maxima occurred in summer or early autumn (Aug/10 and Sep/11) (Figure 7.6). Superimpose to this behaviour a strong interannual signal is also present: for ex-ample in the Nov/09 beach volume is relatively low while in subsequent years the volume at the same month reaches a value closed to the annual maxima.

Norte beach volume variations also show strong spatial gradients with a complex spatiotemporal pattern which are represented in Figure 7.7 as time stack of volume deviations. The analysis of the alongshore standard deviation of the beach volume considering a cut off value of 100 m (Figure 7.7- Bottom) allows to differentiate the beach into a, more variable, southern sector and a northern sector that is more stable.

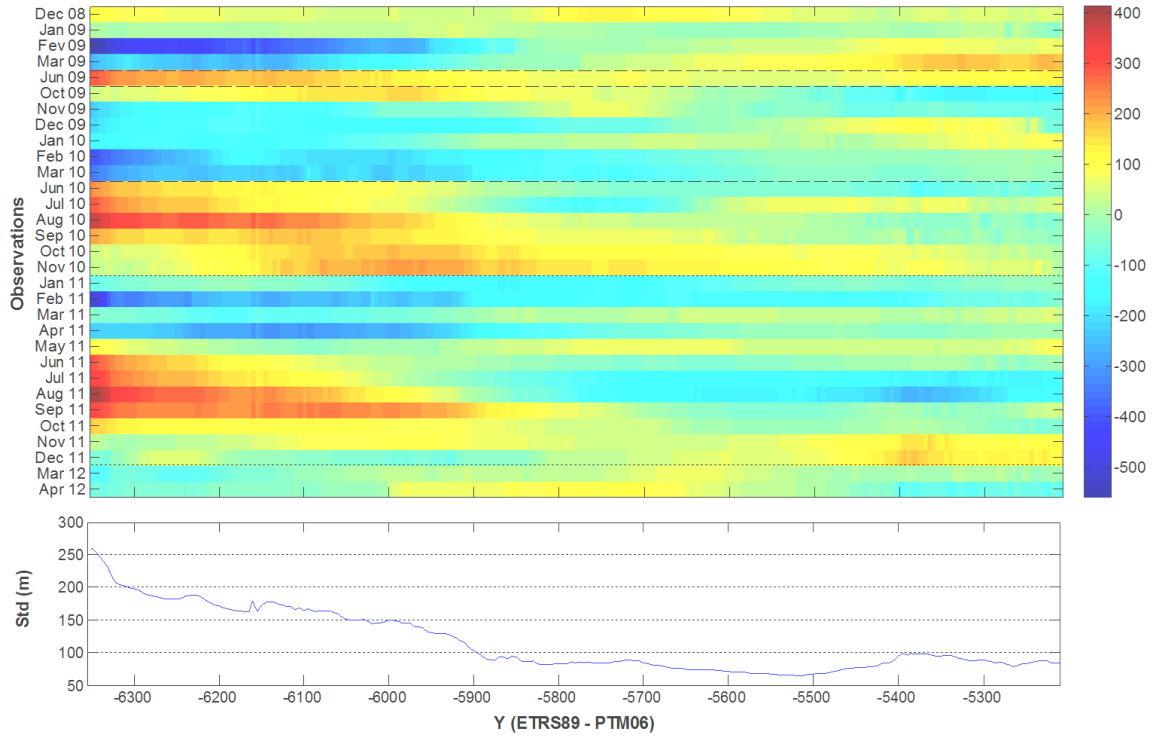


**Figure 7.7 - Time stack of alongshore volume deviation ($m^3$) (top) and standard deviation (Std) of alongshore beach volume (bottom). Long dashed lines represent interruptions longer than 2 months while short dashed lines represent minor (less than 2 months) interruptions.**

The southern sector, adjacent to Nazaré headland (~ -6300 m coordinate), displays a clear seasonal signal similar to the one found for the entire beach: the larger positive deviations are found in August while the minima occurred in February and March. Volume variations

at the southern sector are clearly affected by the presence of the Nazaré headland which acts as a gated sedimentary boundary. At this sector, the morphological responses tend to have a larger magnitude and lag ahead northern changes. In fact, the seasonal signal progressively fades out northward. Additionally, the late summer maxima reveals a spatial delayed phase lag so that at -5900 m coordinate, it occurs in autumn (September to November). At the northern sector the beach volume variability is dominated by the interannual component while the seasonal signal weakens.

The comparison of the total beach volume time series with the offshore incident wave conditions is represented in Figure 7.8**;** weak negative correlation was found for Hs and TP (r = -0.38 in both cases) and a positive, slightly higher, correlation for the wave Dir (r = 0.47). When considering the volume estimated at each sector (Figure 7.9 and Figure 7.10), the correlation improved at the southern sector (r = -0.60, r = -0.69 and r = 0.57 for Hs, Tp and Dir, respectively) and worseness at the northern one (r = 0.17, r = 0.32 and r = 0.06 for Hs, Tp and Dir, respectively). When average wave conditions between volume estimations are considered is possible to get further insights on the North beach morphodynamics response. For example, minimum beach volumes, observed at Feb/2009, Feb/10, Mar/10 and Feb/11, coincide with the more energetic incident wave conditions (Figure 7.5). In contrast, the beach is wider in later summer/early autumn in response to northwest low amplitude waves (for example the period immediately before 28-Aug-10 or 30-Sep-11).

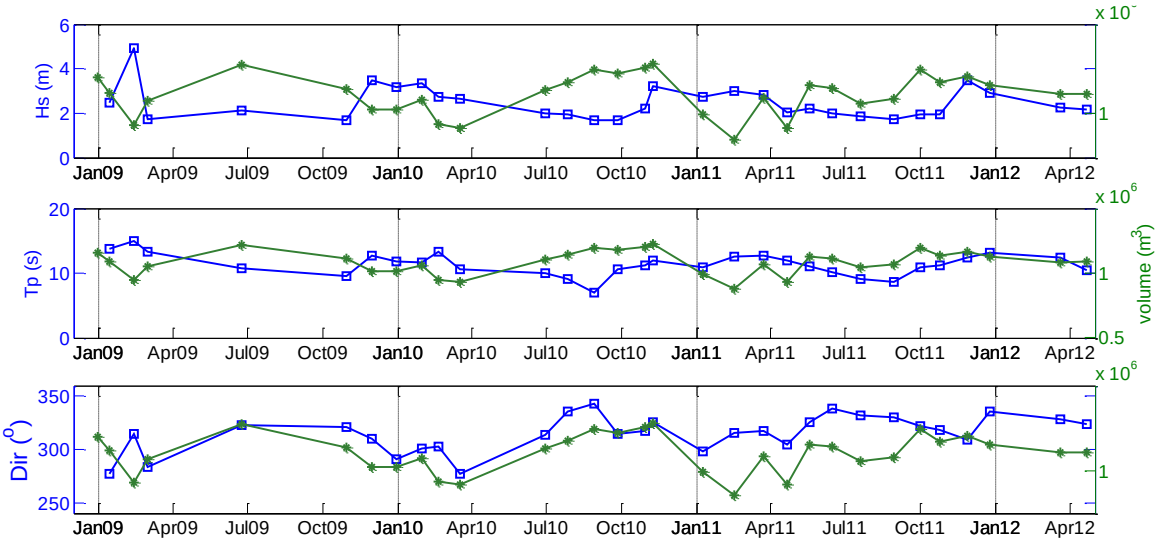


**Figure 7.8 - Time series of total beach volume (green) overlaid with offshore significant wave height (Hs), peak period (Tp) and wave direction (Dir).**

These results support the existence of a relation between forcing and morphologic response, more evident, in the southern sector of the beach. In this sector, beach volume increases in relation with the low energetic, short period, northwest summer waves as they promote southward longshore drift and sedimentary accumulation up-drift of the Nazaré headland. On the other hand, the northern sector exhibits a more stable behavior that is not linearly related to the wave regime. Low frequency phenomena associated to interannual variability and short-term high energetic storm events may play a higher relative influence in this sector of the beach (Figure 7.11).

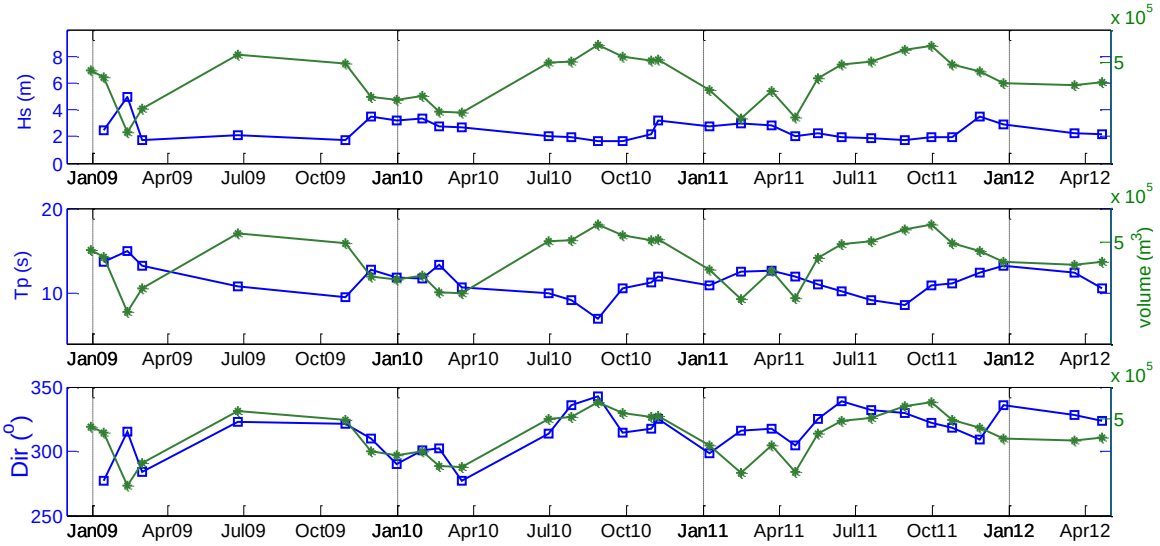


**Figure 7.9 - Time series of beach volume (green), estimated for the Norte beach southern sector, overlaid with off-shore significant wave height (Hs), peak period (Tp) and wave direction (Dir).**

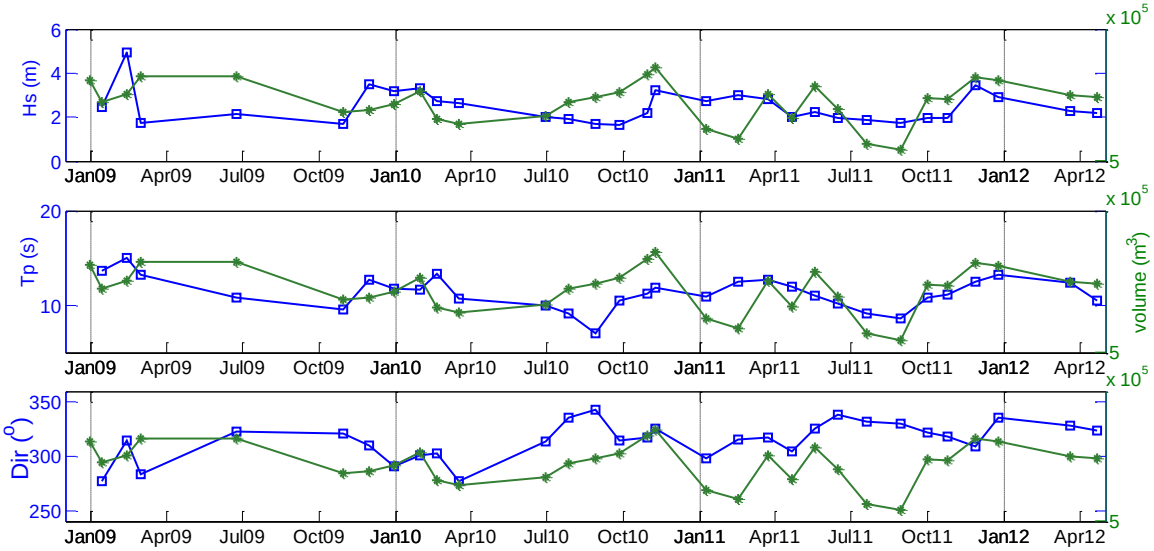


**Figure 7.10 - Time series of beach volume (green), estimated for the Norte beach northern sector, overlaid with off-shore significant wave height (Hs), peak period (Tp) and wave direction (Dir).**

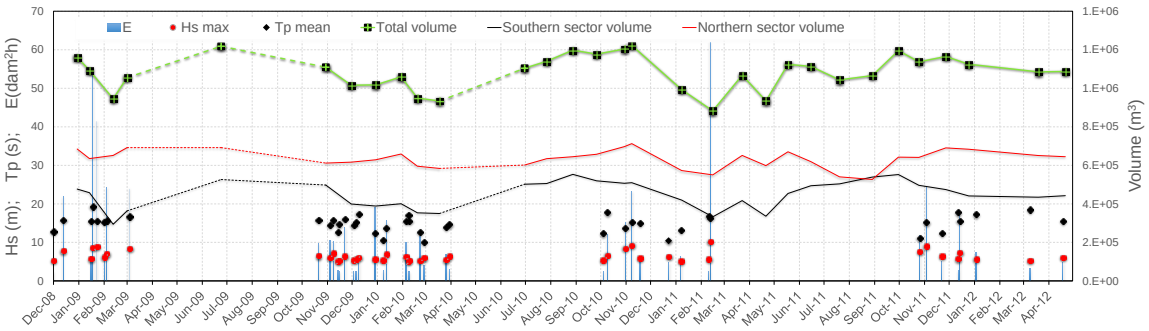


**Figure 7.11 - Norte beach volume time series (total, southern sector and northern sector symbolized by green, black and red lines respectively) and characteristics of storm events (E - Energy, Hs maximum and mean Tp represented by blue lines, red circles and black diamonds, respectively) (dashed lines represent monitoring interruptions longer than 2 months).**

## 7.2. CONCLUSIONS

This work summarizes recent developments on the use of video systems in the understanding of yearly to decadal beach morphological changes. While it is unanimously recognized that these systems have a huge potential, represented for example by the large number of existing systems, the number of long-term studies is still scarce (and mostly supported by the Argus system). This may be related to constraints imposed by the short-term research programs (either in scientific projects or postgraduate programs) that difficult the continuity of monitoring programs. These limitations can be partially overcome

through the implementation of light weighted systems (in what concerns set-up and maintenance costs) combined with simple data exploitation techniques, as exemplified in the case study presented in this work.

In this study the morphodynamics of the Norte beach, Nazaré, Portugal was investigated coupling the wave data acquired by an offshore buoy with beach morphological data derived from video monitoring. The results, encompassing three and a half years of data, enabled to acknowledge the spatio-temporal dependence of the beach evolution in response to incident waves at a large range of temporal scales (storm to inter-annual). This study corroborate previous studies findings which highlight the importance of antecedent morphology in storm response and the connection between longshore and cross-shore processes not only at a seasonal scale but also at an inter-annual scale.

## 7.3. ACKNOWLEDGEMENTS

The authors acknowledge the funding of the PhD grant by FCT (ref. SFRH/BD/ 41762/2007) and the Portuguese Navy for the support in allowing the installation of COSMOS video monitoring system in the Nazaré lighthouse. This work benefits from a contribution of the project B2C - Beach to Canyon Head Sedimentary Processes (PTDC/MAR/114674/2009), supported by FCT.

# CHAPTER 8

# Synthesis of the morphodynamics of the Nazaré coast and Conclusions

# CHAPTER 8 – SYNTHESIS OF THE MORPHODYNAMICS OF THE NAZARÉ COAST AND CONCLUSIONS

**This chapter presents a synthesis and discussion of the Nazaré coast morphodynamic model.**

**This chapter encompasses two main topics: the morphodynamic and sedimentary budget of the Nazaré coast including wave forcing, morphodynamics and the sedimentary budget; and conclusions and future work.**

## 8.1. BEACH MORPHODYNAMICS AND SEDIMENTARY BUDGET

### 8.1.1. WAVE FORCING

#### 8.1.1.1. OFFSHORE

Waves are the primary driver of the coastal morphodynamics thus its correct assessment and characterization is of major importance.

The Nazaré coast is fully exposed to North Atlantic wave regime which is characterized by a predominant swell approaching from the northwest quadrant, superimposed with a less energetic local wind sea with a wider directional spread.

Objective characterization of the wave forcing at the northwest of Portugal goes back to 1966 (Carvalho and Barceló, 1966) where systematic visual estimations were performed at Figueira da Foz. In that work the modal significant wave height is between 1 to 2 m, modal significant period between 9 to 11 s and waves approaching mainly from N80°W to N70°W with a second wave group approaching from SW direction.

In 1979 the installation of wave buoys at several points at the Portuguese coast allowed the compilation of a systematic record of wave characteristics, and subsequently a more robust characterization of the wave regime with results of similar nature.

Costa et al. (2001) and Coelho (2005) reported an important seasonal variability in the wave record with large differences especially between summer and winter month's wave heights. The wave directions also present different behaviours with a predominance of waves approaching from NW and W in summer and an increase of W waves in winter (Costa et al., 2001). In summer wave regime tends to rotate northwards (Coelho, 2005) while the SW and WSW occurrences are more associated with winter months.

Actually, all of these references are based on short and/or non-continuous wave time-series which expose relevant limitations for a correct characterization of the wave climate and its interannual variability. Recent advances in wave modeling and the availability of wind field reanalysis data for the last 60 years has enabled the study of North Atlantic Ocean wave climate since the middle of the XX$^{th}$ century (Dodet et al., 2010 and Pilar et al., 2008).

Based on a hindcast offshore wave time-series data (Dodet et al., 2010), a characterization of the long-term wave statistics was possible, as well as an assessment of the interannual variability of the wave parameters between 1958 and 2008. This study is presented in the *Chapter 5 – Longshore Sand Transport Variability at the Northwest Coast of Portugal* – Silva et al, 2012) of this thesis. Based on the same data set, a similar statistical analysis is presented in Andrade et al. (2013) where the wave climate is characterized through grouped data and frequencies distribution.

In synthesis, the wave climate adjacent to the Nazaré coast, can be described with a mean significant wave height of 2.0 m, mean peak period of 10.5 s and mean wave direction of 307°. The interannual variability of these parameters is also an important result to emphasise, through the coefficient of variation (COV) was realized that wave height displays the greater variability (see Table 5.3 for the results for the three main wave parameters). For instance, some years may be characterized by mean Hs of 1.76 m while others can be described by mean significant wave heights of 2.26 m (these results represent the minimum and maximum mean annual significant wave height, respectively).

In the same Chapter ( *Chapter 5*, particularly in Figure 5.3, Figure 5.4 and Figure 5.5) it can be visualized the variability related to winter and summer months. In fact, summer months (April to September) are less variable than winter months (October to March) in significant wave height, peak period and also in wave direction.

In April 2009 a multi-parametric buoy was deployed in the Nazaré Submarine Canyon at 2000 m depth by the Portuguese Hydrographic Institute in scope of MONICAN project (http://monican.hidrografico.pt/). This buoy named MONICAN01 is located approximately 50 km offshore of Nazaré (Figure 4.3 and Figure 6.1) and records a broad list of wave parameters with a 10 minutes interval.

The beginning of video monitoring on the Norte beach occurred prior to the MONICAN01 installation. Additionally, this buoy wave time-series is not complete due to operational failures or maintenance, for this reason a complete and continuous wave time-series was generated to cover the entire period of video monitoring. Gaps (about 8% of the records) were filled with NOAA (National Oceanic and Atmospheric Administration) hindcast for the

nearest node. The complete data time-series was then resampled to meet the NOAA resolution (3 h interval between samples). A good agreement between data sets was found and the validation results are presented in Silva et al, 2013- *Chapter 6 – Shoreline Variability at the* Norte Beach and Table 6.1.

This procedure resulted in the generation of an offshore wave time-series with significant wave heights, wave peak period and wave direction (with a 3 h interval) between December 1st of 2008 and May 1st of 2012.

The characterization of the wave forcing during this period is presented in *sub-chapter 7.4.3.1 - Wave forcing* where the average Hs is 2.4 m, Tp is 11.1 s and direction 319 °. As expected during summer wave regime is calmer and slightly rotated northward (Hs = 1.8 m; Tp = 8.8 s and Dir = 328 °) while in winter months wave regime is more energetic (Hs = 3.0 m; Tp= 12.6 s and Dir = 311 °) (Figure 7.4 and Figure 7.5A).

#### 8.1.1.2. NEARSHORE

During the monitoring period the wave regime at the Norte beach was estimated with the wave propagation model SWAN (Booij et al., 1999 see *sub-chapter 4.3*, *SWAN Model* for a more detailed description).

The SWAN model was set to run in stationary mode and forced in its boundaries with the offshore wave time-series. Grids used in the modeling include a regional 2000 m resolution grid and two higher resolution nested grids; an intermediate 100 m resolution grid and a local grid with a cell size of 30 m (Figure 8.1). The grid extents were 176 × 198 km, 21.9 × 29.2 km and 3.0 × 5.6 km, respectively for the regional, the intermediate and the local grid.

Propagation results were extracted on cells along the 15 m depth contour line (relative to MSL). The 15 m contour was chosen considering that at this site closure depth is about this value (estimated as 15-16 m at the coast northward of Cabo da Roca; Lapa et al., 2012), the geometry of the ocean floor is relatively constant and, at this depth, the majority of incoming waves have not yet broken. Additionally, at this site/depth the bathymetry is relatively uniform with contours parallel to coastline (with the exception of the southward limit very close to Nazaré headland) therefore suitable for the application of the linear wave theory in the propagation of waves between the 15 m depth and breaking.

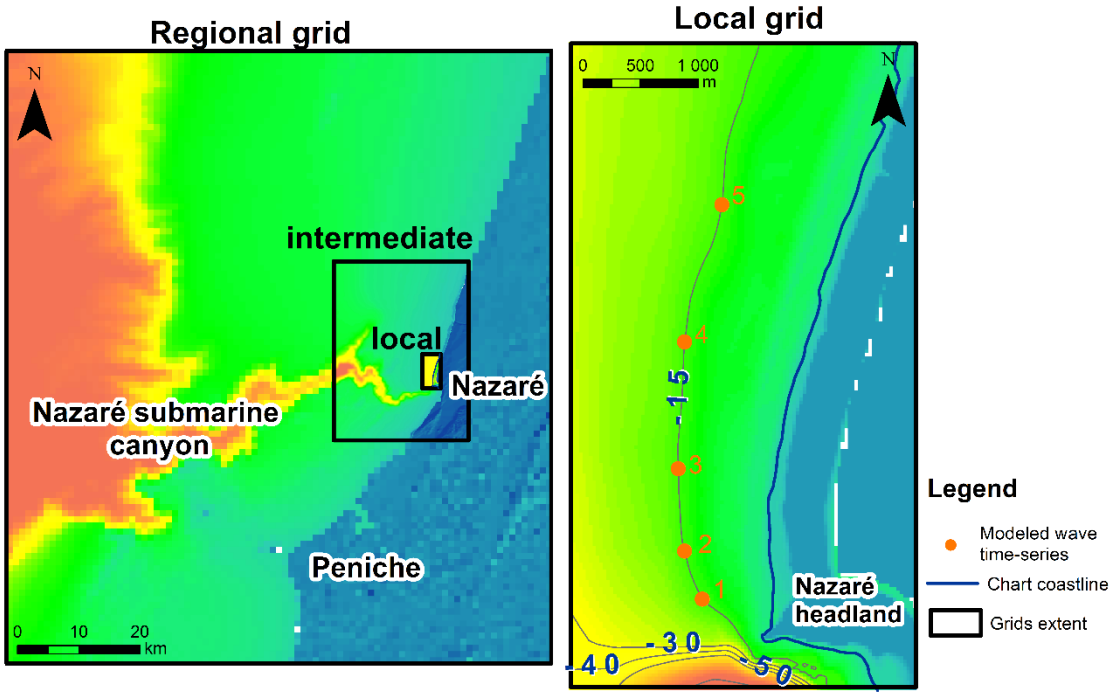


**Figure 8.1 – Bathymetric grids used in wave propagation with SWAN model.**

Amongst the modelled wave time-series (at the 15 m depth) five positions were chosen to be propagated up to the breaker point by the linear wave theory. These five points, defined as positions 1 (southern) to 5 (northern) and identified as red dots in the local grid (Figure 8.1), intend to represent the forcing along the video monitoring area (the three southernmost points) and at the northern sector of the Norte beach for LST estimates (see *Sub-chapter 8.1.4.1. Longshore Sediment Transport Estimates* ).

#### *8.1.1.2.1. THE NAZARÉ WAVE*

Over the last years the Norte beach has received media attention by its particular high waves, an occurrence named "The Nazaré wave". These high waves, responsible for the largest waves surfed in the world (waves that exceed 20 m) occur near the Nazaré headland in a narrowed zone. For instance, in November 1st 2011 the surfer Garrett McNamara surfed a wave which was later certificated by the Guinness as the biggest wave ride with 23.77 m height. At that time, offshore conditions were 5.3 m wave height, 13.8 s wave peak period and wave direction of 307 °.

Modeling results for the aforementioned offshore conditions did not simulate realistically the occurrence, particularly the wave height (Figure 8.2) noticing the large limitations of

this kind of models in the simulation of wave propagation over complex bathymetry. Although wave shoaling effects seem to be correctly located, the maximum wave height modeled was 5.9 m which is 30% less than the observed. Modeled wave directions show a compatible pattern to what is generally observed in the Norte beach, with a southward rotation of the wave crests when approaching the headland induced by the wave refraction over the Nazaré canyon head (Figure 8.2 in the right).

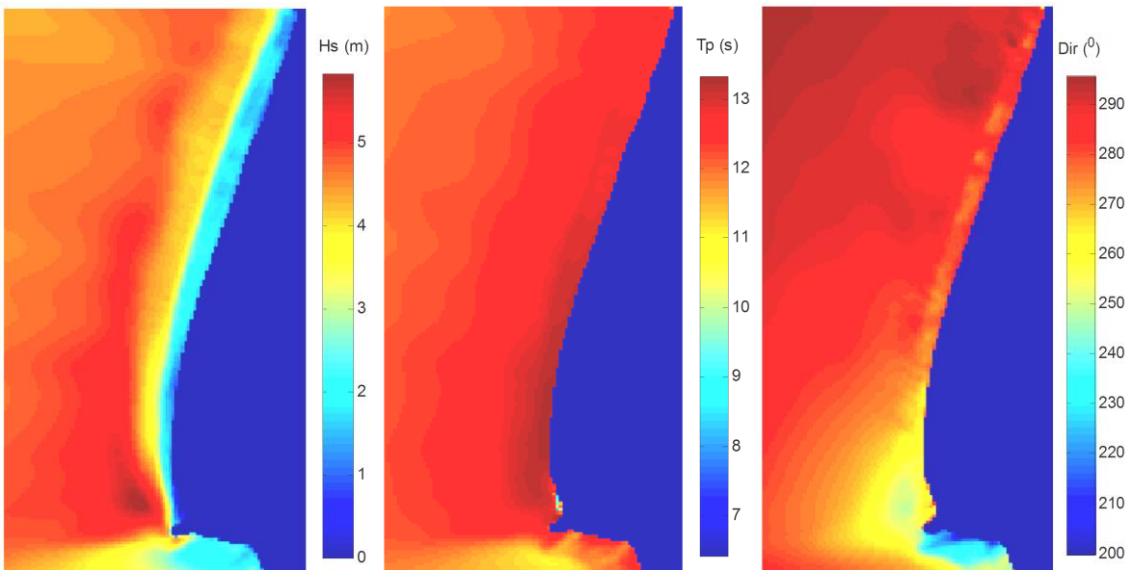


**Figure 8.2 – SWAN modeling results for the offshore conditions during 1st of November 2011.**

Generation of these exceptionally high waves is associated with northwest and west swells, long and high energetic waves. As the waves approach the coast they suffer refraction effects induced by the differences in depth; in the continental shelf the waves tend to reduce progressively its group velocity while within the canyon the velocity reduction induced by the bottom only occur very close to the coast (Figure 8.3).

This phenomena triggers the detachment of an unique wave front into several wave fronts with different group velocities and directions. Particularly, the waves that travel within the canyon experience a southward rotation over the terminal part of the Nazaré canyon (where the canyon head is oriented roughly SW-NE) (Figure 8.3); this group of waves experiences an abrupt increase in depth at the canyon edge (very close to the Nazaré headland) which induces an amplification of the wave height (due to shortening of the wave length); when this group of waves intersect the waves which has propagated over the shelf (in a constant steep morphology) with a northwest (or west) orientation, they

experience another shoaling effect which can double the wave heights and concentrate the wave energy.

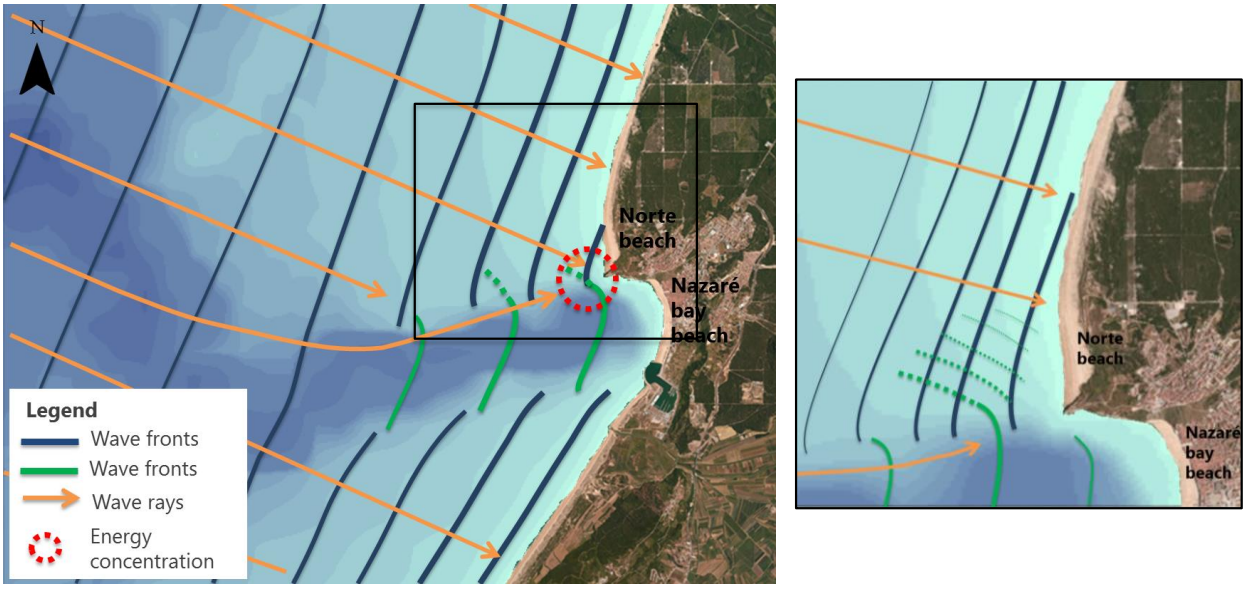


**Figure 8.3 – Schematics of wave propagation at the Nazaré.**

Littoral currents induced by the waves (north-south directed), also transport considerable amounts of water that rises even more the water heights (Figure 8.4) (additional information can be found in the Portuguese Hydrographic Institute website: http://www.hidrografico.pt).

Moreover, interference patterns are frequently observed, it occur when waves from different directions intersect themselves. The interference can be a constructive wave interference when waves are in phase (producing waves larger than the original ones) or a destructive wave interference when waves are out of phase (Whitford, 2002).

In the Norte beach, when the two distinctive wave groups intercept themselves obliquely, a succession of crests and troughs forms a grid pattern which is more intense near the headland (Figure 8.3, Figure 8.5 and Figure 8.6). These occurrences seem also to be related to the occurrence of long waves with an important western component, certainly contributing to increase the wave height in this particular location.


**Figure 8.4 – Images of the Nazaré wave.**

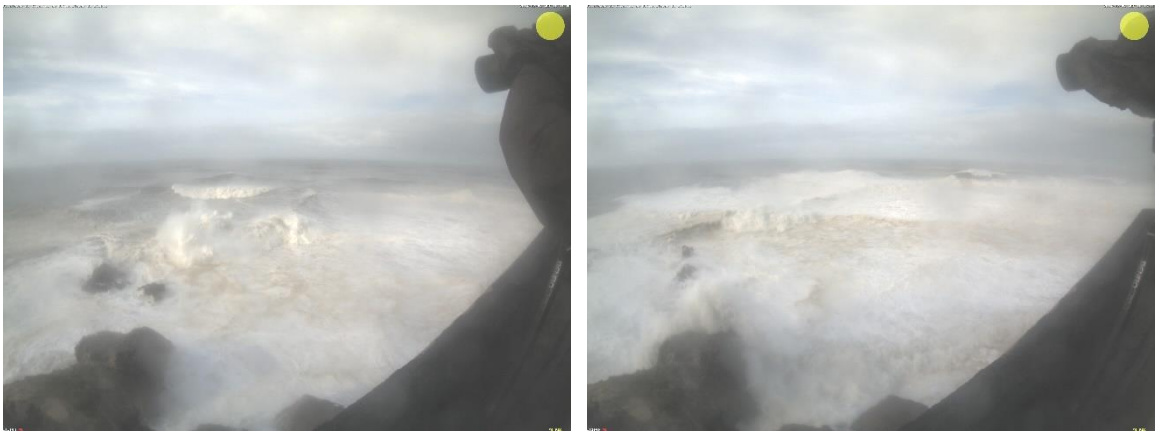

**Figure 8.5 – Snapshot images acquired from the video monitoring system installed at the Forte S. Miguel Arcanjo (from the wide angular camera looking to ocean) where the interference pattern can be identified.**

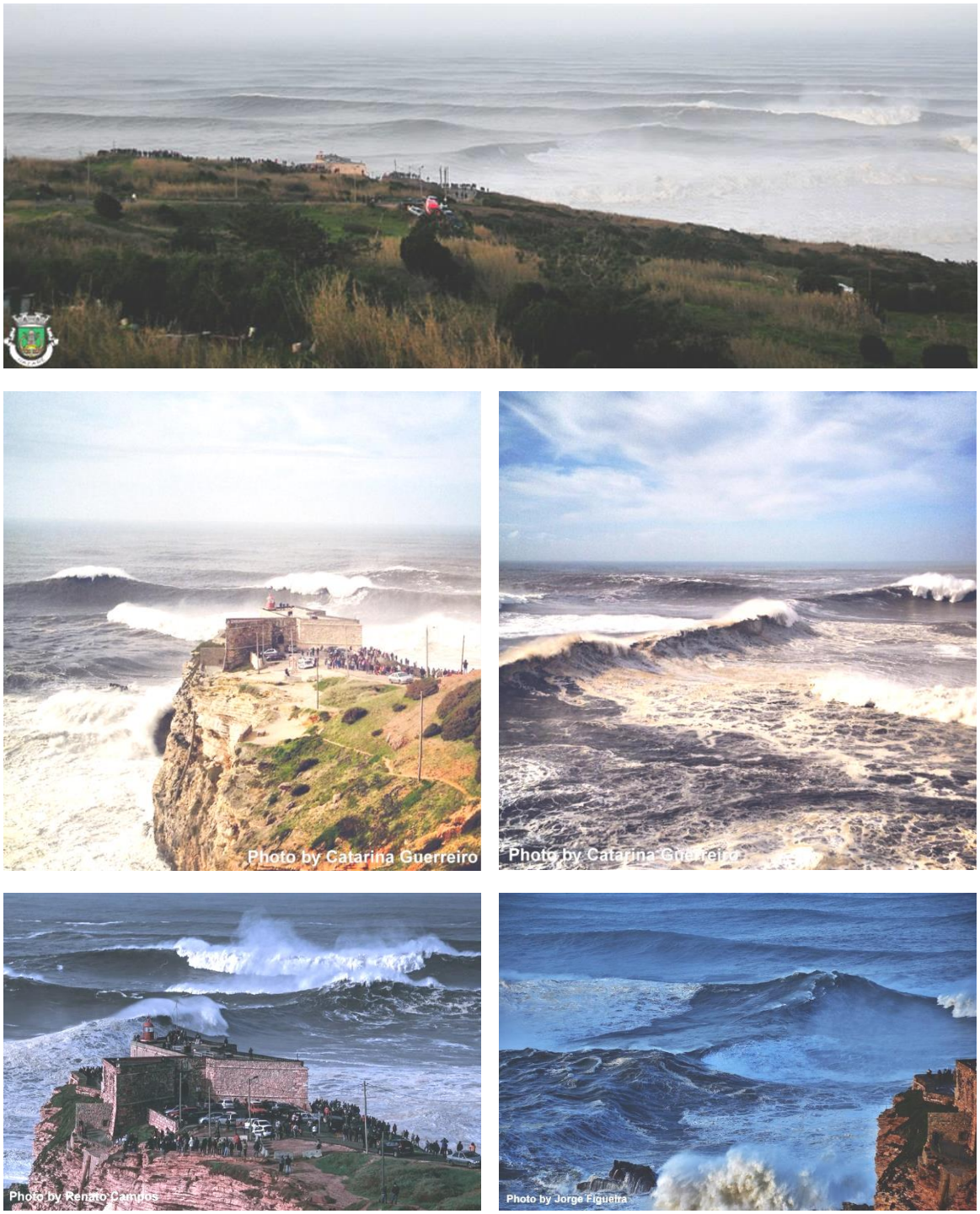


**Figure 8.6 – Images of the interference pattern in the Norte beach.**

As a consequence of the aforementioned processes, the wave modeling at the nearshore of Norte beach and Nazaré headland is a task exceptional difficult. The main concern is that most of wave propagation models do not resolve the wave phase of the incoming

waves, i.e. they are phase-averaged models which resolves the sea surface through the statistical computations on points of a grid.

Although phase-resolving models exist, their applicability is limited to shallow waters since they can be used only for regions of limited size (because the computational grid has to be fine enough to resolve all relevant wave lengths) (Swan Course, 2014). These latter models resolve the sea surface with a grid that includes a vertical component but their use is presently directed to model the waves/sea surface in ports. For these reasons, phase-resolving models are presently incapable to predict the wave propagation over the canyon.

From the above considerations is clear that future work/investigation on wave propagation over the deep canyon and the adjacent shallow shelf should be addressed. Phase-resolving models integrated with currently available deep water propagation models would give insights on the wave behaviour on such environments. The video monitoring system deployed on Nazaré headland can contribute with images for the calibration of those models, namely with information about currents, wave parameters (height, velocity of propagation and direction), location of wave breaking, etc. Moreover, another video camera directed to the ocean was recently set to record images periodically (see Figure 1.1 and Figure 8.5).

#### *8.1.1.2.2. THE NAZARÉ BAY*

The nearshore wave regime at the Nazaré bay is completely distinct from the Norte beach regime. The embayment configuration downdrift of the Nazaré headland creates a shelter effect from the more energetic waves, which normally approach from the north and northwest directions and are subject to wave front divergence. The bottom morphology in front of the Nazaré bay (Figure 8.8 - A) is characterized by several tributaries of the Nazaré canyon head which are located very close to the shore and generally promote wave dispersion and ease energy dissipation. Yet, in particular offshore wave conditions (western long waves and/or storm conditions) the proximity of high depth channels force the energy dissipation to happen very close to the shore which can cause hazardous occurrences, like the overtopping of the sea front during the storm event of February 19th 2013 (Figure 8.7).

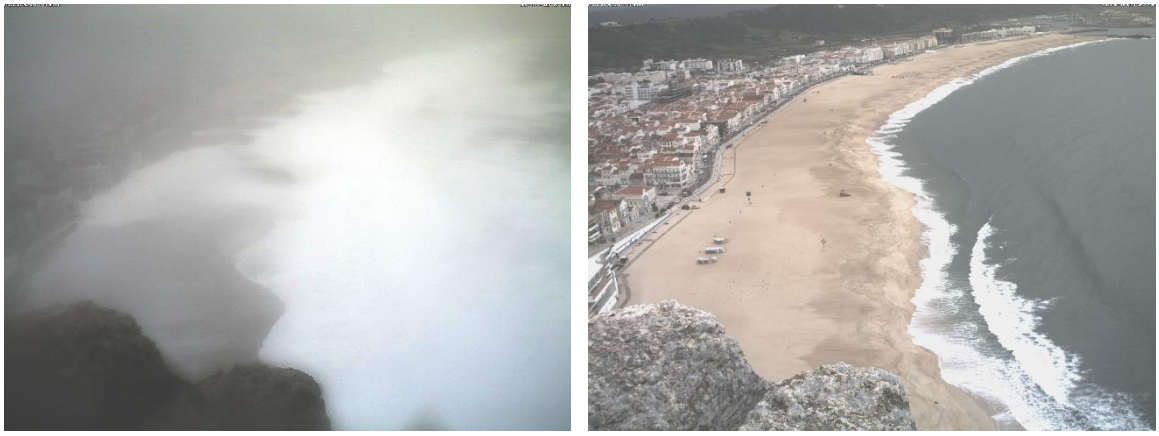

**Figure 8.7 – Snapshot images of Nazaré bay beach during the January 19th storm (left) and during a summer day (right) acquired by the video monitoring system installed in Sítio da Nazaré.**

SWAN modeling results for the propagation of a common offshore wave (Significant wave height Hs = 3.2 m; direction 270 ° and peak period Tp = 9.5 s - Figure 8.8 - B) performed in the scope of a technical study (Taborda et al., 2012), revealed an energy reduction at the Nazaré bay particularly in the northern sector. Even though some energy concentration spots were present, the same study perceived a southward energy decrease of the wave overttopping potential which is in agreement with the video observations during storm events and with an embryonic dune development in the southern sector of the beach.

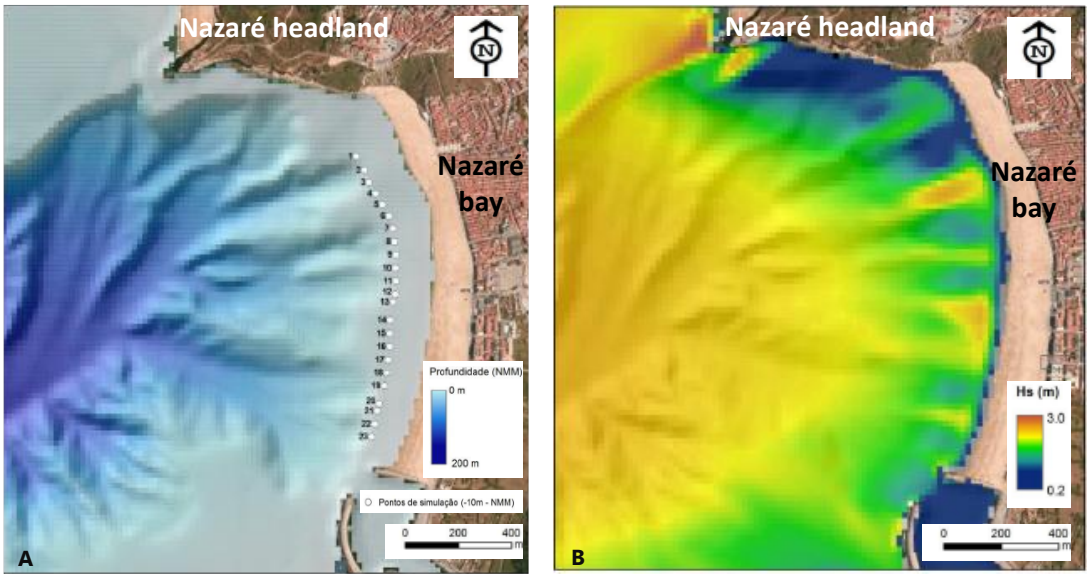


**Figure 8.8 – (A) Bathymetric grid at the Nazaré bay and (B) Spatial distribution of wave height along the Nazaré bay related with a 3.2 m, 9.5 s and 270 ° offshore wave (see text for detailed explanation; adapted from Taborda et al., 2012).**

## 8.1.2. MORPHODYNAMICS

### 8.1.2.1. NORTE BEACH

The initial insights on the morphodynamics of Norte beach were given by the shoreline variability of this beach (see Silva et al, 2013 - *Chapter 6 – Shoreline Variability at the Norte* Beach) where huge seasonal variations were observed. During the monitoring period considered in this study, the shoreline showed a variability up to 160 m in the southern sector and about 70 m at the central and northern sector of the beach.

Analysis of the shoreline variability suggests a clear seasonal imprint which is related to changes in beach configuration from straight to arcuate, mainly due to longshore drift gradients rather than cross-shore sedimentary transferences.

Moreover, the volumetric dynamics of the Norte beach was investigated using the volume model approach, described in Silva and Taborda, 2014 - *Chapter 7 – Norte beach morphodynamics – long-term perspective through video monitoring,* where the beach volume was computed using the coastline position extracted from the video monitoring in a monthly based.

The beach volumes were recomputed with the methodology described in the aforementioned chapter increasing the extent of the study area (Figure 8.9). The area was expanded in the south sector to include the portion of beach that during the winter is normally submerged and the submarine portion of the beach, in order to include the complete beach profile up to the closure depth. The LiDAR data of the submarine beach suggest that the sandy moveable layer does not extend below the 12 m contour (MSL). For this reason, at the study area, the computation of beach volume considered this depth, which is slightly less than the 15-16 m depth of closure proposed to the Portuguese northwest coast (Lapa et al, 2012).

The results are very similar to the ones abovementioned, in what concerns overall tendencies, the magnitudes are naturally higher with a mean beach volume of 6.62 million $m^3$ of sand, ranging from a minimum of 5.75 million $m^3$ and a maximum of 7.43 million $m^3$ (Figure 8.10 and Table 8.1). The maximum amplitude of volume at the Norte beach was 1.67 million $m^3$ of sand (and 1.57 million $m^3$, on average). Sub-aerial beach, above mean sea level, represents about 17% of the total beach volume.

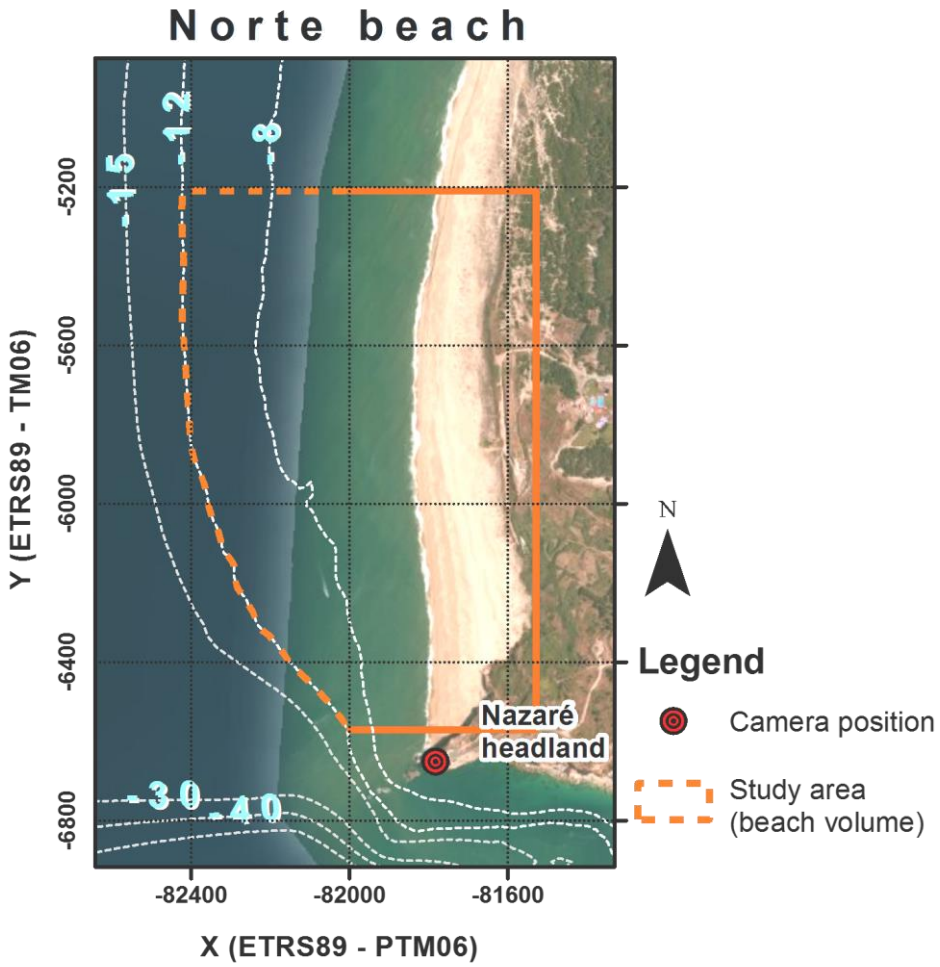


**Figure 8.9 – Extent of the study area for volume estimation.**

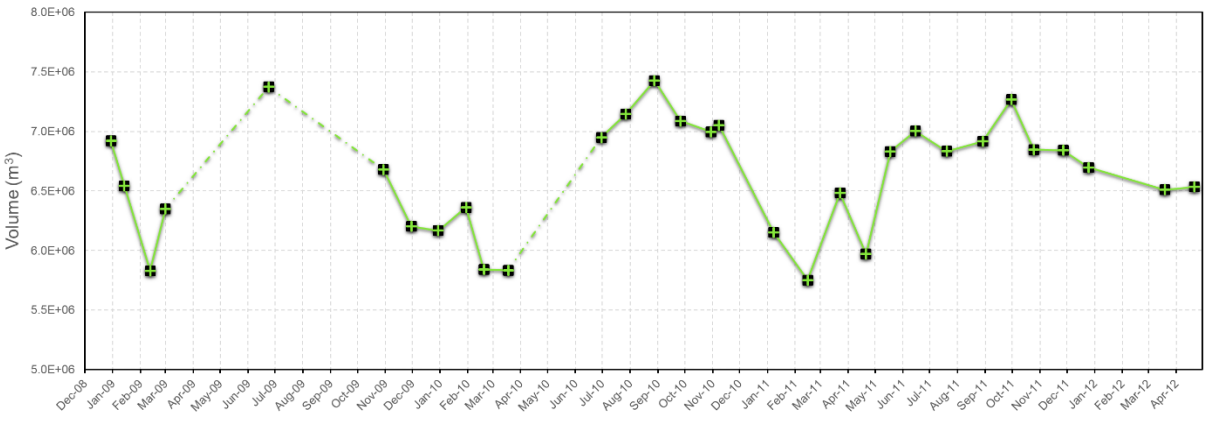


**Figure 8.10 - Norte beach volume time-series up to the closure depth (dashed lines represent monitoring interruptions longer than 2 months).**

**Table 8.1 – Statistics of the volume estimated at Norte beach, between December 2008 and April 2012.**

| | Magnitude ($m^3$) | Occurrence date |
|---|---|---|
| ***Mean*** | $6.62 \times 10^6$ | - |
| ***Minimum*** | $5.75 \times 10^6$ | February 2011 |
| ***Maximum*** | $7.43 \times 10^6$ | August 2010 |
| ***Amplitude (max.)*** | $1.67 \times 10^6$ | - |

The volume variations between maxima and minima values are expressed in Table 8.2, where a regular amplitude of volume variation is shown, about 1.5 million $m^3$. The beach seems to vary repeatedly between a minimum, in winter, and a maximum value in summer (respectively about 5.8 and 7.5 million $m^3$; Figure 8.10). Nevertheless, these extreme values occur in different months representing an interannual variability of beach volume.

**Table 8.2 – Volume amplitudes (between maximum and minimum) and rates of change.**

| | Amplitude ($m^3$) | Change rate ($m^3$/day) |
|---|---|---|
| ***Feb09 – Jun09*** | $1.56 \times 10^6$ | $11.7 \times 10^3$ |
| ***Jun09 – Mar10*** | $-1.54 \times 10^6$ | $-5.77 \times 10^3$ |
| ***Mar10 – Aug10*** | $1.59 \times 10^6$ | $9.77 \times 10^3$ |
| ***Aug10 – Feb11*** | $-1.67 \times 10^6$ | $-9.79 \times 10^3$ |
| ***Feb1 – Sep11*** | $1.52 \times 10^6$ | $6.68 \times 10^3$ |

The alongshore volume deviations from its average magnitude (see detailed explanation on *Sub-chapter* 7.4.2.2 - *Beach volume* and Equation 7.4) is shown at Figure 8.11. The results confirm that the behaviour of the beach volume is very distinctive in the southern and northern sector, with a division near the position -5900 m (Y – ETRS89 PTM06, see Figure 8.9 for spatial reference), similar to the results presented in the earlier chapter.

The seasonality is evident in the southern sector where the major volume deviations occur. The higher volumes happen in summer (June, July, August and September) with great positive volume deviations in the southward limit of the beach, these maxima of volume seem to have a northward progradation, as seen between August and November 2010 and between June and December 2011 (Figure 8.11).

The increase in total beach volume is mainly related to downdrift, north-south direction, sediment transport while the beach volume decrease can be attributed either to sediment

lost to the Nazaré submarine canyon via submarine profile, to sediment transposition of the headland, or to longshore sediment transport northward of the study area. For example, the total volume decrease between October and March 2009 appears to fit in the latter hypothesis since a northward volume transference is recognized at the northern sector (between -5600 and -5210 m Y – ETRS89 PTM06). Additionally, during this period the beach was particularly retreated at the southern sector which difficult the sediment transferences into the Canyon and the sediment bypass of the headland.

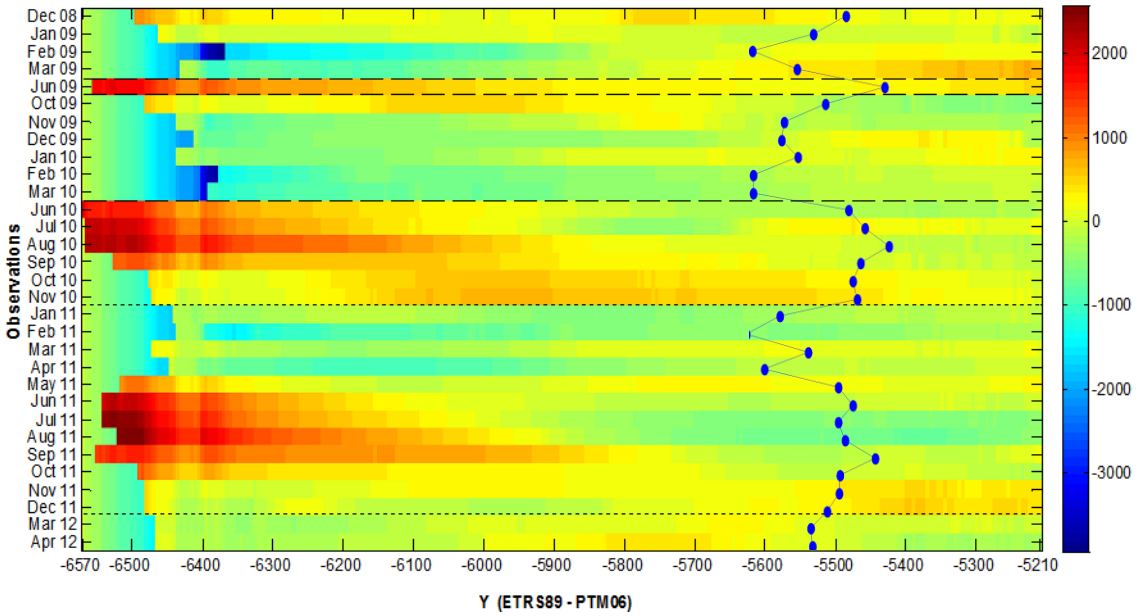


**Figure 8.11 - Time stack of alongshore volume deviation ($m^3$) up to the closure depth. Long dashed lines represent interruptions longer than 2 months while short dashed lines represent minor (less than 2 months) interruptions; blue graph represents Norte beach total volume variation.**

Additionally, the occurrence of a large scale (few hundred meters) irregularity on the shoreline was observed on aerial photography of the Norte beach at March 2010 (Figure 8.12). This perturbation is visible nearly 2 km northward of the Nazaré headland and appears to be related to longshore processes.

**Figure 8.12 – Aerial photography of Norte beach, March 14th 2010 (Source: SIARL – Sistema de Administração do Recurso Litoral and IGP – Instituto Geográfico Português).**

Although the occurrence of these coastline perturbations was not targeted in this thesis, their existence must be taken into account particularly when assessing the sedimentary budget of this coastal stretch (discussed in Sub-chapter 8.1.4 - *Sedimentary budget* ). It is clear though that the monitoring area is too small to capture these events. In future work, satellite imagery namely the Landsat program could give precious insights on this topic since its temporal and spatial coverage is compatible to the recognition and monitoring of these occurrences (Klemas, 2009; Lira and Taborda, 2014).

### 8.1.2.2. PRAINHA BEACH

Still focusing on the morphodynamics of this littoral stretch, in certain years a sedimentary accumulation occurs around the Nazaré headland, named by the locals as "Prainha" (see Figure 1.1 for spatial reference). This phenomena can be described as an ephemeral beach, adjacent to the headland, which connects the Norte beach with the Nazaré beach, its rare occurrence makes this an intriguing event described by the locals to have a recurrence higher than decadal. Historical photographs provided by Nazaré municipality illustrate some of these historical occurrences in 1946, 1951 and 1998 (respectively, Figure 8.13, Figure 8.14 and Figure 8.15). Although it is presently unknown, other occurrences may had happened in the years between.


**Figure 8.13 – Historical photograph of Prainha at August 1946 (photograph taken looking northeast, with Guilhim at the left side of the image; Source: Nazaré municipality).**


**Figure 8.14 - Historical photograph of Prainha at August 1951 (photograph taken looking northeast, with Guilhim at the left side of the image; Source: Nazaré municipality).**

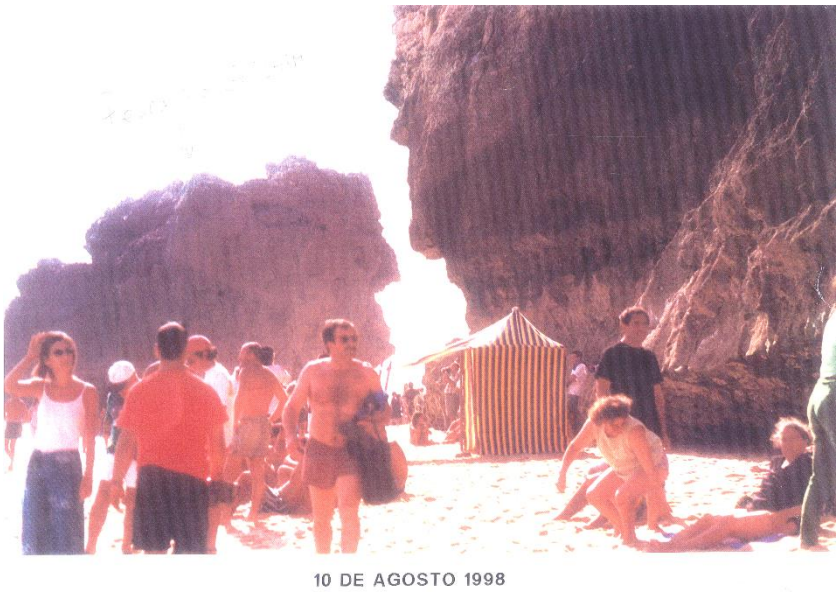


**Figure 8.15 - Historical photograph of Prainha at August 1998 (photograph taken looking east-northwest, with Guilhim at the left side of the image; Source: Nazaré municipality).**

More recently, during the monitoring period on July 23th 2011 this sedimentary accumulation around the Nazaré headland reappeared, connecting the Norte beach and the Nazaré beach through the passage between the headland and Guilhim rock (see Figure 4.8). This connection persisted during a few days and in early August 2011 the passage was no longer possible although an ephemeral beach still existed southward of the headland, which faded away during the subsequent days (Figure 8.16).

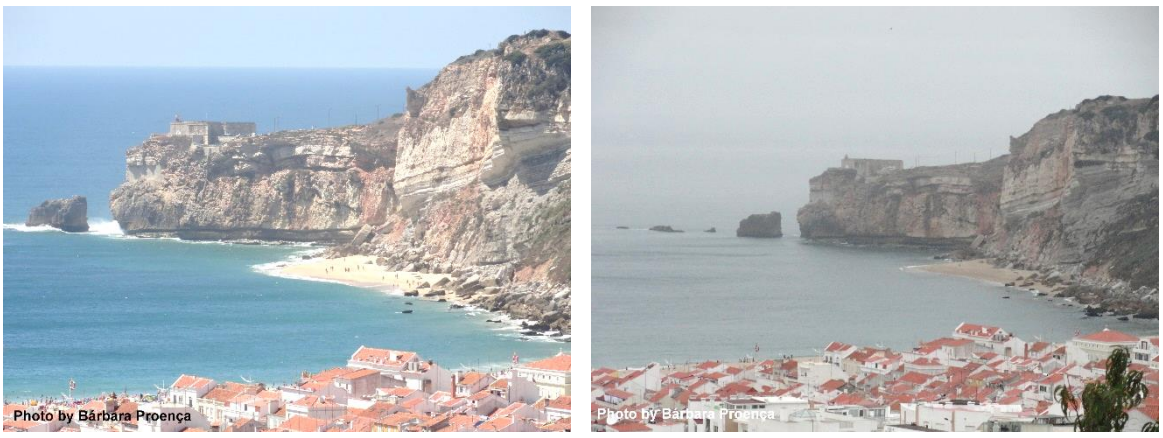


**Figure 8.16 – Images of Prainha on August 7th (left) and August 13th (right) 2011 (photographs taken looking northeast).**

During the summer of 2013, the Prainha phenomena reoccurred, this time the persistence of the beach adjacent to the headland was very long (Figure 8.17). The sedimentary accumulation around the headland, which provided at low tide the connection between both beaches, occurred in August 18$^{th}$ and continued for almost a month, until September 14$^{th}$, 2013.

Based on satellite imagery was possible to monitor this event. It was recognized that the beach adjacent to the headland started to develop in July 2013 and attained its maximum extent by the end of September, afterwards the beach experienced migration eastwards, during the month of October, followed by a beach recede that progressively reduce the beach volume until its disappearance by the end of November 2013 (Lira and Taborda, 2014).

During this event, it was estimated that the sub-aerial portion of Prainha beach reached a maximum sediment volume about 50 000 m$^3$ of sand.

The Prainha beach occurrences are restricted to summer conditions when the Norte beach is at its maximum volume capacity and subaerial sediment bypass occurs. Furthermore, preliminary results of a sedimentary tracer experiment performed during September 2013 at the Norte beach, proved the sediment bypassing over the headland and its presence along the Nazaré bay beach (Duarte et al., 2014).

Additionally, as this event have a non-cyclic recurrence some particular wave/currents and/or persistence forcing conditions need be present for this phenomena to occur. Although it is not yet entirely understood, Lira and Taborda (2014) refer a connection between these beach episodes to the low energetic, short period, northerly waves, which promote the sediment bypassing sub-aerially.

Again, Landsat program which includes historical satellite imagery for the last 40 years could in future work, assist (as demonstrated in Lira and Taborda, 2014) on the search for Prainha occurrences which might not been documented, and contribute with information for the full understanding of this phenomena.


**Figure 8.17 – Images of Prainha on summer 2013 and its evolution (in sequence: August 20th, September 09th September 20th, October 14th and October 23th; photographs taken looking northeast with the exception of the first which is looking southeast).**

### *8.1.2.3. NAZARÉ BAY BEACH*

The Nazaré bay beach embraces an embayed beach limited, at north, by the Nazaré headland and at south by the Nazaré port facilities (Figure 1.1 and Figure 8.8), its terrestrial limit comprehend a physical man-made structure (marginal road) that prevent the beach

migration. Its location facing most of the canyon, apparently active, tributaries suggest that sedimentary transferences between the beach and the canyon may have an increased importance at this site, particularly as the canyon head is located very close to the coast, attaining depths about 20 m a few meter away from the shoreline.

The morphological changes at the Nazaré beach have been evaluated in the previously mentioned technical study elaborated by Taborda et al., (2012) where a beach progradation, in the last tens of years was observed. The beach berm extended between 50 to 100 m, particularly in the southern part of the beach, which is most likely related to the construction of the Nazaré port that acted as a sedimentary retainer of the southward littoral drift.

At the technical report of Silveira et al. (2013) the seasonal variability of Nazaré beach was investigated along three transversal beach profiles. The results suggest a very stable and wide beach, with beach lengths over 100 m which in summer conditions can reach about 180 m length, particularly in the southern sector. Seasonal imprint in the beach profiles provides a variation in the order or tens of metres (40 m; 20 m and 30 m at northern, central and southern sectors of the beach, respectively). Over the last years, in the southern sector of Nazaré bay beach, a vegetated dune had developed at backshore.

### 8.1.3. SEDIMENTARY BUDGET

#### 8.1.3.1. LONGSHORE SEDIMENT TRANSPORT ESTIMATES

The estimates of longshore sediment transport (LST) were done based on the longitudinal component of the wave energy flux at the breaking. The formulation adopted was the CERC formula (Rosati et al., 2002 and equation 5.1) previously described in *Chapter 5 – Longshore Sand Transport Variability at the Northwest Coast of Portugal* ) with the adoption of k = 0.39. A flow chart with the processes and input/output data involved in the LST estimates and observations is presented (Figure 8.18).

The wave characteristics at the breaking zone were assessed based on linear wave theory that was applied to the five nearshore wave time-series defined above (positions 1 to 5, see *sub-chapter 8.1.2 - Nearshore* and Figure 8.1). The wave breaking and its parameters were estimated by the non-iterative approximation of Larson et al. (2010) which enables a simplified solution for the equation of energy flux conservation combined with Snell's law and a breaking criteria of H/d = 0.78 [the relative height of the wave (H) compared to the water depth (d); McCowan, 1891].

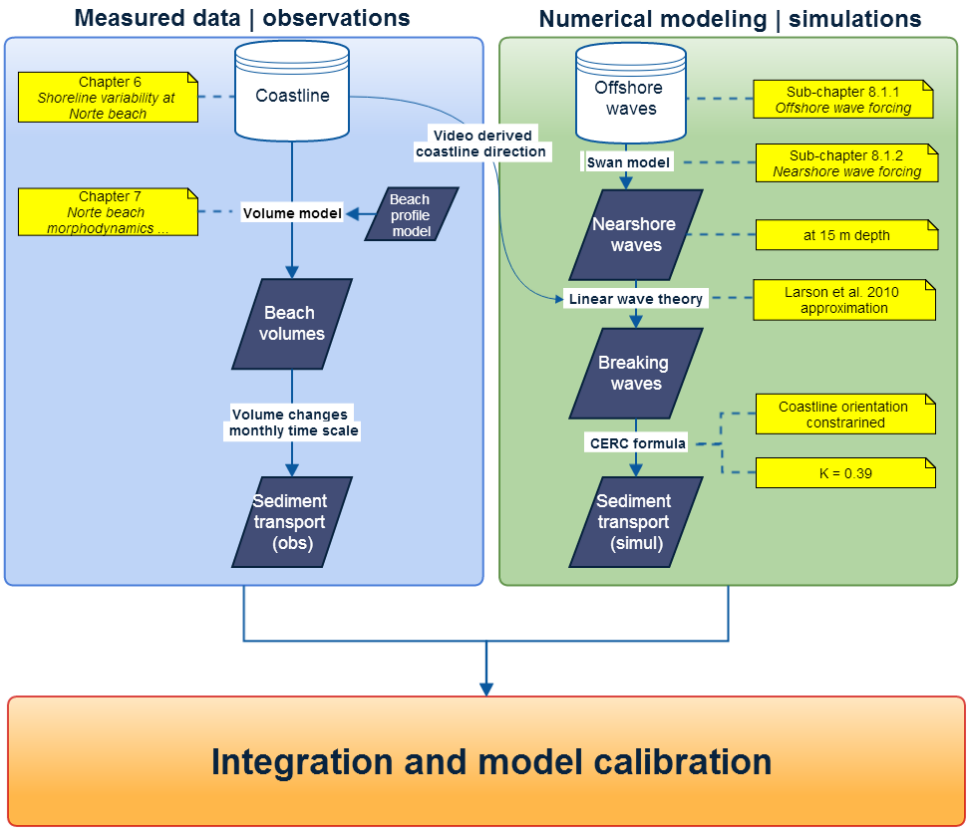


**Figure 8.18 – Work flow for the longshore sediment transport estimates and observations at Norte beach.**

The coastline direction in the two northern positions (4 and 5), outside the video monitoring area, was established based on model estimation expressed by the bathymetry used in SWAN modelling, while within the monitoring area the coastline direction was defined based on the coastline orientations measured with the video.

The video derived coastline directions, for the positions 1 to 3, were determined through several steps: 1) all the video-derived coastlines were interpolated in a 20 m interval, allowing a simplification and attenuation of coastline irregularities; 2) the coastlines were smoothed using a Savitzky–Golay filter (Sgolay - Savitzky and Golay, 1964) with a second degree polynomial fit; 3) every 20 m, interval node of the coastlines, the coastline direction was computed; 4) the resulting directions were smoothed with a Sgolay filter, this time using a first degree polynomial; 5) extraction of the coastline direction at each of the 3 positions, for the dates investigated in the monitoring period and; 6) interpolation of the coastline directions for the whole period of monitoring, i.e. the generation of a coastline

direction time-series, for each point, to meet the breaking wave time-series extent and sampling interval.

The combination of the nearshore wave time-series with the coastline direction time-series, for each 5 positions analysed, enable the computation of the LST with the aforementioned CERC formula during the entire time of monitoring.

The spatial equivalence of the long-term (3.4 years of results) LST was investigated and the LST resultant were incoherent, i.e. presented different LST resultant along the coast. For this reason, the coastline directions were constrained in order to attain equivalent long-term LST results. In fact, as the beach does not present evidences of sedimentary sinks or sources along this area it is reasonable to consider that the magnitude of sand transport is spatially uniform.

The aforementioned coastline direction constraints/adjustments were more significant at the 3 southernmost positions, within the monitoring area, mostly because this area is where the most coastline variability occur. The sensitivity of the numerical modeling to the coastline orientation is particularly visible in these estimations, at those positions the adoption of a constant coastline orientation lead to unrealistic results. The integration of the measured morphological changes of the beach, in a monthly based, improved significantly the results although they only reached realistic results when the coastline angles were computationally constrained.

Naturally, the coupling of the instantaneous LST estimates with their morphological effects on the beach, in terms of the coastline configuration, would reduce significantly the uncertainties related to this critical parameter. In scope of future work, this process based modeling approach involving one-dimensional coastline evolution models like GENESIS (Hanson, 1989) or the ones described in Kamphuis (2000) would simulate more accurately the sedimentary dynamics of this coast (Taborda et al., 2014).

The mean coastline orientations for the 5 positions is expressed in Figure 8.19. The red lines represent the coastline orientation defined by the model, i.e. estimated through the bathymetry (in the 2 northern points) and derived by the video monitoring (in the three southern most points). The green lines represent the adjusted shoreline directions, in this case a softer transition between the shoreline at each position is recognized.

The directional adjustments were maximum at the proximity of the Nazaré headland (6.8° and 10.7° in the position 1 and 2, respectively) and decreased to a minimum at position 3 (0.8°). The northern positions had angular adjustments of 9.2° and 8.4° (position 4 and 5, respectively).

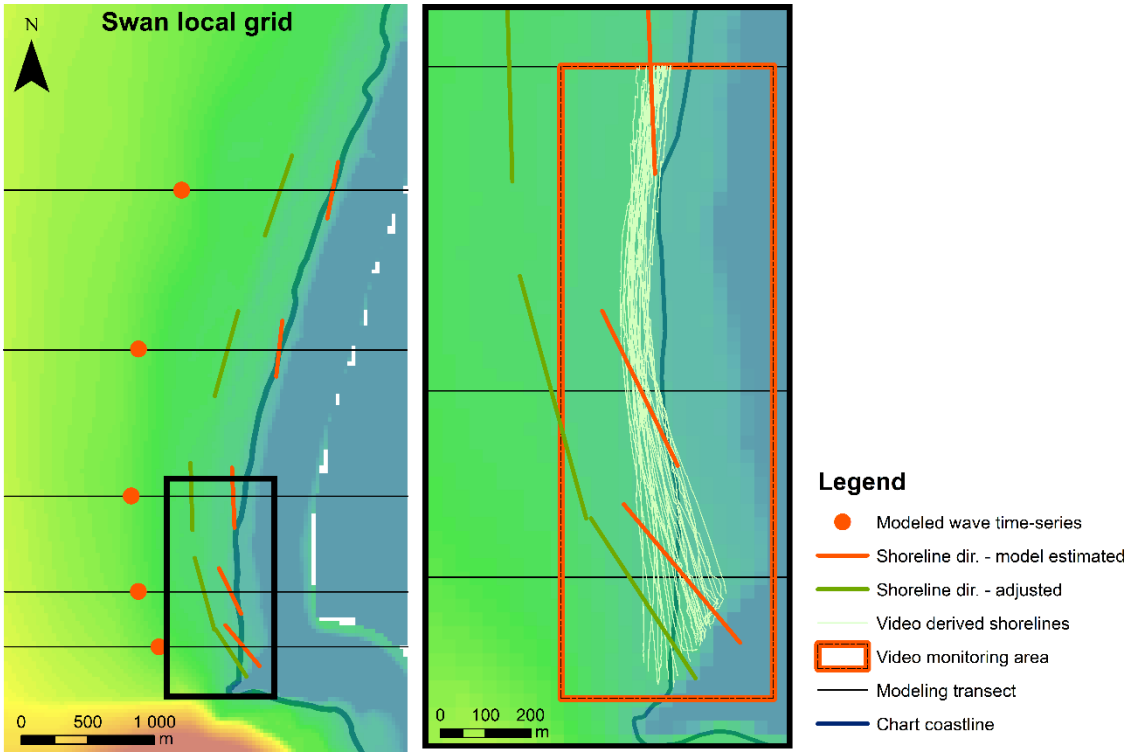


**Figure 8.19 – Coastline directions adopted in the longshore sediment transport estimates.**

In general, the shoreline directions are in agreement with the wave incidence, in this case study the adjusted shoreline directions represent the directions which correspond to the adjustment to wave forcing which was modeled. It was already recognized the modeling limitations of the high wave refraction which occur at this particular place, and this correction in the angle acts as an stability factor for these refraction effects enabling an equilibrium between the modeled wave time-series and the coastline orientation. Additionally, a more frequent update on the coastline response to the morphological variations must be taken into account to improve the results.

The LST results were investigated against the Norte beach volumes, it was possible to detect that the better relations were found when comparing the LST results with the volumes estimated at the southern sector of the beach. This sector, which better describes the seasonal variability of Norte beach, is particularly reactive to the longshore component of the sediment transport while the northern one presents a response more related to the cross-shore sedimentary processes.

Except for the position 3, minor relations were found between observed beach volumes (volume model) and estimated sand volumes (LST estimated through CERC formula). These

results are closely related to the high sensitivity of these methods to the coastline orientation; minor shoreline perturbations can induce huge differences in the LST estimates, particularly true in the vicinity of the headland where the shoreline presented huge variability (positions 1 and 2). Furthermore, the northern positions (4 and 5) also unsuccessfully represented the LST at Norte beach mostly because at those points the refraction effects are negligible, even though they are very influent at Norte beach morphodynamics.

On the contrary, at position 3 on the northern boundary of the video monitoring area, a good agreement is noticeable between the sand volume variability at southern sector of Norte beach (observations) and the sand volume variability estimated (simulations) (Figure 8.20). The records before October 2009 and after December 2011 were dismissed due to the interruptions of video monitoring that caused a lack of observations on those periods.

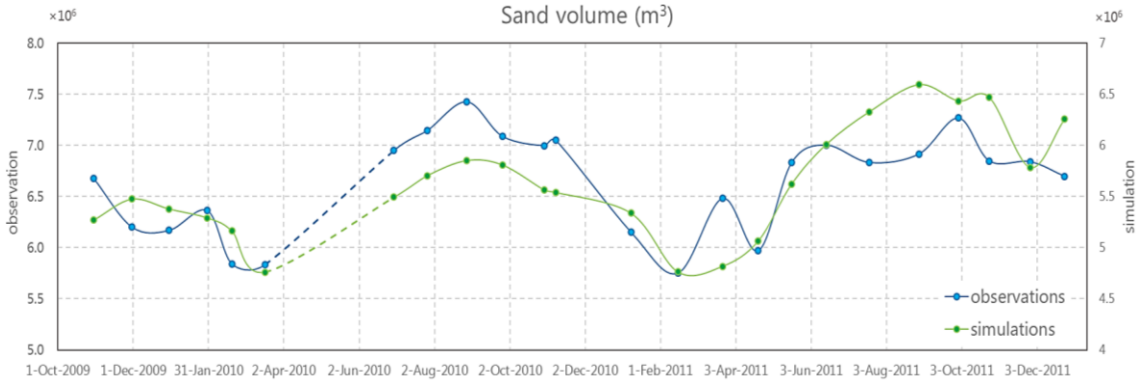


**Figure 8.20 – Sand volume variation along the monitoring period (observations - video derived beach volume and; simulations – estimated with CERC formula).**

Although the overall behaviour of both data sets seems to be well comparable, its correlation factor ($r^2$ = 0.49) is relatively low. This is essentially related to the time that the beach takes to adjust to the wave forcing. When looking to the trimestral behaviour of the sand transport rates, which should attenuate this lag effect, a good agreement between data sets is recognized, $r^2$ = 0.51 (Figure 8.21). Herein, the months were grouped similarly to the wave forcing grouping (the following grouping was used MAM09; JJA09; SON09; DJF10; MAM10; JJA10; SON10; DJF11; MAM11; JJA11 and SON11)[1].

[1] MAM – March, April and May; JJA – June, July and August; SON – September, October and November; DJF – December, January and February.

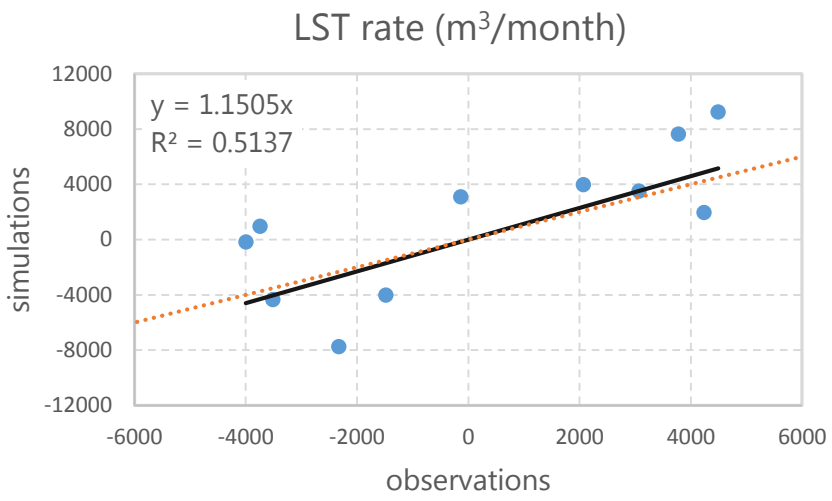


**Figure 8.21 – Longshore sediment transport rates for grouped data (observations *vs* simulations; dark solid line - the best fit line; red dashed line - 1:1 line).**

Linear regression between data sets shows a linear relation expressed by the simulation values being 1.15 times the observations. The adjustment of K empirical parameter of CERC formula, given these outcomes, results in a K parameter of 0.34 slighter below the recommended value of 0.39.

Despite the uncertainties of the LST estimates, related mainly to the coastline orientation, the K coefficient is also very variable contributing likewise to uncertainties on the quantifications of LST (e.g. Komar, 1998; Wang et al., 2002b and Bodge and Kraus, 1991). The K coefficient intends to be a site specific calibration parameter, presently proposed by CERC as 0.39 (considering significant wave height – Hs; and originally 0.77 if considering root mean square wave height - Hrms) based mainly on the field study by Komar and Inman (1970). This value, according to Bodge and Kraus (1991), was supposed to be smaller, as the accurate conversion of the originally K = 0.77 (Hrms) would result in a K = 0.32 (Hs) which is in this regard, surprisingly, close to the one obtained in the present work.

### *8.1.3.2. SEDIMENTARY BUDGET AT THE NAZARÉ COAST*

Based on the above considerations and the concept of budget of littoral sediments, described by Komar (1998) as a simple application of the principle of mass conservation to the littoral sediments, a conceptual sedimentary model can be drawn for the Nazaré

coast, and generalised with the respective limitations/considerations to the widen littoral cell, between the Douro river mouth and the Nazaré.

The sedimentary budget in a pluriannual scale, at Nazaré coast (Figure 8.22), can be described by having sedimentary sources basically related to the longshore sediment transport into the area, in the order of 1 million cubic meters of sand per year, and sinks related to the sediment capture by the submarine canyon. The typical offshore wave forcing induces a net longshore sediment transport (or drift) directed to the south.

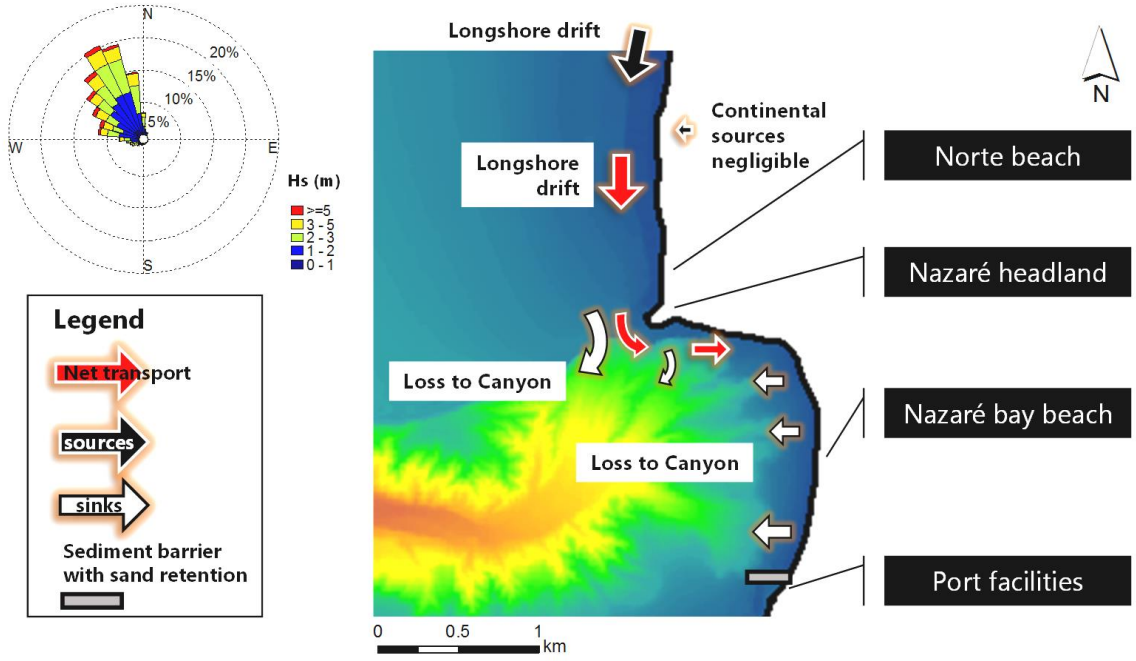


**Figure 8.22 – Long-term sedimentary pattern at Nazaré coast (the rose diagram represents the offshore wave conditions during the monitoring period).**

Continental sediment sources are negligible in this area since there are no rivers nearby. The sinks, at this site are mainly related to sediment capture into the Nazaré Canyon. Part of the southward-directed drift enter the canyon very close to the Nazaré headland, while part of the sediments bypass the headland and redistribute themselves in the Nazaré bay beach (as shown in Duarte et al., 2014) before they enter into the canyon via its tributaries. The sand that reach the southward limit of the Nazaré beach is blocked by the Nazaré port facilities and eventually enter the canyon at the tributary located right in front, closing herein the respective sedimentary cell, since no longshore transferences occur with the adjacent southward littoral.

The sediment transport by the wind at the Norte beach can also be consider a sedimentary sink although, at short-term scales, its relative importance is nearly insignificant. Still, it is worth noting some dune accretion at the Norte beach. Embryonic vegetated dunes are emerging and expanding, they have been responsible, at this site, for coastline progradation over the last decades. Additionally, human-induced sand accretion with dune development had also occurred in south of the Nazaré bay beach driven by construction of the port facilities. However this occurrence was restricted to the period of the sediment infill of the groin and, nowadays, does not act as an important sedimentary sink.

Regarding the cross-shore sediment transference, with exception of the submarine canyon sink, it is believed to be of little influence in the sedimentary balance of this coastal stretch as the cross-shore exchanges with the continental shelf seem to be equivalent in both directions.

Overall, to maintain the sedimentary balance of this coast the magnitude of sources are equivalent to the sinks, therefore the sedimentary balance at the Nazaré coast (Table 8.3) can be considered as in equilibrium, particularly at the Nazaré bay, and minor beach accretion at Norte beach.

**Table 8.3 – Sedimentary budget components on Nazaré coast.**

| | |
|---|---|
| ***Sources*** | • Longshore sediment transport into area<br>• Continental sources – negligible! |
| ***Sinks*** | • Down canyon transport<br>• Wind transport and dune accretion |
| ***Balance*** | • Beach accretion (Norte beach)<br>• Beach in equilibrium (Nazaré bay beach) |

Besides the general sediment dynamics and long-term sedimentary budget observed at the Nazaré coast, very distinctive seasonal sedimentary patterns are observed. In winter (Figure 8.23) is often observed a local LST inversion, i.e. near the Nazaré headland the littoral drift directs northward as a consequence of the aforementioned wave interferences induced by the canyon (see *sub-chapter 8.1.2.1 – The Nazaré wave* ). Although it does not particularly affect the sedimentary balance at this coast, it is responsible for sediment redistribution with impact on the shoreline configuration. As consequence, the Norte beach attains a more arcuate configuration which can be more or less important depending on the magnitude of the northward-directed drift.

During winter, the sediment bypass from Norte beach into Nazaré bay beach seems to be null and the sedimentary exchanges at this later beach are restricted to some sediment loss into the canyon tributaries, probably associated to winter submarine cross-shore profile configuration (that normally redistributes the sediments offshore) and to high energy forcing events.

Concerning the sediment loss into the canyon in front of the Nazaré headland, some doubts remain. It seems unlikely that the submarine beach profile, during winter reaches the vicinity of the canyon head resisting the direct entrance of the sand into the canyon. However, during events of high energetic waves the sediment re-suspension might lead to some sediment loss into the canyon, at this site. The difficulties in submarine profile characterization prevent the correct assessment of the submarine sediment transport trends, although LiDAR bathymetric data exists for the Portuguese coast, it contains a significant amount of errors particularly on the topographic and bathymetric data merging. Moreover this data is limited to one survey making impossible the characterization of the seasonal and temporal variability of the submarine profile.

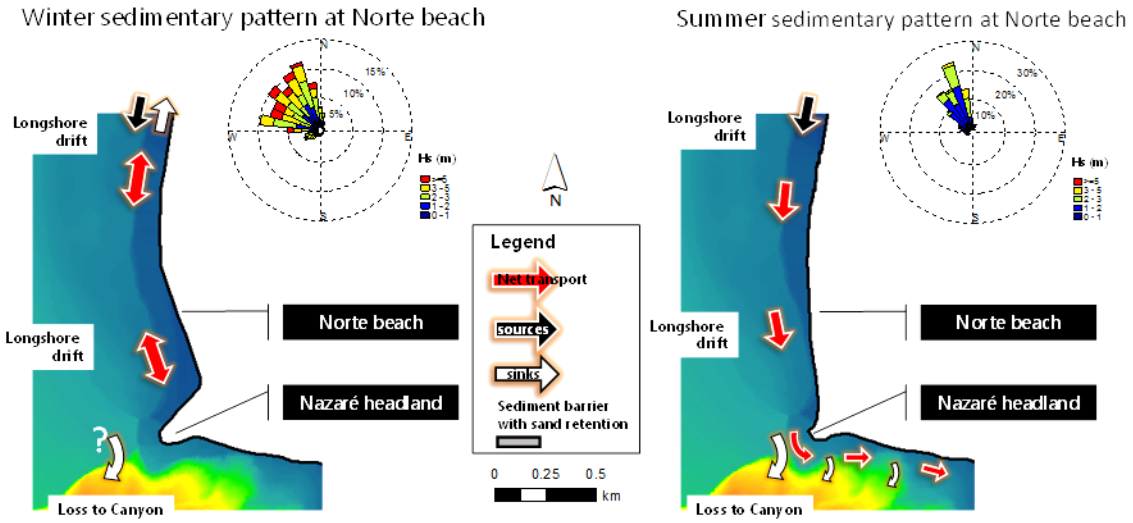


**Figure 8.23 – Winter and summer sedimentary pattern at Nazaré coast (the rose diagrams represent the offshore wave conditions during the monitoring period at winter [DJF] and summer [JJA]).**

The particularities of the summer pattern (Figure 8.23) are related to the Norte beach shoreline configuration that progressively attains a more linear configuration, while the sediments from LST are being retained in the headland. During this typical summer beach

configuration, some sediments enter directly into the canyon while others reach the Nazaré bay beach bypassing the headland via submarine profile.

Occasionally, when the sediment accumulation and bypass are particularly large the Prainha phenomenon occurs and an ephemeral beach arises around the headland, promoting subaerial sand bypass. This sedimentary accumulation can retain, temporarily, sand volumes about 50 000 $m^3$ (see *sub-chapter 8.1.3.2. – Prainha* ) which normally, by the end of the summer, are redistributed in Nazaré bay or lost into the canyon.

## 8.2. CONCLUSIONS AND FUTURE WORK

The Norte beach is a particular place where a rare combination between complex forcing mechanisms with huge morphological responses exists.

During this 3.4 years of video monitoring was possible to quantify great morphological variations on the Norte beach. The seasonality imprint on the Norte beach shoreline position attain magnitudes of variation up to 160 m near the Nazaré headland and the sand volume varies on average 1.57 million of cubic meters every season, within the study area.

Although these variations are mainly related to seasonal recurrences, important interannual variability is recognized in the morphodynamics of this coastal stretch. Despite the long-term monitoring of the Norte beach, this period was not enough to assess the long-term variability of this littoral. In fact, this was already demonstrated in Silva et al, 2012 - *Chapter 5 – Longshore Sand Transport Variability at the Northwest Coast of Portugal* where a minimum of 10 years of monitoring is required to obtain estimates that are ±20 % of the long-term average. For this reason, the future maintenance of the Cosmos video monitoring system at Norte beach is of major importance.

The estimates of the longshore sediment transport at Norte beach were also a challenging task. The measurements of LST were performed through the beach profile model that computes the beach volume, at its change, based on the shoreline position (on a monthly base). LST simulations, on the other hand, resulted from the numerical modeling of the wave regime at the breaking and the application of the CERC formula.

Integration of both approximations revealed small overestimation of the simulations (1.15 times the observations) that led to a re-adjustment of the K coefficient, for this coastal stretch, to a value of 0.34 (relating to Hs) which is surprisingly in agreement with the one recommended in literature.

Additionally, it is worth mentioning that both of those LST approximations are subject to some limitations. The observations of the Norte beach (considered in the integration and model calibration) were limited to the southern sector of the Norte beach since this area reflects particularly the seasonal responses. The simulations considered in the integration and model calibration were restricted to the period without significant video interruptions and to the forcing modelled at the northern limit of the video monitoring area. Another peculiarity of these results is better data agreement when considering the LST trimestral observations/estimations, this is related to the time that the beach takes to adjust to the wave forcing.

As result, a long-term morphodynamic conceptual model was drawn for this coast where 1 million cubic meters of sand (per year) enters this coastal stretch and is transported southward by the prevailing NW wave incidence. The longshore drift is then captured by the submarine canyon tributaries in front of the Nazaré headland or in front of the Nazaré bay beach, closing, at this place, the Douro-Nazaré coastal cell.

Additionally, a distinct sedimentary pattern was recognized at Nazaré coast during winter. The wider wave dispersion, namely the more frequent occurrences of western waves, induce to occasional drift inversion where the LST is directed to the north. This occurrences are restricted to winter conditions and induce an arcuate shoreline configuration together with an escape of sediments (more or less intense) at the northern limit of the monitoring area. During these conditions is still not clear if there is sand transport down-canyon, Norte beach is particularly retreated near the headland (in the vicinity of the Nazaré canyon head) and the lack of information about the submarine beach profile configuration prevents a reliant response to this question.

From the aforementioned achieves it was noticed that the monitoring area should be extended northward to include the evaluation of the magnitude of sand which is temporarily transported northward. Additionally, future work must consider the characterization of the submarine beach profile configuration over time.

Some additional limitations were also found during this work, it was perceived that the nearshore wave characterization, based on the state of the art wave propagation models (SWAN and XBeach) did not simulate truthfully the wave effects over the submarine canyon. Because of its non-resolving wave phase, those models fail on the estimations of the wave effects magnitude particularly the wave highs and interferences in the vicinity of the headland. Future work in wave propagation modeling, at this site, should consider the application of phase-resolving models that consider the wave phase of the incoming

waves. In this scenario, video imagery would provide essential data for the calibration of these models.

Also in what concerns the morphodynamic assessment of Norte beach, an extremely valuable future improvement is related to the morphodynamic modeling using one-dimensional coastline evolution model. This process based approach couples the instantaneous LST estimates with their morphological effects on the coastline configuration, reducing the extreme uncertainties and sensibility related to the coastline orientation.

A brief list of the key findings/achievements is presented:

- Video monitoring techniques were successfully applied in the understanding of the Norte beach morphodynamics. Displacement errors with implications on the coastline detection (of a few metres) are related to the cross-shore positional accuracy, which is the less uncertain direction.
- A long-term video monitoring system (COSMOS) was made operational in the monitoring of Norte beach since the December 2008 (despite gaps related with some technical failures). A long-term record of imagery was compiled, from which about three and half years of the Norte beach imagery data is available, and was analysed within the present work.
- The shoreline variability at the Norte beach was characterized, including its seasonal patterns and the recognition of beach responses that might be more related to interannual (long-term) beach variability. High seasonal coastline variability was identified which exceeds 160 m in the southern sector and 70 m at the central and northern ones. The beach oscillates from a straight (during June to August) and arcuate configuration (during the remaining months).
- The morphological changes and respective variability were also characterized by means of beach volume estimations; this was achieved by the development of a beach volume model which estimates the beach volume based on the position of the Norte beach shoreline. The Norte beach volume varies about 1.5 million of $m^3$ of sand, between around 5.8 and 7.5 million of $m^3$. Also, a seasonal pattern in the volume variability, more visible near the headland, was recognized and quantified.
- It was recognized the high interannual variability of this littoral, for this reason to estimate the longstanding annual drift, at this coastal stretch, a long-term monitoring (5-10 years) program is required.
- SWAN and XBeach were used to model the wave propagation and morphological changes at the Nazaré coast. The developed BeachMM tool has proven its

applicability as it greatly simplifies dataflow effort, reduces the human error and provides a dynamic visualization of the modelling results

- It was established the relation between morphological changes and wave forcing at the Norte beach, from which was possible the assessment of the sedimentary budget at this beach and at the Nazaré coast (including the Prainha and the Nazaré bay beach);
- The relation between LST observations and estimates allowed the improvement of the knowledge about the sedimentary budget of the Douro-Nazaré coastal cell and estimate the K parameter (K = 0.34), at a high-energy environment.
- Based on the morphological evolution of the Norte beach, LST magnitude observations were performed; the annual net drift was estimated in about 1 million cubic meters of sand, directed to the south.
- The sediment circulation pattern at this coast revealed the sedimentary connection between Norte beach and the Nazaré bay beach; part of the longshore drift enters directly into the canyon while part of it bypass the headland and feed the Nazaré bay beach, before it finally enter into the canyon at its tributaries.
- In particular condition the sand passage around the headland occurs sub-aerially, when Prainha phenomena takes place.

# REFERENCES

# REFERENCES


Aagaard, T.; Black, K.P. and Greenwood, B. (2002). *Cross-shore suspended sediment transport in the surf zone: a field-based parameterization.* Marine Geology, 185(3-4), 283–302.

Aarninkhof, S.G.J. (2003). *Nearshore Bathymetry derived from Video Imagery*. Delft: Technical University of Delft, Ph. D. thesis, 175 pp.

Aarninkhof, S.G.J.; Turner, I.L.; Dronkers, T.D.; Caljouw, M. and Nipius, L. (2003). *A video-based technique for mapping intertidal beach bathymetry*. Coastal Engineering, 49(4), 275-289.

Abecasis, C. (1955). *The history of a tidal lagoon inlet and its improvement (the case of Aveiro, Portugal).* Proceedings 5th International Conference Coastal Engineering, Grenoble, 329-363.

Alegria-Arzaburu, A.R. de and Masselink, G. (2010). *Storm response and beach rotation on a gravel beach, Slapton Sands, U.K.*. Marine Geology, 278(1-4), 77–99.

Alexander, P. and Holman, R.A. (2004). *Quantification of nearshore morphology based on video imaging.* Marine Geology, 208(1), 101–111.

Almar, R.; Coco, G.; Bryan, K.R.; Huntley, D.A.; Short, A.D. and Senechal, N. (2008). *Video observations of beach cusp morphodynamics*. Marine Geology, 254(3-4), 216–223.

Andrade, C.; Freitas, M.C.; Cachado, C.; Cardoso, A.C.; Monteiro, J. H.; Brito, P. and Rebelo, L. (2002). *Coastal Zones.* In: Climate Change in Portugal. Scenarios, Impacts and Adaptation Measures. Santos, F.D.; Forbes, K. and Moita, R. [Eds.]; SIAM Project, Gradiva, Lisboa, 173-219.

Andrade, C.; Pires, O.; Taborda, R. and Freitas, M.C. (2007). *Projecting future changes in wave climate and coastal response in Portugal by the end of the 21st century*. Journal of Coastal Research, SI50, 263 – 267.

Andrade, C.; Taborda, R.; Oliveira, M.A.; Alves, M. and Carapuço, A.M. (2013). *Caracterização do clima de agitação ao largo*. Criação e implementação de um sistema de monitorização no litoral abrangido pela área de jurisdição da administração da região hidrográfica do Tejo, APA - Agência Portuguesa do Ambiente, 14 pp, (in Portuguese).

Antunes, C. (2007). *Previsão de Marés dos Portos Principais de Portugal*. In: http://webpages.fc.ul.pt/~cmantunes/hidrografia/hidro_mares.html accessed in November 2012.

Archetti, R.; Schiaffino, C.; Ferrari, M.; Brignone, M. and Rihouey, D. (2008). *Video systems for coastal monitoring*. Beach erosion monitoring. Pranzini, E. and Wetzel, L. [Eds.]; Beachmed-e/OpTIMAL Project, 111-118.

Armaroli, C. and Ciavola, P. (2011). *Dynamics of a nearshore bar system in the northern Adriatic: A video-based morphological classification*. Geomorphology, 126(1-2), 201–216.

Armaroli, C.; Ciavola, P.; Balouin, Y. And Gatti, M. (2004). *An integrated study of shoreline variability using GIS and ARGUS techniques.* Journal of Coastal Research, SI39, 473-478.

Baptista, P. (2006). *O Sistema de Posicionamento Global Aplicado ao Estudo de Litorais Arenosos*. Ph.D. thesis, University of Aveiro, Portugal, 260 pp, (in Portuguese).

Barceló, J.P. (1970). *Experimental Study of the Hydraulic Behaviour of Inclined Groyne Systems*. Proceedings 12th Coastal Engineering Conference, ASCE, 1021-1040.

Battjes, J. A. and Janssen, J.P.F.M. (1978). *Energy loss and set-up due to breaking of random waves.* Proceedings 16th International Conference Coastal Engineering, ASCE, 569-587.

Bauer, E. (2001). *Interannual changes of the ocean wave variability in the North Atlantic and in the North Sea*. Climate Research, 18, 63–69.

Beach, R. and Sternberg, R. (1988). *Suspended sediment transport in the surf zone: response to cross-shore infragravity motion*. Marine Geology, 80, 61–79.

Bertin, X.; Castelle, B.; Chaumillon, E.; Butel, R. and Quique, R. (2008). *Longshore transport estimation and interannual variability at a high energy dissipative beach: St Trojan Beach, SW Oléron Island, France.* Continental Shelf Research, 28(10-11), 1316–1332.

Bodge, K.R. and Dean, R.G. (1987). *Short term impoundment of longshore transport*. Proceedings Coastal Sediments. ASCE, New York, 468-483.

Bodge, K.R. and Kraus, N.C. (1991). *Critical examination of longshore transport rate magnitude*. Proceedings Coastal Sediments '91. ASCE, New York, 139-155.

Booij N.; Ris R.C. and Holthuijsen, L.H. (1999). *A third-generation wave model for coastal regions. 1. Model description and validation*. Journal of Geophysical Research, 104(7), 649–666.

Brandmeyer, J.E. and Karimi, H.A. (2000). *Coupling methodologies for environmental models*. Environmental Modelling & Software, 15, 479–488.

Carvalho, J.R. and Barceló, J. (1966). *Agitação marítima na costa Oeste de Portugal Metropolitano – Contribuições para o seu estudo.* Memórias Laboratório Nacional Engenharia Civil, 290, Lisboa, 34 pp, (in Portuguese).

Cascalho, J.; Bosnic, I.; Taborda, R.; Ribeiro, M.; Lira, C. and Carapuço, M. (2012). *Beach sediment grain size variability based on image analysis*. Proceedings 2as Jornadas de Engenharia Hidrografica, Lisboa, 287-290.

CERC (1984). *Shore Protection Manual*. U.S. Army Corps of Engineers, Coastal Engineering Research Center. U.S. Government Printing Office, Washington, D.C.

Cheng, W.; Wang, K. and Zhang, X. (2010). *Implementation of a COM-based decision-tree model with VBA in ArcGIS*. Expert Systems with Applications, 37, 12-17.

Ciavola, P.; Taborda, R.; Ferreira, Ó. and Dias, J.M.A. (1997). *Field measurements of longshore sand transport and control processes on a step meso-tidal beach in Portugal.* Journal Coastal Research. 13, 1119-1129.

Coelho, C.D.B. (2005). *Riscos de Exposição de Frentes Urbanas para Diferentes Intervenções de Defesa Costeira.* Ph.D. thesis, Universidade de Aveiro, Aveiro, Portugal, 404 pp, (in Portuguese).

Coelho, C.; Silva, R.; Veloso-Gomes, F. and Taveira-Pinto, F. (2009). *Potential effects of climate change on northwest Portuguese coastal zones*. ICES Journal of Marine Science, 66, 1497–1507.

Conley, D.C.; Trangeled, A.; Zappa, G.; Gualdesi, l.; Guerrini, P. and Holman, R.A. (2007). *Rapid environmental assessment in the nearshore*. Journal of Marine Systems, 69(1-2), 74-85.

Costa, C.L. (1994). *A Wind wave climatology of the Portuguese Coast*, Final report of sub-project. Report PO-WAVES 6/94-A, IH/LNEC, Lisbon, 80 pp.

Costa, M.; Silva, R. and Vitorino, J. (2001). *Contribuição para o estudo do clima de agitação marítima na costa portuguesa.* Actas das 2ªs Jornadas Portuguesas de Engenharia Costeira e Portuária. Associação Internacional de Navegação, Sines, 20 pp, (in Portuguese).

Crossman, N.D.; Perry, L.M.; Bryan, B.A. and Ostendorf, B. (2007). *CREDOS: A Conservation Reserve Evaluation And Design Optimization System.* Environmental Modelling & Software, 22, 449-463.

Davidson, M.; Van Koningsveld, M.; de Kruif, A.; Rawson, J.; Holman, R.; Lamberti, A., Medina, R.; Kroon, A. and Aarninkhof, S. (2007). *The CoastView project: developing video-derived coastal state indicators in support of coastal zone management*. Coastal Engineering, 54(6-7), 463-475.

Dean, R.G. (1991). *Equilibrium Beach Profiles: Characteristics and Applications*. Journal of Coastal Research 7(1),53-84

Dean, R.G.; Berek, E.P.; Bodge, K.R. and Gable, C.G. (1987). *NSTS measurements of total longshore transport.* Proceedings Coastal Sediments. ASCE, New York, 452–667.

Delft (2005). *Delft3D-WAQ: Detailed description of processes*. Technical Reference Manual. 397 pp.

Deltares (2011). *Validation of dune impact models using European field data.* Report 1002266, DeltaResearch

Dessy, C.; Schiaffino, C.; Corradi, N. and Ferrari, M. (2008). *Nourishment of Levanto (Italy): a webcam-aided evaluation of a mixed sand and gravel beach fill*. In: Beach erosion monitoring. Pranzini, E. and Wetzel, L. [Eds.], Beachmed-e/OpTIMAL Project, 119-128.

Di Luzio, M.; Srinivasan, R. and Arnold, J.G. (2004). *A GIS-Coupled Hydrological Model System for the Watershed Assessment of Agricultural Nonpoint and Point Sources of Pollution*. Transactions in GIS, 8(1), 113-136.

Dias, J.M.A.; Jouanneau, J.M.; Gonzalez, R.; Araújo, M.F.; Drago, T.; Garcia, C.; Oliveira. A.; Rodrigues, A.; Vitorino, J. and Weber, O. (2002). *Present day sedimentary processes on the northern Iberian shelf*. Progress on Oceanography, 52(2-4), 249–259.

Dodet, G.; Bertin, X. and Taborda, R. (2010). *Wave climate variability in the North-East Atlantic Ocean over the last six decades*. Ocean Modelling, 31(3-4), 120–131.

Downing, J.P.; Sterberg, R.W. and Lister, C.R.B. (1981). *New instrumentation for the investigation of sediment suspension processes in the shallow marine environment.* Marine Geology, 42, 19–34.

Dronkers, T. (2001). *Intertidal morphodynamics at Narrowneck Reef*. Delft: Technical University of Delft, Master's thesis, 55 pp.

Duane, D.V. and James, W.R. (1980). *Littoral transport in the surf zone elucidated by an eulerian sediment tracer experiment.* Journal of Sedimentary Petrology 50(93), 929-942.

Duarte, J.; Taborda, R.; Ribeiro, M.; Cascalho, J.; Silva, A. and Bosnic, I. (2014). *North beach (Nazaré) sand tracer experiment.* Geophysical research abstracts, Vol. 16. EGU2014.

ESRI (2010). *ArcGIS - A Complete Integrated System.* Environmental Systems Research Institute, Inc., Redlands, California. Available via http://esri.com/arcgis. Accessed August 2010.

Falqués, A. (2006). *Wave driven alongshore sediment transport and stability of the Dutch coastline.* Coastal Engineering, 53, 243-254.

Fields, M.L. and Weishar, L.L. (1987). *Distribution of sediment tracers seaward of the breaker zone – Duck85.* Proceedings Coastal Sediments. ASCE, New York, 848-864.

Foster, R.A. (2012). *Shoreline variation and beach rotation of Pauanui beach*. University of Waikato.

Freire de Andrade (1937). *Os vales submarinos portugueses e o diastrofismo das Berlengas e da Estremadura*. Mem. Serv. Geol. Port., 1, (in Portuguese).

Freire, P. (2003). *Morphological and sedimentary evolution of estuarine banks (Tagus Estuary, Portugal)*. University of Lisbon, LNEC, Ph.D. thesis, 380 pp, (in Portuguese).

Freire, P.; Taborda, R. and Silva, A.M. (2007). *Sedimentary Characterization of Tagus Estuarine Beaches (Portugal). A contribution to the sediment budget assessment.* Journal of Soils and Sediments, 7(5), 296–302.

Guillén, J.; García-Olivares, A.; Ojeda, E.; Osorio, A.; Chic, O. and González, R. (2008). *Long-Term Quantification of Beach Users Using Video Monitoring*. Journal of Coastal Research, 246, 1612–1619.

Guza, R.T. and Thornton, E. B. (1981). *Wave set-up on a natural beach*. Geophysical Research, 86(C5), 4133–4137.

Hanson, H. (1989). *GENESIS — a generalized shoreline change numerical model*. Journal of Coastal Research 50 (1), 1–27.

Harley, M.D.; Turner, I.L.; Short, A.D. and Ranasinghe, R. (2011). *Assessment and integration of conventional, RTK-GPS and image-derived beach survey methods for daily to decadal coastal monitoring*. Coastal Engineering, 58(2), 194–205.

Haxel, J. and Holman, R.A. (2004). *The sediment response of a dissipative beach to variations in wave climate.* Marine Geology, 206(1-4), 73–99.

Heikkila, J. and Silvén, O. (1997). *A four-step camera calibration procedure with implicit image correction*. IEEE Computer Society Conference on Computer Vision and Pattern Recognition (CVPR'97), San Ruan, Puerto Rico, 106-1112.

Holland, K.T. (1998). *Beach cusp formation and spacings at Duck, USA*. Continental Shelf Research, 18(10), 1081–1098.

Holland, K.T.; Holman, R.A. and Lippmann, T.C. (1997). *Practical Use of Video Imagery in Nearshore Oceanographic Field Studies*. IEEE Journal of Oceanic Engineering, 22(1), 81-92.

Holman, R.A. (1986). *Extreme value statistics for wave run-up on a natural beach*. Coastal Engineering, 9, 527-544.

Holman, R.A. and Stanley, J. (2007). *The history and technical capabilities of Argus*. Coastal Engineering, 54(6-7), 477-491.

Holman, R.A.; Sallenger, J.; Lippmann, T.C. and Haines, J.W. (1993). *The application of video image processing to the study of nearshore processes.* Oceanography, 6(3), 78-95.

Hughes, M.G.; Moseley, A.S. and Baldock, T.E. (2010). *Probability distributions for wave runup on beaches.* Coastal Engineering, 57(6), 575-584.

Hurrel, J.W. (1995). *Decadal Trends in North Atlantic Oscillation: Regional temperatures and Precipitation.* Science, 5224, 676-679.

Kalnay, E.; Kanamitsu, M.; Kistler, R.; Collins, W.; Deaven, D.; Gandin, L.; Iredell, M.; Saha, S.; White, G.; Woollen, J.; Zhu, Y.; Chelliah, M.; Ebisuzaki, W.; Higgins, W.; Janowiak, J.; Mo, K. C.; Ropelewski, C.; Wang, J.; Leetmaa, A.; Reynolds, R.; RoyJenne, R. and Joseph, D. (1996). *The NCEP/NCAR 40-year reanalysis project*. Bulletin of the American Meteorological Society, 77, 437-472.

Kamphuis, J.W. (1991). *Alongshore sediment transport of sand*. Journal of Waterway, Port, Coastal, and Ocean Engineering, ASCE, 117(6), 624-641.

Kamphuis, J.W. (2000). *Introduction to Coastal Engineering and Management*. World Scientific, Singapore.

Klemas, V. (2009). *Sensors and Techniques for Observing Coastal Ecosystems.* In: Remote Sensing and Feospatial Technologies for Coastal Ecosystem Assessment and Management. Lecture Notes in geoinformation and Cartography. Yang, X. Ed. Springer-Verlag Berlin Heidelberg. 561pp.

Komar, P.D. (1998). *Beach Processes and Sedimentation.* Prentice Hall, New Jersey. 544 pp.

Komar, P.D. (1990). *Littoral sediment transport*. In: Handbook of Coastal and Ocean Engineering. Herbich, J. [eds.], vol. 2 Gulf Pub. Co, Houston, TX, 681-714.

Komar, P.D. and Inman, D.L. (1970). *Longshore sand transport on beaches*. Journal of Geophysical Research. 75(30), 5514-5527.

Konicki, K. and Holman, R.A. (2000). *The statistics and kinematics of transverse sand bars on an open coast*. Marine Geology, 169(1-2), 69–101.

Kraus, N.C. and Dean, J.L. (1987). *Longshore sediment transport rate distribution measured by trap*. Proceedings Coastal Sediments. ASCE, New York, 881–896.

Kraus, N.C.; Isobe, M.; Iagrashi, H.; Sasaki, T.C. and Horikawa, K. (1981). *Field experiments on longshore sand transport in the surf zone.* Coastal Engineering Jpn. 24, 171-194.

Kraus, N.C.; Farinato, R.S. and Horikawa, K. (1982). *Field experiments on longshore sand transport in the surf zone.* Proceedings 18th Coastal Engineering Conference ASCE, 969-988.

Kroon, A.; Larson, M.; Möller, I.; Yokoki, H.; Rozynski, G.; Cox, J. and Larroude, P. (2008). *Statistical analysis of coastal morphological data sets over seasonal to decadal time scales*. Coastal Engineering, 55(7-8), 581–600.

Lapa, N.; Rodrigues, A.; Taborda, R.; Duarte, J. and Pinto, J. (2012). *The sedimentary processes of the Portuguese inner shelf off Almagreiro Beach (Peniche).* Actas das 2as Jornadas de Engenharia Hidrográfica. Instituto Hidrográfico, 279-282.

Laranjeiro, S.H.C.D.; Oliveira, F.S.B.F.; Taborda, R. and Silva, R. (2004). *Dinâmica Sedimentar do Trecho Litoral Praia da Vieira - Praia Velha. Caracterização de Parâmetros Morfodinâmicos*. 7º Congresso da Água, APRH, CD-ROM.

Larson, M. and Kraus, N. (1994). *Temporal and spatial scales of beach profile change, Duck, North Carolina*. Marine Geology, 117, 75–94.

Larson, M.; Capobianco, M. and Jansen, H. (2003). *Analysis and modeling of field data on coastal morphological evolution over yearly and decadal time scales. Part 1: Background and linear techniques*. Journal of Coastal Research, 19(4), 760–775.

Larson, M.; Hoan, L. and Hanson, H. (2010). *Direct Formula to Compute Wave Height and Angle at Incipient Breaking*. Journal of Waterway, Port, Coastal, and Ocean Engineering, 136(2), 119–122.

Liao, H. and Tim, U.S. (1997). *An interactive modeling environment for nonpoint source sollution control*. Journal of American Water Resources Association, 33(3), 591–603.

Lira, F.C. and Taborda, R. (2014). *Advances in Applied Remote Sensing to coastal environments using free satellite imagery.* In: Advances in Coastal and Marine Resources: Remote Sensing and modelling. Finkl, C.W., Klein, A.H.F. and Makowski, C. [Eds.], Springer.

Liu, H.; Arii, M.; Sato, S. and Tajima, Y. (2012). *Long-term nearshore bathymetry evolution from video imagery: a case study in the Miyazaki coast*. Proceedings of 33th International Conference on Coastal Engineering, ICCE2012, Santander, Spain.

Luterbacher, J.; Xoplaki, E.; Dietrich, D.; Jones, P.D.; Davies, T.D.; Porties, D.; Gonzalez-Rouco, J.F.; von Storch, H.; Gyalistras, D.; Casty, C. and Wanner, H. (2002). *Extending North Atlantic oscillation reconstructions back to 1500*. Atmospheric Science Letters, 2, 114-124.

Madsen, A.J. and Plant, N.G. (2001). *Intertidal beach slope predictions compares to field data*. Marine Geology, 173, 121-139.

Madsen, O.S; Poon, Y-K. and Graber, H.C. (1988). *Spectral wave attenuation by bottom friction: theory*. Proceedings 21th International Conference Coastal Engineering, ASCE, 492–504.

Masselink, G. and Short, A. (1993). *The effect of tide range on beach morphodynamics and morphology: A Conceptual Beach Model.* Journal of Coastal Research, 9(3), 785-800.

Masselink, G. and Pattiaratchi, C.B. (2001). *Seasonal changes in beach morphology along the sheltered coastline of Perth, Western Australia*. Marine Geology, 172(3-4), 243–263.

McCall, R.T.; de Vries, J.S.M.V.T.; Plant, N.G.; Van Dongeren, A.R.; Roelvink, J.A.; Thompson, D.M. and Reniers, A.J.H.M. (2010). *Two-dimensional time dependent hurricane overwash and erosion modeling at Santa Rosa Island.* Coastal Engineering, 57, 668–683.

McCowan, J. (1891). *On the Solitary Wave*. London, Philosophical Magazine, 32(194), 45-58.

Miller, J.K. and Dean, R.G. (2007). *Shoreline Variability via Empirical Orthogonal Function Analysis: Part I Temporal and Spatial Characteristics*. Coastal Engineering, 54(2), 111–131.

Nielsen, P. (1989). *Wave Setup and Runup: An Integrated Approach*. Coastal Engineering, 13(1), 1-9.

Ojeda, E.; Guillén, J. and Ribas, F. (2011). *Dynamics of single-barred embayed beaches*. Marine Geology, 280(1-4), 76–90.

Oliveira, A.; Santos, A.; Rodrigues A. and Vitorino J. (2007). *Sedimentary particle distribution and dynamics on the Nazaré canyon system and adjacent shelf (Portugal)*. Marine Geology. 246(2-4), 105-122.

Oliveira, F.S.B.F.; Oliveira, T.C.A.; Silva, R. and Larangeiro, S.H.C.D. (2004). *Dinâmica Sedimentar do Trecho Litoral Praia da Vieira - Praia Velha. Hidrodinâmica e transporte longitudinal de sedimentos.* 7º Congresso da Água, APRH, (in Portuguese)

Pilar, P.; Guedes Soares, C. and Carretero, J.C. (2008). *44-year wave hindcast for the North East Atlantic European coast.* Coastal Engineering, 55, 827-842.

Pinheiro, J.P.T. (2008). *Avaliação dos processos de transposição artificial de sedimentos em embocaduras.* University of Porto, Engineering faculty. Master thesis, 96 pp, (in Portuguese).

Pires, H.N. and Pessanha, L.E. (1986). *Wave power climate of Portugal, In:* Hydrodynamics of Ocean Wave-energy Utilization. Evans, D. and Falcão, A. [Eds.], IUTAM Symposium, Lisboa, 157-167.

Plant, N.G. and Holman, R.A. (1997). *Intertidal beach profile estimation using video images*. Marine Geology, 140, 1-24.

Portela, L. and Neves, R. (1994). *Numerical Modelling of Suspended Sediment Transport in Tidal Estuaries: a Comparison Between the Tagus and the Scheldt.* Netherlands Journal of Aquatic Ecology, 28(3-4), 329-335.

Pullar, D. and Springer, D. (2000). *Towards integration GIS and catchment models*. Environmental Modelling & Software, 15, 451-459.

Python Software Foundation (2010). *Python Programming Language*. Python Soft-ware Foundation, Hampton, NewHampshire. Available via http://python.org. Accessed August 2010.

Quartel, S.; Kroon, A. and Ruessink, B.G. (2008). *Seasonal accretion and erosion patterns of a microtidal sandy beach.* Marine Geology, 250(1-2), 19–33.

Ranasinghe, R.; Symonds, G.; Black, K. and Holman, R.A. (2004). *Morphodynamics of intermediate beaches: a video imaging and numerical modelling study*. Coastal Engineering, 51(7), 629–655.

Roberts, J.J.; Best, B.D.; Dunn, D.C.; Treml, E.A. and Halpin, P.N. (2010). *Marine Geospatial Ecology Tools: An integrated framework for ecological geoprocessing with ArcGIS, Python, R, MATLAB, and C++*. Environmental Modelling & Software, 25, 1197-1207.

Roelvink, J.A.; Reniers, A.; Van Dongeren, A.; De Vries, J.V.T.; Lescinski, J. and Walstra, D.J. (2007). *Modeling hurricane impacts on beaches, dunes and barrier islands*. Proceedings 10th workshop on Waves and Coastal Hazards, North Sore, Oahu.

Roelvink, D.; Reniers, A.; Van Dongeren, A; De Vries, J.V.T.; McCall, R. and Lescinski, J. (2009). *Modeling storm impacts on beaches, dunes and barrier islands*. Coastal Engineering, 56(11-12), 1133-1152.

Roelvink, D.; Reniers, A.; Van Dongeren, A.; De Vries, J.V.T.; Lescinski, J. and McCall, R. (2010). *XBeach Model description and Manual*. Unesco-IHE Institute for Water Education, Deltares and Delft University of Tecnhology. Report June, 21 2010 version 6.

Rosati, J.D.; Gingerich, K.J.; Kraus, N.C.; Smith, J.M. and Beach, R.A. (1991). *Longshore sand transport rate distributions measured in Lake Michigan*. Proceedings Coastal Sediments. ASCE, New York, 156–169.

Rosati, J. D.; Walton, T. L. and Bodge, K. (2002). *Longshore sediment transport*. Coastal Engineering Manual, Part III, Longshore sediment transport, Chapter III-2, Engineering Manual, 1100-2-1100. U.S. Army Corps of Engineers, Washington, DC.

Santos, L.I.V.; Tavare, A.O. and Antunes do Carmo, J.S. (2013). *Dealing with expertise and non expertise knowledge about coastal risk*. Procedia – Social and Behavioral Sciences, 83, 83-87.

Savitzky, A and Golay, M.J.E. (1964). Smoothing and differentiation of data by simplified least squares procedures. Analytical Chemistry, 36, 1627–1639.

Schoonees, J. S. (2000). *Annual variation in the net longshore sediment transport rate.* Coastal Engineering, 40, 141-160.

Shi-Leng, X. and Teh-Fu, T. (1987). *Long-term variation of longshore sediment transport*. Coastal Engineering, 11, 131-140.

Siegle, E.; Huntley, D. A. and Davidson, M.A. (2007). *Coupling video imaging and numerical modelling for the study of inlet morphodynamics.* Marine Geology, 236(3-4), 143–163.

Silva, A.N.; Taborda, R.; Rodrigues, A.; Duarte, J. and Cascalho, J. (2007). *Longshore Drift Estimation Using Fluorescent Tracers: New Insights from an Experiment at Comporta Beach, Portugal*. Marine Geology, 240, 137–150.

Silva, A.N.; Taborda, R.; Catalão, J. and Freire, P. (2009). *DTM Extraction using video-monitoring techniques: application to a fetch limited beach*. Journal of Coastal Research, SI56, 203-207.

Silva, A.N.; Taborda, R.; Bertin, X. and Dodet, G. (2012). *Seasonal to Decadal Variability of Longshore Sand Transport at the Northwest Coast of Portugal*. Journal of Waterway, Port, Coastal, and Ocean Engineering, 138(6), 464-472.

Silva, A.N.; Taborda, R.; Antunes, C.; Catalão, J. and Duarte, J. (2013). *Understanding the coastal variability at Norte beach, Portugal.* Journal of Coastal Research, SI65, 2173–2178.

Silva, R.; Silva, A.J.; Rusu, E.; Oliveira, F.S.B.F.; Larangeiro, S.H.C.D. and Taborda, R. (2005). *Evaluation of the longshore current for a sector of the Portuguese west coast: application of different methodologies*. Proceedings 29th International Conference Coastal Engineering, ASCE, 2, 1455-1467.

Silveira, T.M.; Diogo, Z.; Taborda, R.; Andrade, C.; Sousa, H.; Carapuço, A.M. and Silva, A.N. (2013). *Caracterização da variabilidade morfodinâmica sazonal das praias-piloto representativas do litoral em estudo*. Criação e implementação de um sistema de monitorização no litoral abrangido pela área de jurisdição da administração da região hidrográfica do Tejo, APA - Agência Portuguesa do Ambiente, 147 pp, (in Portuguese).

Smit, M.W.; Aarninkhof, S.G.J.; Wijnberg, K.M.; González, M.; Kingston, K.S.; Southgate, H.N.; Ruessink, B.G.; Holman, R.A.; Siegle, E.; Davidson, M. and Medina, R. (2007). *The role of video imagery in predicting daily to monthly coastal evolution*. Coastal Engineering, 54(6-7), 539–553.

Smith, R.K. and Bryan, K.R. (2007). *Monitoring Beach Face Volume with a Combination of Intermittent Profiling and Video Imagery*. Journal of Coastal Research, 23(4), 892-898.

Southgate, H.; Wijnberg, K.; Larson, M.; Capobianco, M. and Jansen, H. (2003). *Analysis of field data of coastal morphological evolution over yearly and decadal timescales. Part 2: Non-linear techniques*. Journal of Coastal Research, 19(4), 776–789.

Stockdon, H.; Holman, R.A.; Howd, P. and Sallenger Jr, A. (2006). *Empirical parameterization of setup, swash, and runup.* Coastal Engineering, 53(7), 573-588.

SWAN (2009). *Scientific and Technical Documentation (version 40.51)*. Delft University of Technology, Environmental Fluid Mechanics Section. Available via http://www.fluidmechanics.tudelft.nl/swan/index.html. Accessed August 2010.

SWAN Course (2014). *SWAN Course*. Available via: http://tamtie.nl/digital-hydraulics/index.php?pag=Swan_course.htp Accessed September 2014.

Taborda, R. and Silva, A. (2012). *COSMOS: A lightweight coastal video monitoring system*. Computers & Geosciences, 49, 248-255.

Taborda, R.; Ferreira, Ó.; Dias, J.M.A. and Moita, P. (1994). *Field observations of longshore sand transport in a high energy environment.* Proceedings Littoral 94. Second International Symp. Europ. Coastal Zone Assoc. Sci. Technol. EUROCOAST, Portugal, Lisbon, 479–487.

Taborda, R.; Ciavola, P.; Ferreira, Ó. and Dias, J.M.A. (1999). *Measurements of suspended sediment transport on a reflective mesotidal beach in southern Portugal*. Revista do Instituto Español de Oceanografia. 15, 229–241.

Taborda, R.; Magalhães, F. and Ângelo, C. (2005). *Evaluation of Coastal Defence Strategies in Portugal*. In: Environment Friendly Coastal Protection Structures. Dean, B. and Zimmermann, C. [Eds.], Kluwer, Netherlands. 255-265.

Taborda, R.; Silveira, T; Andrade, C.F.; Carapuço, A.M.; Duarte, J.F. (2012). *Galgamento marinho do edifício de talassoterapia na área dominial do porto de abrigo da Nazaré.* Tecnhical report by Instituto Dom Luiz and Centro de Geologia, 17 pp, (in Portuguese).

Taborda, R.; Andrade, C.F.; Silva, A.; Silveira, T.; Lira, C.; Freitas, M.C. and Pinto, C. (2014). *Caparica-Espichel longshore sediment transport model.* IX Congresso Nacional de Geologia (IX CNG) e 2º Congresso de Geologia dos Países de Língua Portuguesa (2º CoGePLiP) [IX CNG/2º CoGePLiP], Porto, 18 a 24 Julho 2014. (in Portuguese).

Taveira-Pinto, F.; Pais-Barbosa, J. and Veloso-Gomes, F. (2009). *Coastline Evolution at Esmoriz-Furadouro Stretch (Portugal).* Journal of Coastal Research, SI56, 673-677.

Teixeira, S. (1994). *Dinâmica sedimentar da ria de Aveiro (Portugal)*. Ph.D. thesis, University of Lisbon, Portugal. 396 pp, (in Portuguese).

Teixeira, S. (2009). *Alimentação artificial de praias com dragados*. In: 1º Curso Técnico de Dragagens, Aveiro, (in Portuguese).

Tolman, H.L. (2009). *User manual and system documentation of WAVEWATCH III version 3.14*. NOAA/NWS/NCEP/MMAB Technical Note 276, 194 pp.

Turner, I. L.; Whyte, D.; Ruessink, B.G. and Ranasinghe, R. (2007). *Observations of rip spacing, persistence and mobility at a long, straight coastline*. Marine Geology, 236, 209 – 221.

Van Dongeren, A.; Bolle, A.; Vousdoukas, M.I.; Plomaritis, T.; Eftimova, P.; Williams, J.; Armaroli, C.; Idier, D.; Van Geer, P.; De Vries, J.V.T.; Haerens, P.; Taborda, R.; Benavente, J.; Trifonova, E.; Ciavola, P.; Balouin, Y. and

Roelvink, D. (2009) *MICORE: Dune Erosion and Overwash Model validation with Data from Nine European Field Sites*. Proceedings of Coastal Dynamics 2009, 82, 1-15.

Van Enckevort, I.M.J. and Ruessink, B.G. (2003a). *Video observations of nearshore bar behaviour. Part 1: alongshore uniform variability*. Continental Shelf Research, 23(5), 501–512.

Van Enckevort, I.M.J. and Ruessink, B.G. (2003b). *Video observations of nearshore bar behaviour. Part 2: alongshore non-uniform variability*. Continental Shelf Research, 23(5), 513–532.

Van Koningsveld, M.; Davidson, M.; Huntley, D.; Medina, R.; Aarninkhof, S.; Jiménez, J.A.; Ridgewell, J. and Kruif, A. (2007). *A critical review of the CoastView project: Recent and future developments in coastal management video systems*. Coastal Engineering, 54, 567-576.

Vicente, C.M. and Clímaco, M. (2012). *Trecho de costa do Douro ao Cabo Mondego: caracterização geral do processo erosivo.* Laboratório Nacional de Engenharia Civil, LNEC report, 56 pp, (in Portuguese).

Vila-Concejo, A.; Ferreira, Ó.; Ciavola, P.; Matias, A. and Dias, J.M.A. (2004). *Tracer studies on the updrift margin of a complex inlet system*. Marine Geology, 208, 43–72.

Vincent, C.; Hanes, D.M. and Bowen, A.J. (1991). *Acoustic measurements of suspended sand on the shoreface and the control of concentration by bed roughness*. Marine Geology, 96, 1–18.

Vincent, C.E. and Green, M.O. (1990). *Field measurements of the suspended sand concentration profiles and fluxes and of re- suspension coefficient $\gamma$ 0 over a rippled bed*. Journal of Geophysical Research 95, 11591–11601.

Vision Caltech (2009). www.vision.caltech.edu/bouguetj/calib_doc, acceded on January 2009.

Vriend, H. and Capobianco, M. (1993). *Approaches to long-term modelling of coastal morphology: a review*. Coastal Engineering, 21, 225-269.

Wang, P.; Kraus, N.C. and Davis, R.A. (1998). *Total longshore sediment transport rate in the surf zone: field measurements and empirical predictions*. Journal Coastal Research, 14, 269–282.

Wang, P.; Smith, E.R. and Ebersole, B.A. (2002a). *Large-scale laboratory measurements of longshore sediment transport under spilling and plunging breakers*. Journal Coastal Research, 18, 118–135.

Wang, P.; Ebersole, B.A. and Smith, E.R. (2002b). *Longshore sand transport – Initial results from large-scale sediment transport facility.* CHETN-II-46, Coastal and Hydraulics Laboratory, U. S. Army Corps of Engineers, Vicksburg, Mississippi, USA.

Watts, G.M. (1953). *A Study of Sand Movement at South Lake Worth Inlet, Florida*. U.S. Army Corps of Engineers, Beach Erosion Board Technical Memo N. 42.

Whitford, D.J. (2002). *Teaching ocean wave forecasting using computer-generated visualization and animation – Part 1: sea forecasting*. Computers & Geosciences, 28, 537-546.

Winterton, R.L. and Livermore, R.A. (2004). *A Customised GIS to Aid Gondwana Research*. Gondwana Research, 7 (1), 287–292.

Wolf, P. and Dewitt, B. (2000). *Elements of photogrammetry with applications in GIS*, 3rd ed., McGraw-Hill Book Company, Boston, Massachusetts, USA, 607 pp.

Woolf, D.K.; Challenor, P.G. and Cotton, P.D. (2002). *Variability and predictability of the North Atlantic wave climate.* Journal of Geophysical Research, 107(C10), 3145.

Wright, L. and Short, A. (1984). *Morphodynamic variability of surf zones and beaches: a synthesis*. Marine geology, 56, 93–118.

Wright, L.; Short, A. and Green, M. (1985). *Short-term changes in the morphodynamic states of beaches and surf zones: an empirical predictive model*. Marine geology, 62(3-4), 339-364.

Zundel, A.K. (2000). *Surface-water modeling system reference manual*. Brigham Young University, Environmental Modeling Research Laboratory, Provo, UT.

# APPENDIX A

## Abbreviations

# APPENDIX A - ABBREVIATIONS

$\alpha_b$ – Breaking wave direction

**ANOVA** – Analysis of Variance

**AT** – Astronomic Tide

**BeachMM** – Beach Morphodynamic Model

**CERC** – Coastal Engineering Research Center

**CIL** – Coastal Imaging Laboratory

**COV** – Coefficient Of Variation

**Dir** – Wave direction

**DJF** – December, January and February

**DTM** – Digital Terrain Model

**E** – Total storm wave Energy

**GCP** – Ground Control Points

**GIS** - Geographic Information System

**Hs** – Significant wave height

$\mathbf{H_{s,b}}$ – Breaking significant wave height

**JJA** – June, July and August

**K** – Factor (or coefficient) of calibration of the wave energy flux approach

**LiDAR** – Light Detection And Ranging

**LST** – Longshore Sediment Transport

**MAM** – March, April and May

**MCR** – MATLAB Compiler Runtime

**MSL** – Mean Sea Level

**Mwd** – Mean Wave Direction

**NAO** - North Atlantic Oscillation

**NMM** – Nível Médio do Mar

**NOAA –** National Oceanic and Atmospheric Administration

**non-IT** – non-information technology

**NRMSE** – Normalized Root Mean Square Error

**PCA** – Principal Component Analysis

**Q** – Volumetric sand transport rate

**Rmax** – maximum run-up level

**RMS** – Root Mean Square

**RMSE** - Root Mean Square Error

$\mathbf{R_{x\%}}$ - Run-up x exceedance level

**Sgolay** – Savitzky–Golay

**SON** – September, October and November

**Tanβ -** Beach face slope

**TIMEX** – Time Average

**TIN** – Triangulated Irregular Network

**Tp** – Peak period

**TSL** – Transporte Sedimentar Longilitoral

**TWL** – Total Water Level